

Spring 5-16-2014

## **An Analysis of the Green Knoll Salt Dome, located in the Southeast Green Canyon, Deep Water Gulf of Mexico**

Randal J. Broussard  
*University of New Orleans, rjbrouss@uno.edu*

Follow this and additional works at: <https://scholarworks.uno.edu/td>



Part of the [Geology Commons](#), [Geophysics and Seismology Commons](#), and the [Stratigraphy Commons](#)

---

### **Recommended Citation**

Broussard, Randal J., "An Analysis of the Green Knoll Salt Dome, located in the Southeast Green Canyon, Deep Water Gulf of Mexico" (2014). *University of New Orleans Theses and Dissertations*. 1858.  
<https://scholarworks.uno.edu/td/1858>

This Thesis is protected by copyright and/or related rights. It has been brought to you by ScholarWorks@UNO with permission from the rights-holder(s). You are free to use this Thesis in any way that is permitted by the copyright and related rights legislation that applies to your use. For other uses you need to obtain permission from the rights-holder(s) directly, unless additional rights are indicated by a Creative Commons license in the record and/or on the work itself.

This Thesis has been accepted for inclusion in University of New Orleans Theses and Dissertations by an authorized administrator of ScholarWorks@UNO. For more information, please contact [scholarworks@uno.edu](mailto:scholarworks@uno.edu).

An Analysis of the Green Knoll Salt Dome, located in the Southeast  
Green Canyon, Deep Water Gulf of Mexico

A Thesis

Submitted to the Faculty of the  
University of New Orleans  
in partial fulfillment of the  
requirements for the degree of

Master of Science  
in  
Earth and Environmental Sciences  
Geology

by

Randal John Broussard

B.S. The University of New Orleans, 2011

May, 2014



## Acknowledgement

First and foremost I would like to thank my family and my wife, because without their love and support I would not be where I am today. I would like to appreciate BOEM very much for providing the hardware, software and expertise for the research. A large amount of gratitude is extended to WesternGeco for allowing us to use their seismic data. I would also like to extend a large amount of gratitude to Midland Valley and their structural geology experts. Particular recognition is extended to Thierry DeCort and Richard Wells at BOEM. Lastly, special thanks are in order to all of the BOEM geoscientists who aided in the completion of this work.

## Table of Contents

List of Figures .....	iv
List of Tables .....	v
Abstract .....	vi
Section 1.....	1
Introduction.....	1
Background and Literature Review .....	2
Methods and Data Sets.....	7
Geologic Setting.....	13
Interpretation.....	15
Section 2.....	41
Structural Restoration .....	41
Methods.....	41
Interpretation.....	45
Conclusions.....	58
Work Cited.....	60
Vita.....	64

## List of Figures

Figure 1 Location of Analysis.....	2
Figure 2	
Figure 3 Location of Seismic Data .....	9
Figure 4 Stratigraphic Correlation .....	17
Figure 5 Redwood Well Log.....	18
Figure 6 Isopach Map .....	19
Figure 7A Seismic Resolution of Variable Area .....	20
Figure 7B Basemap Reference for Fig 7A.....	21
Figure 8 Basemap of Borehole Locations.....	22
Figure 9A Seismic Line A-A' .....	23
Figure 9B Basemap Reference for Fig 9A.....	24
Figure 10A Seismic Line B-B' .....	27
Figure 10B Basemap Reference for Fig 10A.....	28
Figure 11A Seismic Line C-C' .....	29
Figure 11B Basemap Refernce for Fig 11A .....	30
Figure 12A Seismic Line D-D' .....	31
Figure 12B Basemap Refernce for Fig 12A .....	32
Figure 13A Seismic Line E-E' .....	33
Figure 13B Basemap Reference for Fig 13A.....	34
Figure 14A Seismic Line F-F' .....	35
Figure 14B Basemap Reference for Fig 14A.....	36
Figure 15A Depth Reference of 3 Max-Amp Extractions .....	37
Figure 15B The 17,500 ft Max-Amp Extraction .....	38
Figure 15C The 20,000 ft Max-Amp Extraction .....	39
Figure 15D The 22,500 ft Max-Amp Extraction .....	40
Figure 16 Present day.....	47
Figure 17 Upper Pleistocene decompacted.....	47
Figure 18 Middle Pleistocene unfolded .....	48
Figure 19 Middle Pleistocene decompacted .....	48
Figure 20 Lower Pleistocene unfolded .....	49
Figure 21 Lower Pleistocene decompacted .....	49
Figure 22 Pliocene unfolded .....	50
Figure 23 Pliocene decompacted .....	50
Figure 24 Miocene-Pliocene unfolded.....	51
Figure 25 Miocene-Pliocene decompacted.....	51
Figure 26 Upper Miocene unfolded.....	52
Figure 27 Upper Miocene decompacted .....	52
Figure 28 Middle Miocene unfolded .....	53
Figure 29 Middle Miocene decompacted .....	53
Figure 30 Lower Miocene unfolded .....	54
Figure 31 Lower Miocene decompacted.....	54
Figure 32 Oligocene unfolded .....	55
Figure 33 Oligocene decompacted.....	55
Figure 34 Eocene unfolded .....	56
Figure 35 Eocene decompacted .....	56

Figure 36 Cretaceous-Paleocene unfolded.....	57
Figure 37 Cretaceous-Paleocene decompacted.....	57

## List of Tables

Table 1 Time Processing of Seismic Data .....	10
Table 2 Depth Processing of Seismic Data.....	11
Table 3 Stratigraphy of intervals for Restoration .....	43
Table 4 Rock Properties for Restoration.....	44

## Abstract

The western portion of the Mississippi/Atwater fold belt in the Gulf of Mexico contains what is known as The Green Knoll Salt Dome. The creation and growth of this salt diapir is punctuated by salt deposition, salt migration, sediment loading, and is linked to the “Frampton” fold belt. An indicator of these growth periods is exhibited in the Miocene-Pliocene angular unconformity (halo-kinetic sequence boundary). The objective Miocene sand in the “Redwood” (Green Canyon 1001) borehole was thin due to this unconformity. An evaluation of seismic and well log data provided by Bureau of Ocean Energy Management indicated that the unconformity might not provide the seal needed to trap hydrocarbons on the flank of the salt dome, or it did not allow enough sand to be deposited. A palinspastic structural restoration of the Green Knoll Salt Dome revealed that the growth of the Green Knoll and Frampton are connected.

Keywords: salt dome; Gulf of Mexico; restoration; halo-kinetic sequence boundary; hydrocarbon reservoir

## **Introduction**

The Gulf of Mexico is separated into three main sections; Western, Central and Eastern Planning areas, and those three areas are further separated into different protractions where each protraction contains a number of blocks. The area of each block is 3 miles<sup>2</sup> (4.8 km<sup>2</sup>). This geological analysis involves seismic data that covers 10 blocks located in the southeast corner of the Green Canyon protraction area, which is located in the deep waters of The Central Planning Area. These 10 blocks contains a geologic feature known as The Green Knoll Salt Dome, which is a massive salt diapir located outboard of the Sigsbee Escarpment. The Sigsbee Escarpment is the termination limit of allochthonous salt bodies that have been slowly migrating overall in a southeastern direction in this area (Trudgill 1999).

The Green Knoll is situated in southeast Green Canyon among the western portion of the Mississippi Fan Fold Belt or Atwater Valley fold belt system, where one of the fold belts, known as The “Frampton Anticline” fold, extends from the northeast to the southwest terminating against the Green Knoll. The west side of the Green Knoll consists of the other side of the fold belt with a much different geometry than the east side (Figure 3a). The diapir has an angular unconformity (halo-kinetic sequence boundary) that surrounds it (Rowan 2000). This feature is termed halo-kinetic angular unconformity because the unconformity was formed due to an increased growth rate of the salt diapir during the Miocene/Pliocene boundary and the interval that this unconformity contains was analyzed for the existence of hydrocarbons. Salt diapirs are attractive geologic structures because the interval that rides up onto the flank of the diapir, against the salt, can create a trap (Figure 1).

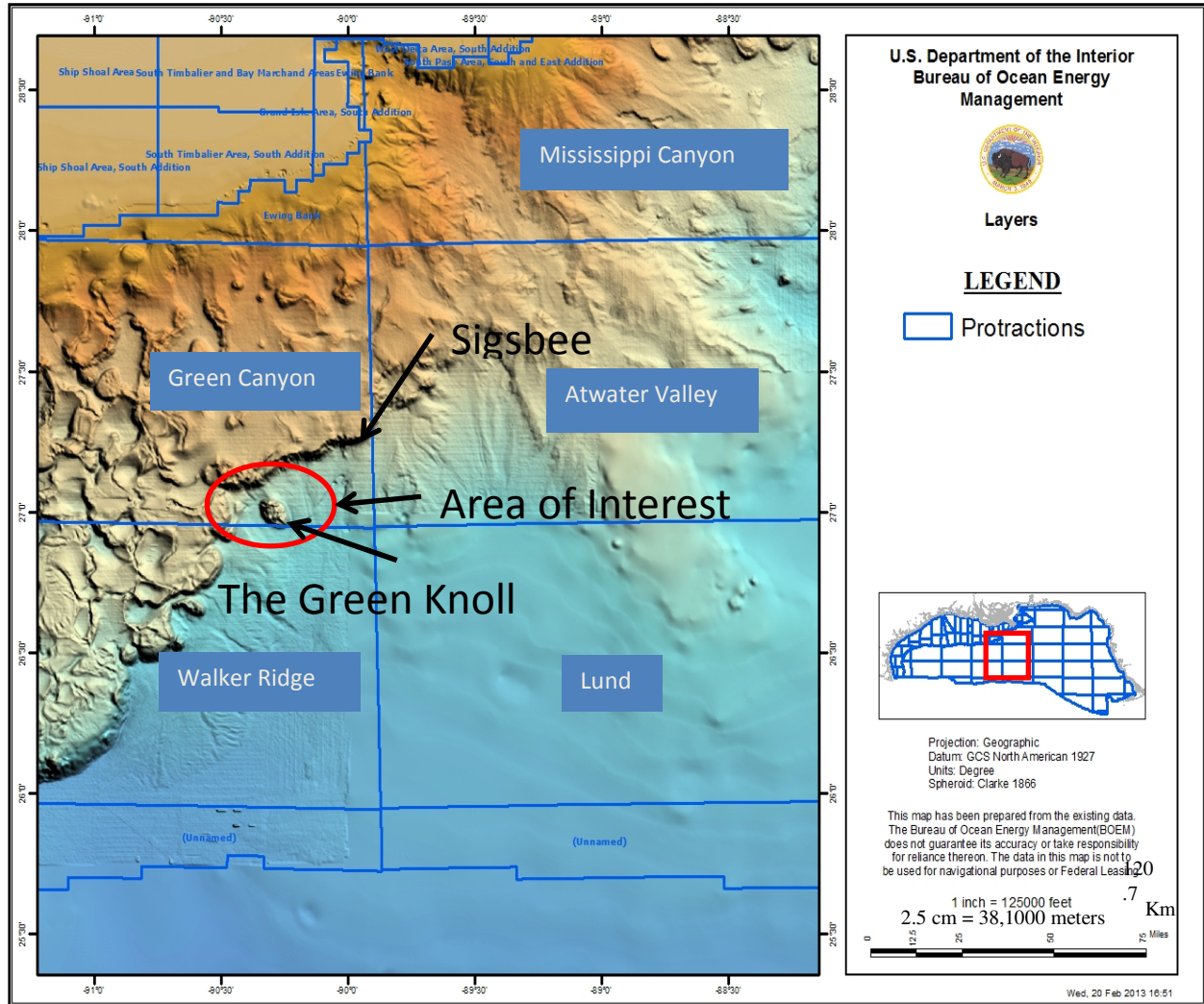


**Figure 1.** Location of the analysis. The Green Knoll Salt Dome is located in the southeast corner of the protraction area Green Canyon in The Gulf of Mexico. (Sea floor datum NAD 1927 projection.)

## Background and Literature Review

Stern and Dickinson (2010) hypothesized that The Gulf of Mexico is a back arc basin where it acted as a spreading center as a result of the late Paleozoic and early Mesozoic breakup of Pangaea. The back arc basin grew behind the Nazas arc, which was formed due to an east dipping subduction zone in the Late Jurassic. (Stern and Dickinson 2010) The middle Jurassic is the main period of rifting while oceanic spreading conceivably continued into the Late Jurassic.



A set of northeast-southwest trends of half grabens and tilted fault blocks together with northwest-southeast trending transverse faulting were created as a result of the rifting continental margin. These northwest-southeast transverse structural features are observed among the Perdido fold belt and Atwater fold belt regions (Grando et al. 2004). Rowan et al. (2000) suggested that the eastern Atwater Valley fold belt experienced two major phases of deformation followed by periods of relative inactivity. First, during the upper Jurassic to Cretaceous post rift thermal subsidence phase, small wavelength folds developed due to gravity gliding above a basinward dipping basal salt detachment. Then during the Cretaceous to middle Miocene phase a period of quiescence occurred, which consisted of thermal subsidence waning while the basinward tilt of the decollement layer was reversed by flexural sedimentary loading on the upper slope. Lastly during the middle Miocene to Pliocene phase there was renewed large wavelength folding caused by gravity spreading as the clastic margin prograded basinward over a landward-dipping detachment (Rowan et al., 2000). Stephens (2009) states that the rift architecture of The Gulf of Mexico provided the complicated basement fabric for the deposition and movement of autochthonous and subsequently allochthonous salt bodies. Rowan et al. furthers this notion by suggesting that the Atwater Valley fold belt formed at the basinward limit of the middle Jurassic Louann salt and the original deposition limit of the salt may have been locally controlled by the basement structures (Figure 2) (Rowan et al., 2000). Deigel et al. (1995) and Rowan et al. (1999) contend that the general movement and geologic structures that the salt undergoes is theorized to be from differential sediment loading into the basin during time. There is a complex relationship where the basement fabric of the basin initially influenced the position and movement of the salt, and the differential sediment loading then controlled the movement of the salt more directly. Since the salt has the lowest shear strength of all the lithological components in the Gulf of Mexico it migrates through the weakest points in the sediment due to sediment loading. Galloway et al. (2011) explains that there was an increase in sedimentation rates during the Miocene and by the end of the Miocene the sediment accumulation had increased throughout the basin to the point where there was enough sediment load to cause the salt in the Green Knoll to grow substantially forming the halo-kinetic angular unconformity.

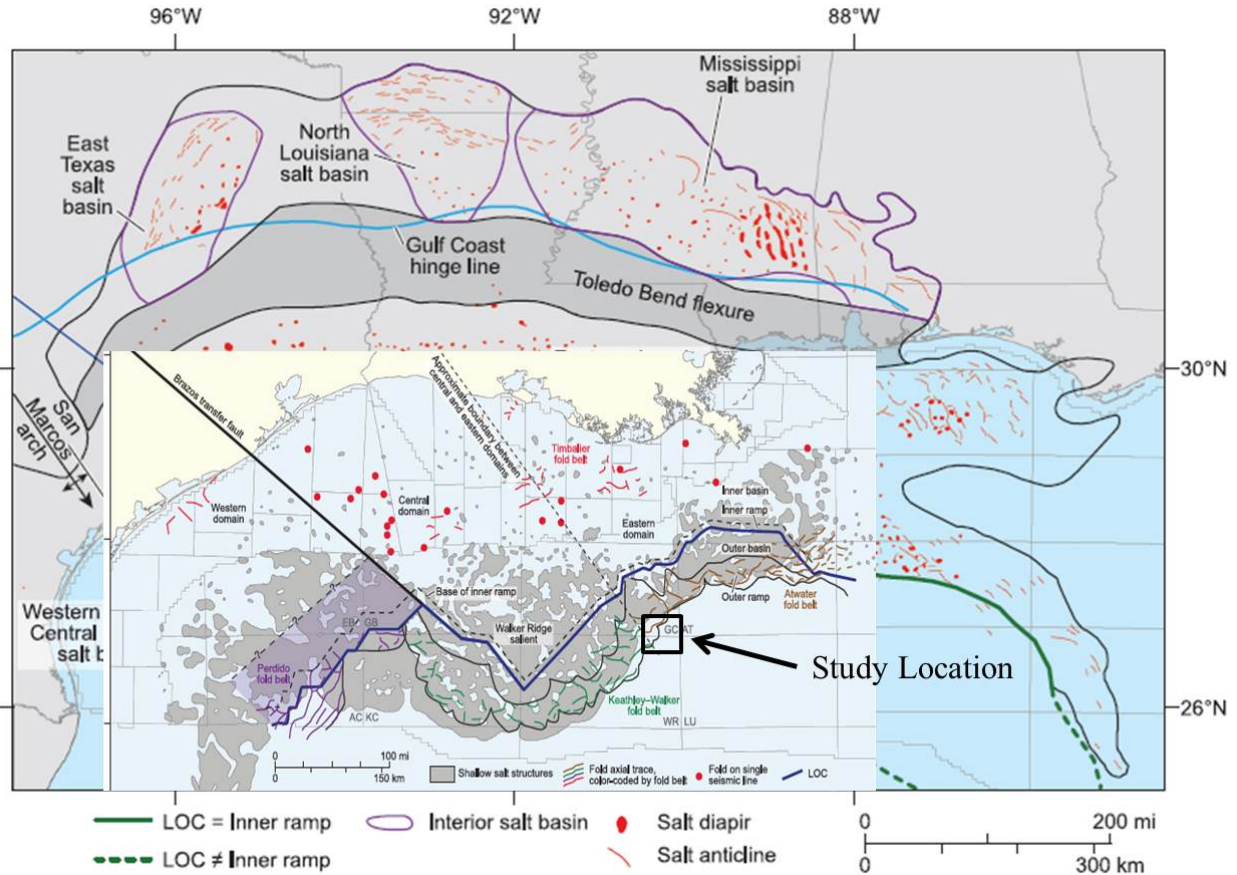


**Figure 2.** Tectonic map with study location. The Green Knoll is situated on the boundary of central and eastern domains where there is a structural change in the fold belt provinces that exist along the Sigsbee Escarpment. (Modified from Hudec et al. 2013)

Rowan and Vendeville (2006) explained that the salt at the decollement level of fold belts apply a strong influence on the structural styles that are formed. The thickness of the salt layer in the salt-cored fold determines whether it will be a salt-cored fold with detachment folds or if a thrust fold develops. Since diapirs are the weakest parts of the rock volume they become preferentially squeezed. After salt deposition occurred in the Gulf of Mexico it started to move relatively immediately, within a few million years. It is still unclear what initially caused deformation in the basin. Rowan (1997) affirms that there was an early, minor phase of gravity gliding of the salt and its overburden, which was caused by the thermal subsidence of oceanic crust in the deep basin that controlled the basinward tilt of the margin. However, Wu et al. (1990) believes that the basinward movement of salt was in response to updip depositional loading. Regardless, localized differential loading became dominant once the salt highs and lows

were established. Hudec et al. (2013) terms the autochthonous salt that moved along a decollement layer as parautochthonous. The original Louann salt bodies that migrated along the basement during the Jurassic are parautochthonous since they are no longer in their original depositional position but still contains an autochthonous component because they are still on top of the basement (Figure 2) (Hudec et al. 2013).

During the late Pliocene and early Pleistocene the Mississippi Fan was deposited, 4km thick in some locations. It is a mud-dominated submarine fan that was deposited in the deep waters of The Gulf of Mexico, beyond the Sigsbee Escarpment. (Weimer 1990) This submarine fan deposit is what bounds the halo-kinetic unconformity with the Miocene. The Frampton Fold Belt, which is located among the Atwater Valley Fold Belt system, developed as a result of the regional salt canopy that started to deform during the early Cretaceous. (Morrison and Weimer 2004) The fold belt formation includes factors like compressional forces from sediment loading where the sediment deposited down slope occurring at the loading fringes of the basin, which is the present day Sigsbee Escarpment. Mercier et al. (2007) provides evidence through modeling that the amplification of folding occurs through hinge migration. Hudec and Jackson (2011) explain the combination of factors that create a salt diapir that is shaped like an hour glass and fold belt formation in their text book *The Salt Mine: A Digital Atlas of Salt Tectonics*. The explanation for the hour glass shape of the salt diapir is that the salt in the diapir rose faster than the aggradation of sediments surrounding it. This particular salt dome is a passive diapir that was reactivated during the Miocene/Pliocene sequence boundary. It is also a relatively young diapir since the top of the dome has not been completely dissolved by the sea water. Typically, an older diapir has a flat top from dissolution and contains sediment that is deposited on top (Hudec and Jackson, 2011).

Mount et al. (2010) explains that the trap development and timing are typically related to the subsidence of sedimentary depocenters (which contain Mesozoic source rocks) into the underlying autochthonous salt layer and emplacement of an allochthonous salt canopy at a shallow structural level through a system of salt stock feeders. Prather et al. (1998) explains the idea of increased sediment supply by second order sea level fall by explaining the capture of large drainage areas from the Mississippi River during the Pleistocene, which are the primary controls on developing a large-scale stratigraphic architecture of intraslope basins.

Lawless et al. (1997) affirmed this idea in a previous study by explaining that the sand rich submarine fans are deposited within sequences of second-order sea level fall. Combellas-Bigott (2002) and Galloway (2002) analyzed the sandy submarine fan that was deposited during the middle Miocene creating a favorably porous package of sandstone that was deposited over allochthonous salt bodies. This is one of the submarine fan sands that is believed to be productive in the Mad Dog Field, because the porosity is around 30% making it conducive for the extraction of hydrocarbons. Rowan et al. (1999) came up with a classification system that defines the different styles of faults, welds, and salt related structures. They describe break thrusts that are high-angle reverse faults that cut one or both limbs of detachment folds, which is a good description of the faults contained in the Frampton Fold belt.

Jurassic source rocks are responsible for the most reservoired thermogenic hydrocarbons existing in the Gulf of Mexico. According to Hood et al. (2002) the source rocks for hydrocarbon accumulation in southeast Green Canyon is the Tithonian hydrocarbon system that is in the uppermost Jurassic aged interval and the Oxfordian, which is an upper Jurassic aged interval as well. The Tithonian source rock consists of organic-rich calcareous shales that contain marine type unbiodegraded oil systems with high, moderately high and moderate sulfur contents. The Oxfordian source rocks are mainly organic-rich carbonates with elevated salinity contents. The Oxfordian hydrocarbon system found in seeps and stains from the deep central Gulf of Mexico are also found in Mobile Bay, which confirms a widespread basin occurrence of this source interval. The stratigraphic column that Hood et al. (2002) generated shows Mesozoic source intervals for the offshore Gulf of Mexico. This column reveals that source intervals coincide with second-order transgressions in a sequence-stratigraphic framework. Their core and cuttings analyses indicate that source richness can vary significantly within an interval, possibly reflecting temporal variations in the environment. The two most likely mechanisms for creating cross-stratal channels are salt movement and faulting. In order to be effective the deep source intervals must be connected to younger Tertiary reservoirs by potential migration pathways (Hood et al. 2002).

The middle Miocene has created one of the most prolific hydrocarbon-producing intervals in the Gulf of Mexico. The submarine fan system that existed was long-lived because of the Harang collapse. Since the shelf margin collapsed (Harang embayment) due to a large load of

sediment during the lower Miocene in combination with salt evacuation, a large influx of sediment bypassed the slope depositing large volumes of sediment basinward of the slope. According to Combellas-Bigott and Galloway (2006) this fan system evolved from a structurally controlled elongated fan to a radial one. The elongated fan consisted of sand-rich to mixed sand and mud, where the radial fan consisted of mixed sand and mud. The complex salt-sediment interaction controlled the distribution and relation of shelf, slope and basin-floor depositional systems. This middle Miocene sand fan is what is productive in Mad Dog and has been found to contain hydrocarbons in Mission Deep (Combellas-Bigott 2006).

## **Methods and Data Sets**

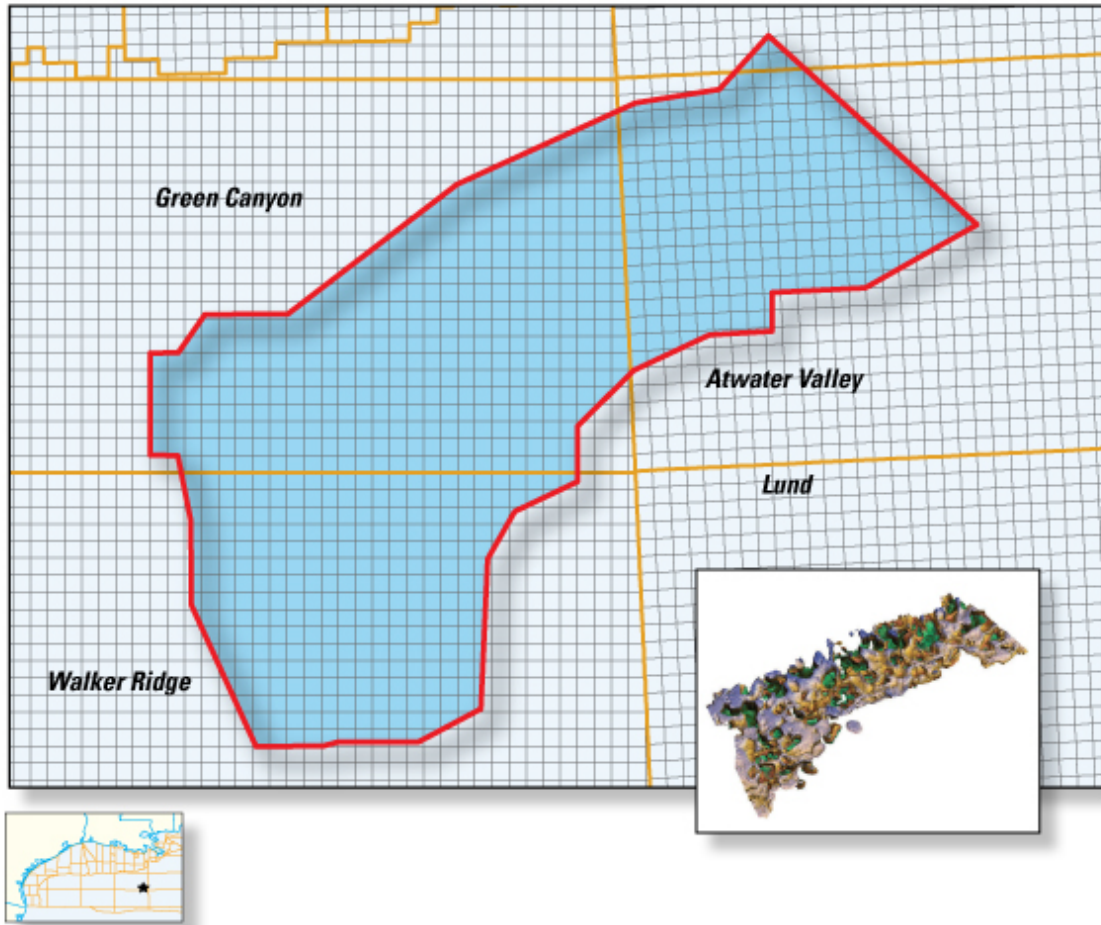
The allochthonous and parautochthonous salt bodies were mapped as well as the middle Miocene horizon. The top and bottom of the angular unconformity was also mapped. The Green Knoll is comprised of both an allochthonous and parautochthonous unit connected by a theoretical “stock”. The autochthonous Louann “mother salt” was not originally deposited in this area, but migrated south-southeast very early on by gliding along a decollement layer. This is where the salt in the salt diapir and the salt in the salt-cored fold at the Frampton fold originated. The terms parautochthonous and allochthonous salt is used for convenience when discussing the structural components of the salt diapir. The parautochthonous component is the part of the salt diapir that existed before the salt diapir grew into its present orientation. The allochthonous component is the section that the parautochthonous component grew into after the second major growth period. The depth imaged 3D seismic data set used to map these elements is the (196\_002\_dm2) E DOG GC/WR/AT from WesternGeco (Figure 3). For optimal clarity and resolution WesternGeco performed both Kirchhoff Migration and one-way Wave Equation Migration (WEM). Some methodologies included the use of boreholes with paleontological data to make the correct ties for the mapping of chronostratigraphic horizons.

We used a Geoframe IESX software package to load the 3D seismic data used in the analysis of the Green Knoll Salt Dome. The 3D seismic data was used to map the middle Miocene horizon in order to generate a structure map within the basemap using the project mapping tool (Figures 9A & B – 15A & B). Using paleontological information from boreholes that were posted on the basemap and 3D seismic data (provided by BOEM), we were able to map the correct depth of the middle Miocene horizon. There are 4 boreholes located within the 3D

seismic data used for tying the middle Miocene horizon together. Three of these boreholes are located outside of the allowable seismic display zone and one of the boreholes is located within it, which is outlined in pink (Figures 9B – 15B). The fault tool in the 3D seismic interpretation package was used to map the top (blue), base and stock (red) of the allochthonous salt body and the autochthonous salt body (light blue) (Figures 9A – 15A). Since the salt varies greatly in lithology from the other lithological components there is a bright seismic reflector, due to the great acoustic impedance, that shows up at the contact between the sediment and the salt. We decided to also map the unconformity using the fault tool on the 3D seismic data because the fault tool allows the interpreter to construct a line without the constraints of having one z value corresponding to one x value like the horizon tool. We noticed two unconformity surfaces on the 3D seismic data so we mapped them with the upper (purple), secondary (green) and base (dark purple) faults represented by dotted lines exhibiting the different stratigraphic relationships (Figures 9A – 15A).

Basemap, 3D seismic, GeoViz, and Wellpix were used from the Geoframe IESX package. The GeoViz tool allowed the 3D seismic data to be loaded as a cube and it was used to pan through the data in real time to gain a better understanding of the relationships of the geological features. Wellpix was used to stratigraphically hang the Mad Dog, Mission Deep and Redwood electronic logs together to reveal the thinning of the middle Miocene sand as it rises up on the flank on the Green Knoll Salt Diapir (Figure 4). An isopach map was also created to show the thinning middle Miocene sand on the flank of the Green Knoll Salt Dome (Figure 6). Figures 7A & 7B were created to show the limited seismic resolution for the construction of the isopach map. Figure 8 shows the location of the 5 well logs used to calculate the average sand amount in the middle Miocene intervals that are located around the Green Knoll Salt Dome. The “Redwood” well log is used for the analysis of the lithology at the unconformity as well as for paleontological markers. As I stated earlier, a structure map was created from the middle Miocene chronozone for the area that encompasses the Green Knoll Salt Dome since it is one of the most attractive hydrocarbon bearing sands in the region. Depth slices were gathered at 2500 ft (760 m) intervals at 17,500ft (5,334m), 20,000ft (6,096m) and 22,500ft (6,858m) for a different perspective of the salt bodies and the angular unconformity. The maximum amplitude extraction tool was used to image the geological features because it focuses on bringing out the

max amplitudes, which allows the stratigraphy and sediment to salt interface to be imaged more easily (Figures 15A, 15B, 15C, 15D).



FULL VOLUME PRESTACK DEPTH MIGRATION

Multiclient Services



**Figure 3.** Data coverage of the (169\_002\_dm2) E DOG GC/WR/AT depth survey, UTM Zone 15 Clarke 1866 NAD 27 (Courtesy of WesternGeco)

<b>Input Surveys</b>
Atwater Valley Area 1
Atwater Valley Phases 5 & 6
Green Canyon VI
Green Canyon Phases 7 through 13
Green Canyon 16
Walker Ridge 1 through 5
<b>Processing Flow</b>
<b>Time Processing</b>
SEG-D conversion to internal format
Navigation merge
Resample to 4 ms
Anomalous noise attenuation (ANA shot domain)
Designature (zero phase)
Surface related multiple elimination (SRME)
Weighted least squares radon
Anomalous noise attenuation (ANA-CMP domain)
Shot and channel consistent scaling
Phase and amplitude matching
Residual de-bubble
Water velocity correction
Inverse Q correction (phase only)
Gun and cable static correction
Resample to 8 ms

**Table 1.** Input surveys and time processing of the (I96\_002\_dm2) E DOG GC/WR/AT survey (Courtesy of WesternGeco)



<b>Processing Flow</b>
<b><i>Depth Processing</i></b>
Sediment tomography
Sediment flood - pick top of salt 1
Salt flood 1 - pick bottom of salt 1
Salt body 1 - pick top of salt 2
Salt flood 2 - pick bottom of salt 2
Salt body 2
Subsalt tomography
Full salt body velocity model
Final Kirchhoff and WEM migrations
Residual moveout correction - Kirchhoff only
3D Tau-P coherency filter, Kirchhoff and WEM
Final volumes: Kirchhoff PSDM stack volume and offset gathers WEM PSDM stack volume and angle gathers (25 Hz)
Processing completed September 2006

**Table 2.** The depth processing flow of the (196\_002\_dm2) E DOG GC/WR/AT survey (Courtesy of WesternGeco)

## Seismic Data

A Geoframe IESX workstation (courtesy of BOEM) was used for the mapping of the interpretation of seismic data, which includes horizons, faults, an unconformity and allochthonous, autochthonous and parautochthonous salt bodies. The survey (196\_002\_dm2) E DOG GC/WR/AT (courtesy of WesternGeco) is a depth survey that is a combination of the following surveys: Atwater Valley Area 1, Atwater Valley Phases 5 and 6, Green Canyon IV, Green Canyon Phases 7 through 13, Green Canyon 16, and Walker Ridge 1 through 5 (Table 1). The sampling rate of the data is 32 ft/sec (9.8 m/sec) and the vertical resolution is 250 ft (76.2 m). In the final depth processing of the seismic data there was one salt flood and three salt bodies used for migration. The maximum depth of the survey reaches 60,160 ft (18,336 m), the output fold used was 26, and the output grid was 164 x 131 ft (50 x 40 m). The record length is 6,000 ft (1828.8 m) with a distance between crosslines of 41.01 ft (12.5 m) and a distance between inlines of 65.62 ft (20 m).

This particular survey encompasses the protractions of Green Canyon, Atwater Valley, and Walker Ridge (Figure 3). It is a full volume with pre-stack depth migrated data that consists of WEM and Kirchhoff migrations.

Pre-stacked data allows for a more true representation of the amplitudes as oppose to the post-stacking method, which was used in the past. The Kirchhoff migration uses Ray tracing to solve the wave equation where the WEM uses numerical solution of the one-way wave equation in the frequency domain. The WEM method creates a more complicated velocity model with irregular features while the Kirchhoff method is moderately complicated that requires smoothing. The Kirchhoff method is better suited for steep dips and model building and these are the reasons that the Kirchhoff migration was used for this project (Vinje, 2010). Table 2 shows the final processing techniques used for the depth imaging of the data, which was finished in 2006 by WesternGeco.

The stratigraphy of the Frampton/Green Knoll area were subdivided into five megasequences, two growth periods, an inter-growth period and a post-growth period by Grando et al. (2004) in order to correlate the depositional units with the tectonic events. The first megasequence consists of the syn-rift-post-rift tectonic event, which took place during early Jurassic to early Cretaceous. The deposition consisted of continental clastics, Louann salt and carbonates. The second megasequence contains the first growth period that took place during the middle to the upper Cretaceous. There is a transition from shallow marine carbonates to deep marine shales and marls, which is indicative of a transgressive phase. During this depositional episode early salt pillow structures formed.

The third megasequence consists of an inter-growth period that takes place from the middle Cretaceous Sequence Boundary to the mid-late Miocene. The older portion of this depositional unit consists of deep marine shales & marls. By the early Miocene siliciclastics that are described as coarse-grained turbidites entered the basin and started to reach this area. The fourth megasequence takes place from the mid-late Miocene to the middle Pliocene and it contains the second growth period. The significant growth strata in this interval represent the time of greatest fold amplification and uplift. This is the interval that is defined by the halo-kinetic angular unconformity. The fifth megasequence takes place from the middle Pliocene to the present and is characterized as the post growth interval.

The Mississippi Fan is a part of this sequence and is dominated by slump related sediments and channel levee deposits. This stratigraphy is consistent with the stratum that rides up onto the flanks of the salt dome since they are continuous from the fold belt (Grando et al., 2004).

### **Geologic Setting**

The Louann salt that was deposited during the middle Jurassic has created a very complicated structural fabric of geologic formations that are conducive for hydrocarbon maturation, migration and trapping. Hall (2002) states that a number of structural traps developed between allochthonous and autochthonous salt levels are due to the shapes of the strata that were formed from feeder systems driven by autochthonous salt flow. The salt deposition and differential migration has made it possible to successfully discover and extract hydrocarbons that would otherwise be too difficult to reach. This basin contains many different styles of faults, salt related structures, and salt remnant structures. Some examples include 3-way hydrocarbon traps against the stocks of salt domes or salt feeders and salt welds, which are spaces where salt has evacuated out due to sediment load. These remnant features are sediment packages “welded” to other sediment packages with a very thin layer of salt left over leaving a bright reflector in the seismic image. Often, these welded areas follow weak points in the strata, like faults.

The Green Knoll Salt Dome rises through the sea floor creating about 1500 ft (450 m) of relief. The salt diapir has a classic hourglass shape with a mushroom cap at the sea floor. This salt dome is believed to still be fed by a parautochthonous salt root. The M/P (Miocene/Pliocene) angular unconformity that is present (halo-kinetic sequence boundary) is the evidence of a major growth period of the salt dome at the Miocene and Pliocene chronostratigraphic boundary. The halo-kinetic angular unconformity is much more pronounced on the western and eastern sides. It creates a thinning of productive Miocene sands analogous to nearby Mad Dog Field (GC 826) and Mission Deep Field (GC 955) (Figures 4 & 6).

The Green Knoll is located among the western portion of the Atwater Valley fold belt province. This geologic setting of fold belts and salt domes are common to an area that experiences compressional forces at the fringes of a basin, like at the Sigsbee Escarpment where the slope allows for sediment accumulation and loading.

The general setting in this area consists of a wave train of folds, which are located underneath the allochthonous salt canopy, that contain landward dipping salt-cored normal faults dominating the structures. The most distal fold belt in the wave train is a counter-regional salt-cored reverse fault that dips basinward, and it is located outboard of the Sigsbee Escarpment (allochthonous salt sheet), hence the Frampton fold belt. This region consists of only one salt diapir that is located outboard of the Sigsbee escarpment, the Green Knoll Salt Dome. The two landward folds among the wave train have traps with announced oil discoveries (Mad Dog and K2/Timon). As mentioned in a previous section the fringe of the basin acted like a buttress controlling the extent of the parautochthonous salt bodies movements along the decollement layer. Morris and Weimer (2004) explain that the folds overlie the regional detachment of the Louann salt, which are the parautochthonous salt bodies that migrated basinward along a glide plane. According to Stephens (2009) the Sabine Transfer Fault extends from the Ouchita front, across the Texas Gulf Coast shelf and through the Sigsbee salt canopy in a northwest-southeast trending fashion. Stephens (2009) affirms that the Sabine Transfer Fault is the most prominent of all of his hypothesized transfer faults that extends beneath the abyssal plane. The Hackberry Transfer Fault is located east of the Sabine Transfer Fault and travels parallel with the Sabine Transfer Fault. This corridor located between faults generally extends underneath the Green Knoll Salt Dome, which has implications on the limit at which the parautochthonous salt bodies migrated to, and the implied structural controls that the faulting had on the formation of the Green Knoll and Frampton fold belt. This may provide further insight on why the amount of salt that migrated to this region piled up to form the Green Knoll and the compressional features like the connected fold belt (Stephens 2009).

The Frampton anticline fold belt extends for about 15 mi (24 km) from east to west terminating against the east side of the Green Knoll salt dome, then starts again on the west side of the Green Knoll extending for another 8 mi (12.5 km) where Mission Deep (GC 955) is located. The length of the entire fold belt is about 23-25 mi (37-40 km). Grando et al. (2002) describes the eastern most profile as a symmetric detachment fold with well-developed kink bands between planar axial surfaces and sharp angular hinges. The fold progressively becomes a faulted detachment fold to the west where the hinges become more rounded. The salt diapir and the fold belt experienced the same growth periods due to the halo-kinematics revealing that both structures are linked by the same structural controls.

## **Interpretation**

The Green Knoll is located past the Sigsbee Escarpment where there are no allochthonous salt bodies present, except for the top half of the salt diapir. The salt diapir has extensional faulting associated with the growth on the flanks, which is most pronounced on the northern and southern flanks. There is also a small salt pillow associated with the halo-kinetic unconformity that formed on the northwestern flank of the salt dome (Figures 9A and 9B). This small salt pillow billowed out as the Green Knoll was rising as a result of the large influx of Miocene sedimentary loading taking place. The salt pillow contains evidence of the halo-kinetic angular unconformity where the side of the salt pillow meets the base. The base is a high amplitude reflector that is juxtaposed to the stock of the salt diapir representing the sequence boundary at which the Green Knoll's rate of upward growth was outpacing deposition. This is direct evidence of the "halo-kinetic" component of the sequence boundary.

Grando and McClay (2003) performed a palinspastic restoration of the Frampton fold belt to gain insight on the structural evolution of this feature. The results revealed salt punctuations of two main growth periods: the first during the early deformation stage (salt inflation) following the middle Jurassic Louann Salt deposition and the second that is the Miocene/Pliocene boundary growth period. Evidence of the second growth period is in the halo-kinetic angular unconformity that marks the Miocene/Pliocene boundary. The "Redwood" Prospect (GC 1001) was drilled onto the flank of the Green Knoll Salt Dome attempting to reach the productive middle Miocene sands found in The Mad Dog Field (GC 826). The well missed the objective sands because it was drilled too far up dip along the angular unconformity. The halo-kinetic angular unconformity caused the middle and upper Miocene sands to be pinched out where the well was drilled. The thinning of the Miocene sands is due to a non-depositional unconformity. As the Miocene was loading the area with sediment, The Green Knoll diapir had already existed but was not as pronounced as it is presently. As the large influx of Miocene sediment caused the diapir to rise more rapidly, the deposition of the Miocene simply did not reach all the way up the flanks of the diapir.

The halo-kinetic angular unconformity that surrounds the Green Knoll Salt Dome has two main components. One is the main discontinuity surface and the other is a less pronounced discontinuity surface.

The dark purple dashed line in Figure 10A represents the main discontinuity surface while the green dashed line represents the secondary discontinuity surface. In Figures 10A and 10B, middle Miocene strata terminate onto the discontinuity surface in an onlapping fashion as the strata rises up onto the flank of the Green Knoll. The angle of the strata is much steeper on the east side as opposed to the west side which is most likely due to the absence of allochthonous salt on the east side of the salt diapir to disrupt the angle of strata growth. This halo-kinetic unconformity was created by the punctuation of salt growth around the Miocene/Pliocene chronostratigraphic boundary surrounding the Green Knoll Salt Dome. The borehole of the Redwood Prospect was deviated at a 45-degree angle towards the salt diapir in order to test the prospective Miocene sands but those sands were missed. The Miocene sands are present further down dip from the salt diapir. The “Redwood” (GC 1001) well log revealed the thinning of middle Miocene sands. The well logs in Figure 4 were hung stratigraphically on the middle Miocene sand. The well log correlation shows the thinning of the middle Miocene sand in the Redwood well. The three biostratigraphic markers used in the well log correlation are *Sphenolithus heteromorphus* (S heta), *Helicosphaera ampliaperta* (H hete) and *Catapsydrax dissimilis* (C diss). *Sphenolithus heteromorphus* is a calcareous nannoplanktic paleo-marker found in middle middle Miocene sediment. *Helicosphaera ampliaperta* is also a calcareous nannoplanktic paleo-marker found in the lower part of middle Miocene sediment, and *Catapsydrax dissimilis* is a foraminiferal planktic paleo-marker found in the upper portion of lower Miocene sediment (Figure 4) (Witrock et al. 2003). The borehole locations for the well logs used in Figure 4 are located on the well log referenced basemap (Figure 8).

The upper Pliocene sits right on top of the middle middle Miocene and below that is a condensed section of lower Miocene, Oligocene and upper Eocene strata providing direct evidence of the condensed package of thinning strata that rides up on the flank of the salt diapir (Figure 4). The Green Knoll area is near the deposition limit of the middle Miocene deposode and may explain why the upper Miocene did not reach the upper flanks of the salt diapir. The gamma ray signature in the “Redwood” well log reveals a thin sand package and limestone present at the boundary of the halo-kinetic unconformity, which may have allowed any hydrocarbons to escape if they migrated to this area (Figure 5).

The mud log revealed limestone at the interval of the unconformity, which could be present from the formation of a carbonate hard-ground chemosynthetic community where hydrocarbons seeped through the sediment while this section was exposed to the sea floor at the Miocene/Pliocene boundary (Figure 5). This could further the notion of a non-depositional unconformity but it is speculative whether it happened or not. There is no direct evidence leading to a carbonate hard-ground existing on the flank of the salt diapir at the end of the Miocene. However it would further prove the existence of hydrocarbons, since they could have migrated up and seeped out at this location forming the supposed chemosynthetic community.

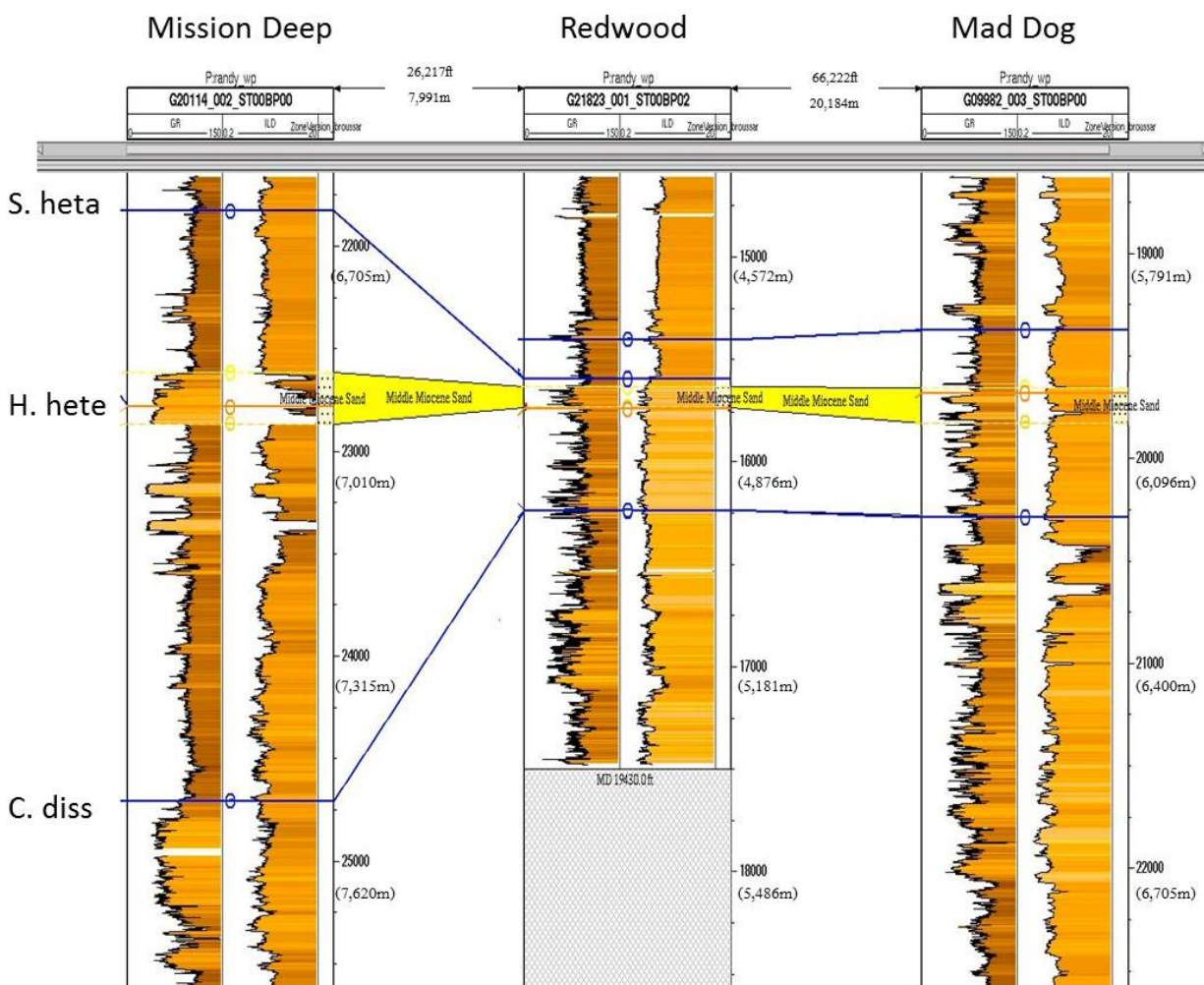


**Figure 4.** Stratigraphic Correlation of middle Miocene sand. The three biostratigraphic markers used in the well log correlation are *Sphenolithus heteromorphus* (S heta), *Helicosphaera ampliaptera* (H heta) and *Catapsydrax dissimilis* (C diss). *Sphenolithus heteromorphus* is a calcareous nannoplanktic paleo-marker found in middle middle Miocene sediment. *Helicosphaera ampliaptera* is also a calcareous nannoplanktic paleo-marker found in the lower part of middle Miocene sediment, and *Catapsydrax dissimilis* is a foraminiferal planktic paleo-marker found in the upper portion of lower Miocene sediment. Courtesy of BOEM (Witrock et al. 2003).



# GC 1001 "Redwood" Well

Gamma Ray

Resistivity

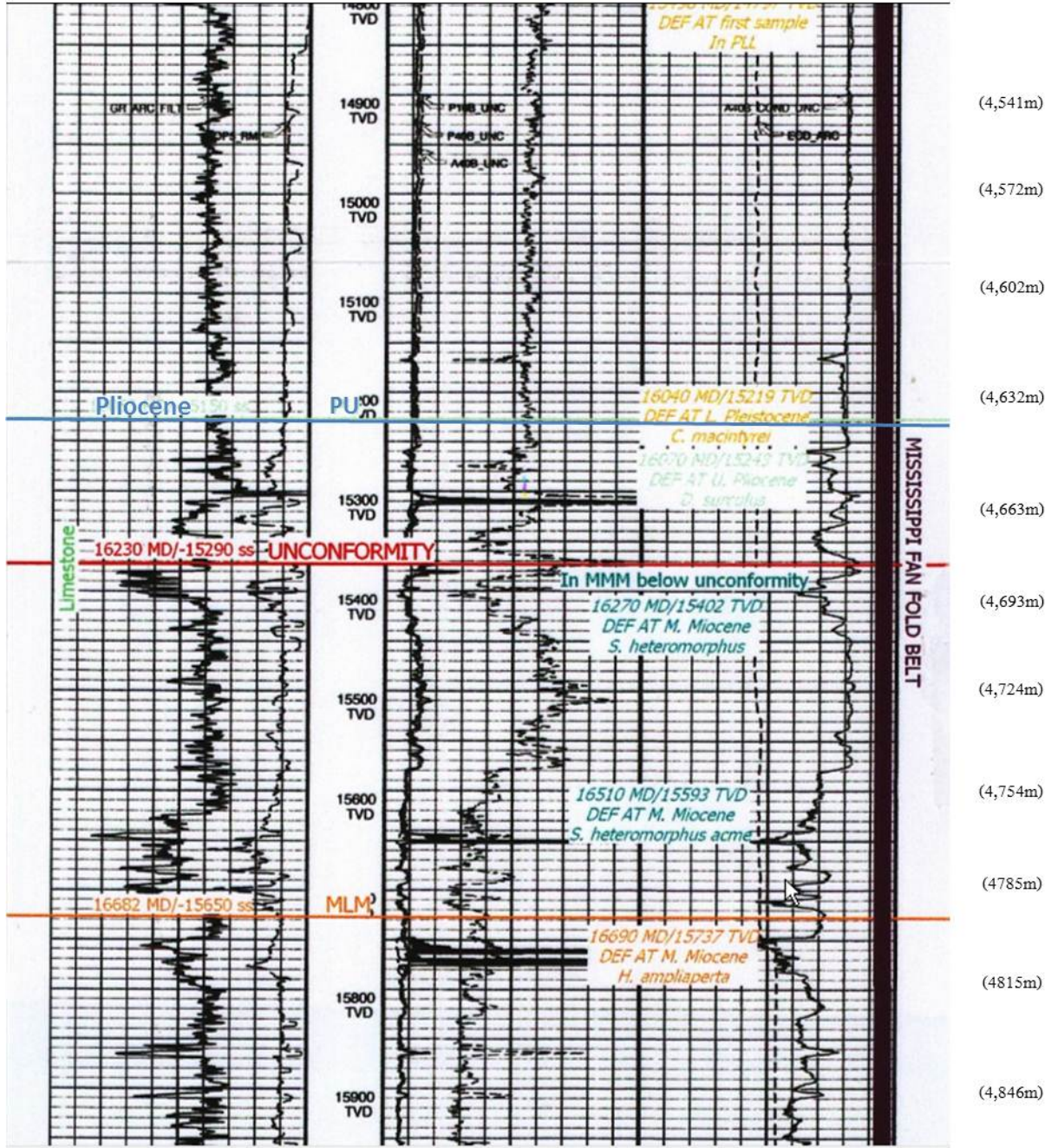


**Figure 5.** Redwood well log with the halo-kinetic unconformity present. The whole upper Miocene section is non-existent, and the Pliocene is lying on top of the middle Miocene. There is limestone present at the unconformity. The Mississippi Fan Fold Belt is included within the interval of the Pliocene-Miocene package.



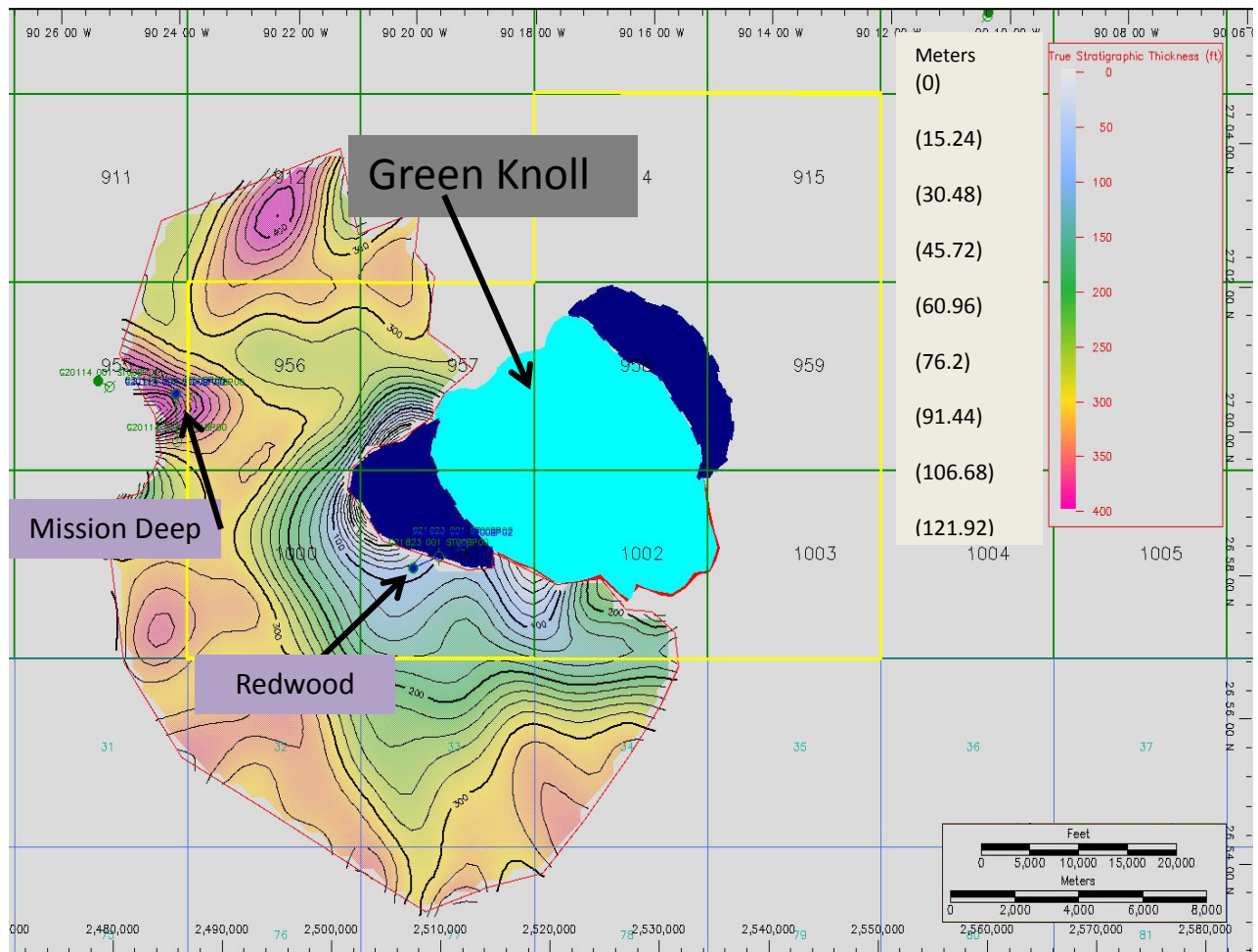


**Figure 6.** Isopach map of the middle Miocene mapped from the Mission Deep (GC 955) well to the Redwood well (GC 1001). Courtesy of BOEM.

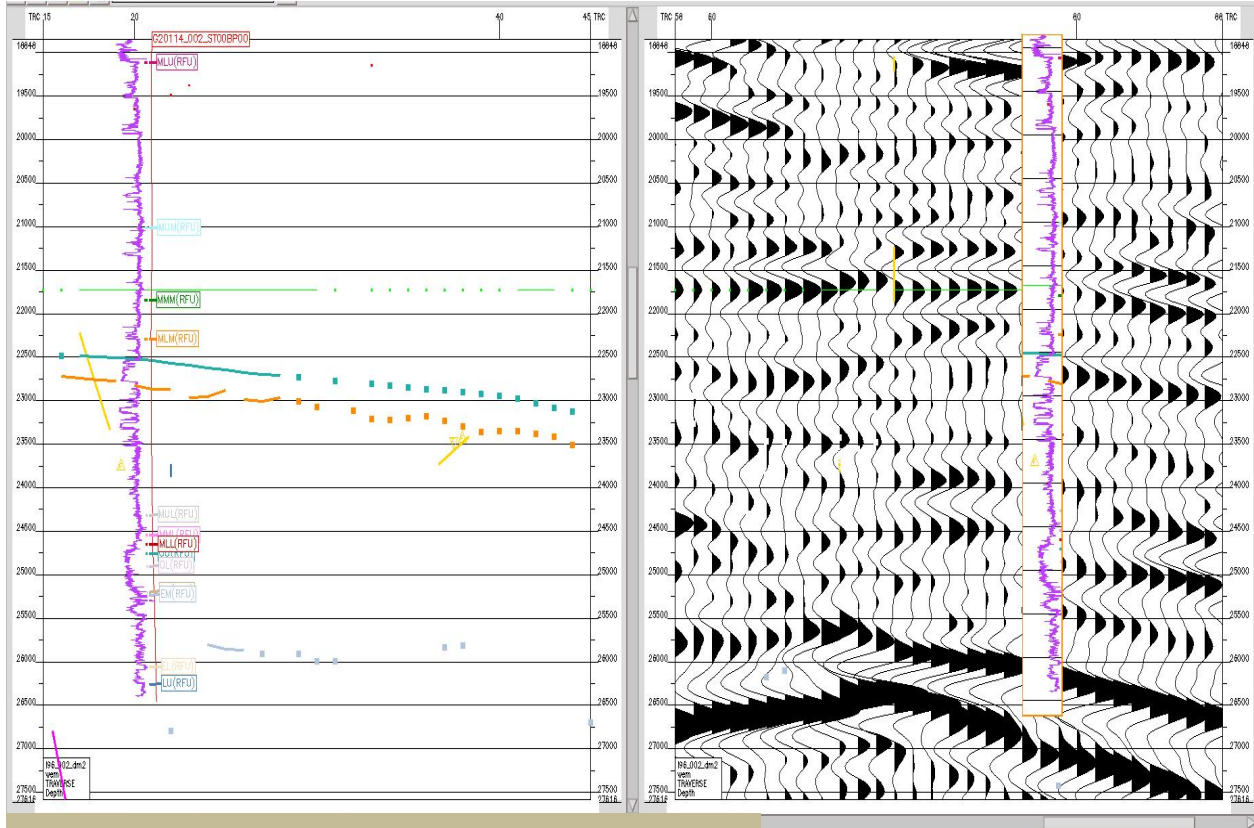


**Figure 7a.**  
 Depth Survey I96\_002\_dm2 Kirchhoff migrated  
 Variable area posted on the right for seismic resolution  
 Courtesy of WesternGeco

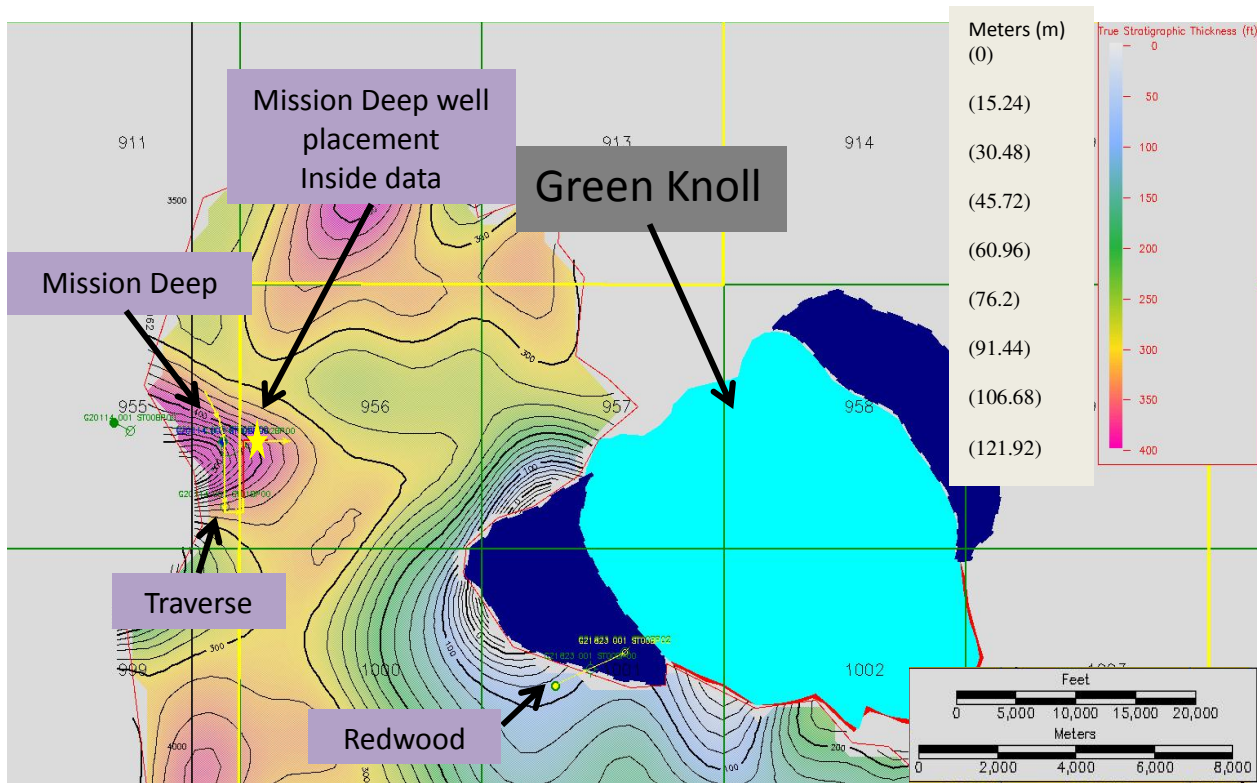


**Figure 7a & 7b.** Seismic resolution with the associated basemap to show the traverse and placement of the Mission Deep borehole. Figure 7a shows the variable area of the seismic and the Mission Deep borehole posted to show the resolution of the 250 ft sand in Mission Deep. These two images exhibit the limited resolution of the data for the construction of the isopach map. Courtesy of WesterGeco.





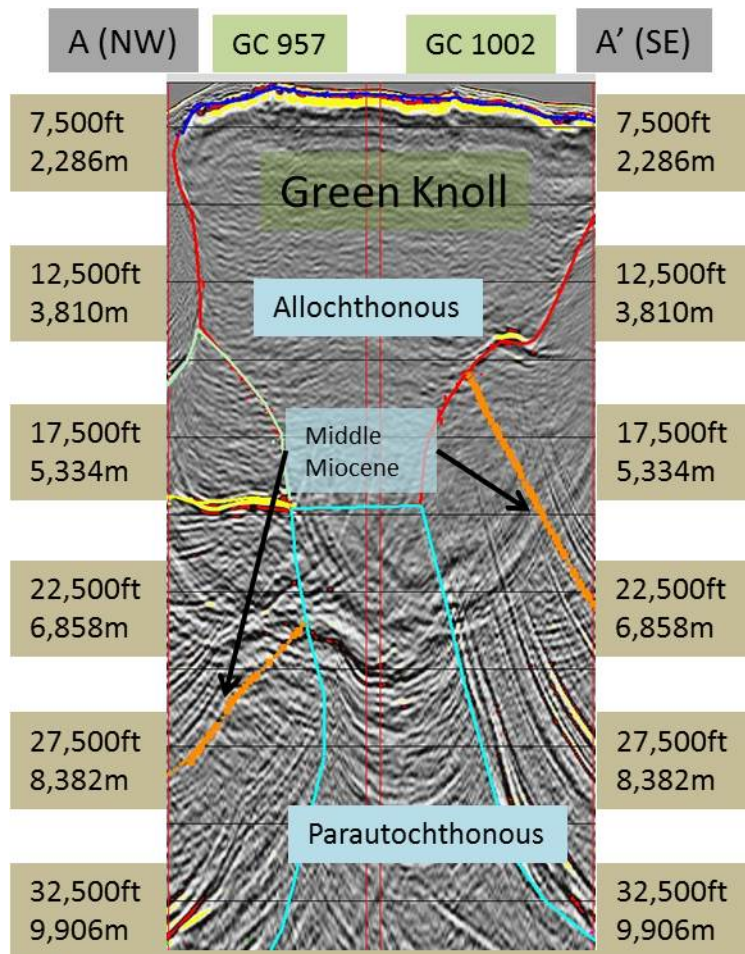
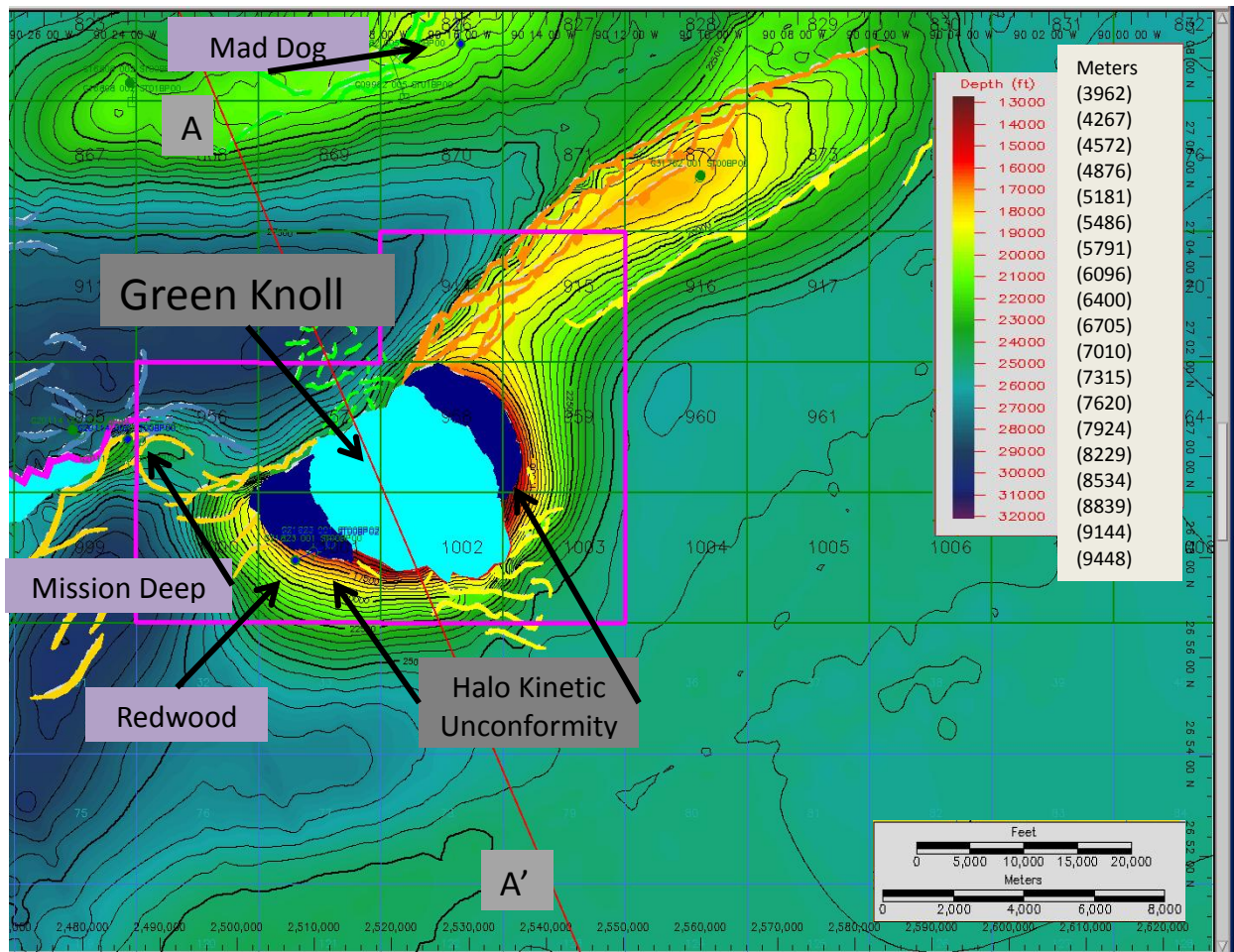


**Figure 9a.**  
 Depth Survey I96\_002\_dm2 Kirchhoff migrated  
 Courtesy of WesternGeco



**Figures 9a. & 9b.** The seismic line and basemap with the associated traverse for a graphic of The Green Knoll Salt Dome where the allochthonous and parautochthonous components are connected at the stock, from north to south. The small salt body located on the northwest of The Green Knoll was formed during the formation of The Green Knoll. The image is annotated with the transect direction and the blocks that the data is covering. Structure Map of the Middle Miocene Depth Survey 196\_002\_dm2 Kirchhoff migrated (Courtesy of WesternGeco).

Figure 6 is an isopach map created to show the thinning of a hydrocarbon bearing sand on the flank of the Green Knoll Salt Dome. Since the resolution of the seismic is 250-300 ft (76.2-91.4 m) it is difficult to resolve anything thinner than 250 ft (76.2 m). Instead we mapped the interval of the wavelet shown in Figure 7a from Mission Deep (GC 955) to the Redwood (GC 1001) well. Since the isopach map is not an accurate true thickness of the sand, five of the closest wells that contain the middle lower Miocene section were used to average the sand content among the intervals so the true stratigraphic thickness of the sand is understood within the

context of these maps. The average interval among the 5 wells is 940 ft (286.5 m) with an average total sand thickness of 280 ft (85.3), which yields a 30% of sand content among those intervals (Figure 8).

The isopach map that has been generated shows a hydrocarbon bearing sand interval from Mission Deep which is around 250 ft (76.2 m) thick, mapped to the Redwood well which contains about 50 ft (15.24 m) of sand. The sampling rate of the seismic is 32 ft (9.7 m) but the resolution of the “peak to trough” wavelet is 250-300 ft (76.2-91.4 m). The left image in Figure 7a shows the Mission Deep gamma ray log posted on a section of seismic that is located outside of the zone of proprietary seismic that I am allowed to show. The image on the right of Figure 7a shows the seismic with the variable area of the wavelets posted within the zone of seismic that I am allowed to show. Since I cannot show the seismic where Mission Deep has been drilled, I posted it on the right to exhibit the resolution of the wavelet that encompasses the 250 ft (76.2 m) sand located in the middle lower Miocene interval. The yellow star among the traverse in Figure 7b exhibits the approximate location of where Mission Deep has been placed in the right image. The flattening tool was used with the green horizon to remove dip so the reader can image the wavelet with the gamma ray signature better as a reference for the resolution of the seismic.

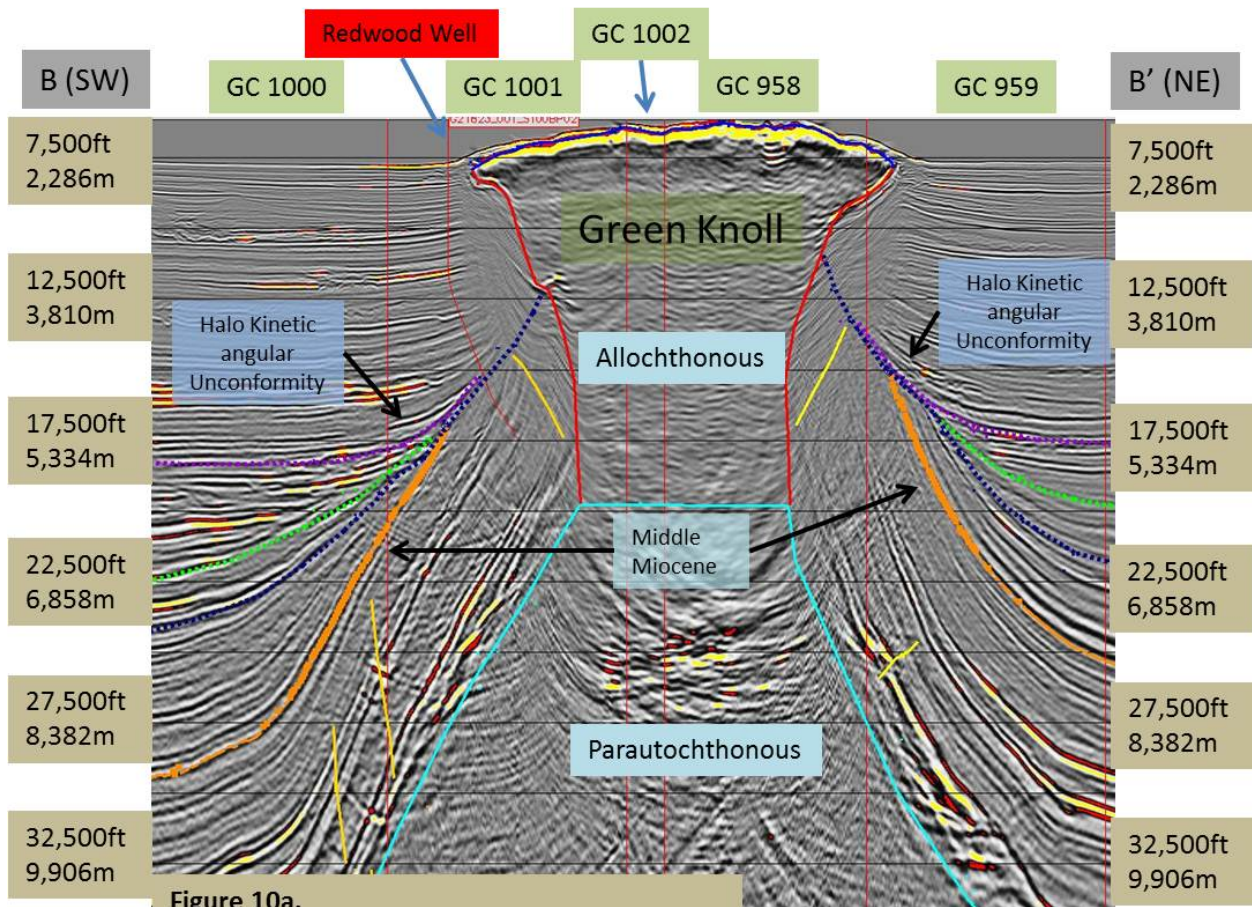
Grando et al. (2003) states that the western limit of the Frampton fold belt is the Green Knoll Salt Dome, yet the fold belt continues on the western side of the salt diapir for another 8 mi (12.5 km). If the amount of salt present was less and the Green Knoll diapir didn't form, the fold belt would have been uninterrupted by the diapir. Therefore the full length of the fold belt is approximately 23 mi (37 km) long. The Frampton Fold Belt can be imaged on both sides of the Green Knoll Salt Dome as it extends from east to west “through” the parautochthonous portion of the salt diapir. The Frampton Fold on the west side of the Green Knoll has multiple folds and is shorter in height as opposed to the east side of the Green Knoll. The eastern side contains the crest of the fold belt and is a much more pronounced anticlinal fold (Figures 11A & 11B and Figures 12A & 12B).

The amount of parautochthonous salt that was present on both sides of the salt diapir as the fold belt was forming has implications on the different style of folding on each side. The halo kinetic unconformity is present at the top of the fold belt, which reveals the connection of the salt diapir and the fold belt. One will also see the presence of the middle Miocene within the

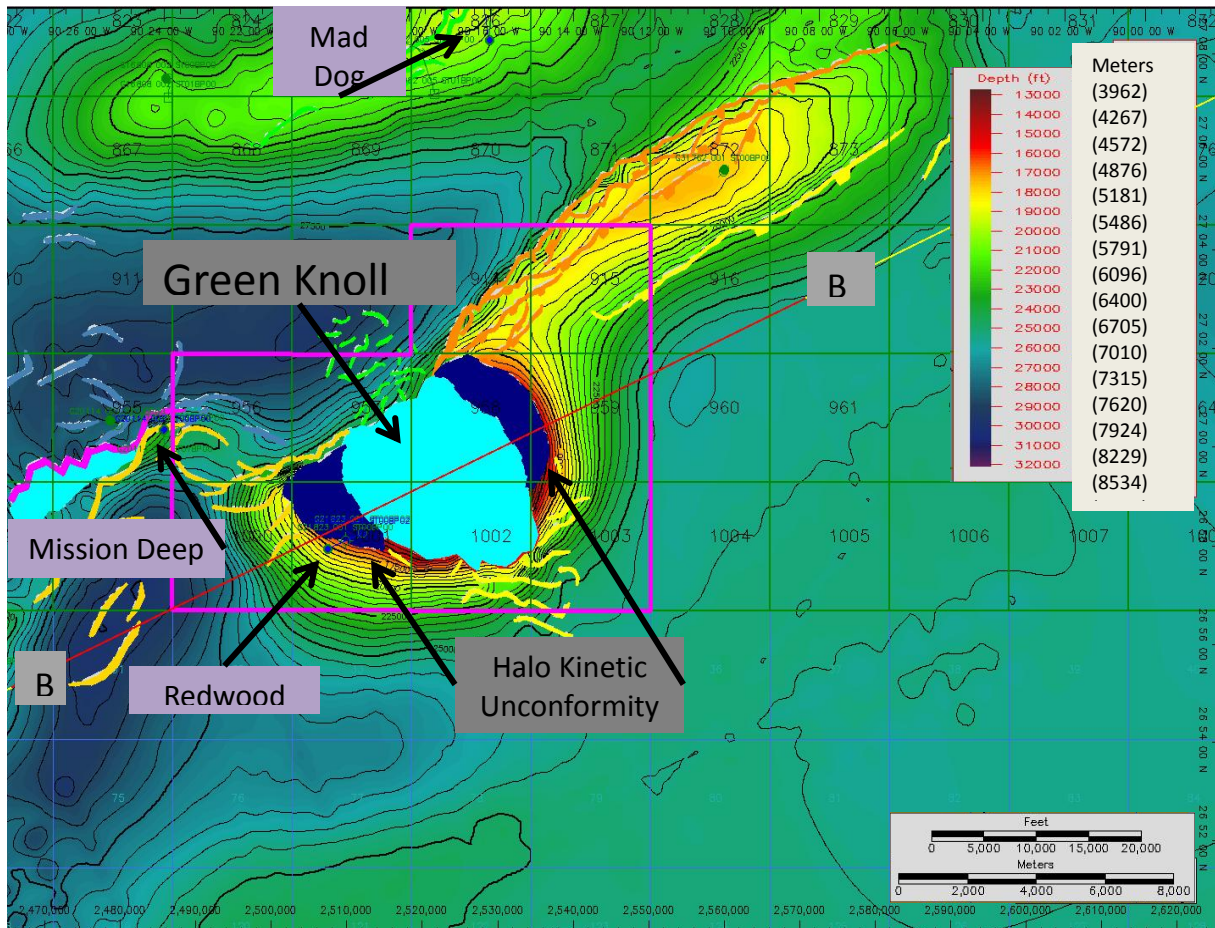
Frampton Fold Belt. On the east side of the Green Knoll the fold from east to west starts as a symmetric box-fold and ends as an asymmetric fold with a reverse fault dipping basin ward as the dominant orientation. The fold on the west side of the Green Knoll is an asymmetrical “crinkled” fold that is dominated by multiple faults. The fold belt dips basinward instead of landward because during the formation of the fold belt the parautochthonous salt found a weak spot on the north side of the fold belt and started to migrate up through it dominating its present orientation. The downdip portion was buttressed by the landward tilt of the crust due to the flexural sedimentary loading. The buttress dominated the migration of salt to flow upwards and landward simultaneously as deposition caused compression. Figure 13A provides the best perspective for viewing the Green Knoll, Frampton fold and the halo kinetic angular unconformity. Figure 14A is similar to Figure 13A except the traverse travels through the north side of the diapir imaging the salt pillow that formed due to the M/P halo-kinetic growth period. Notice the base of the pillow as it is a strong reflector signifying the growth sequence. The halo kinetic unconformity provides the evidence of the growth and formation of the structures. In Figures 15A, 15B, 15C and 15D depth slices were taken at 17,500ft (5,334m), 20,000ft (6,096m) and 22,500ft (6,858m) intervals to show the halo kinetic angular unconformity from a different perspective. The bright amplitude on the south west side of the salt diapir could contain a pocket of hydrocarbons, or it could have been the hard ground chemosynthetic-community that was hypothesized earlier in this paper. This amplitude extraction is an example of what a possible hydrocarbon trap or wet sand might look like on the base map. The strong reflector that the acoustic impedance is creating is caused by lithologies that are very different from each other but stacked right on top of each other, or fluid filled sands that are surrounded by shale. Usually hydrocarbons create a positive-negative-positive relationship because sound will travel faster through a denser material (shales), slower through a less dense material (fluid filled sand), and then fast again through a denser material. Yet, in Figure 15A the seismic amplitude signature is a negative-positive-negative sequence. The chemosynthetic community hypothesis could make sense with this sequence of acoustic impedance because a dense carbonate could be sitting in between less dense sands.



Notice the flat beds, steeply dipping beds and the salt in the middle in Figures 15B, 15C and 15D. The unconformity is the boundary between the steeply dipping beds and the flat beds. The flat beds have a “cloudy” character while the steeply dipping beds appear to be thin and tightly stacked segments on each other. The salt has the typical jumbled up look in the center of Figures 15B, 15C and 15D, where the stock is located.

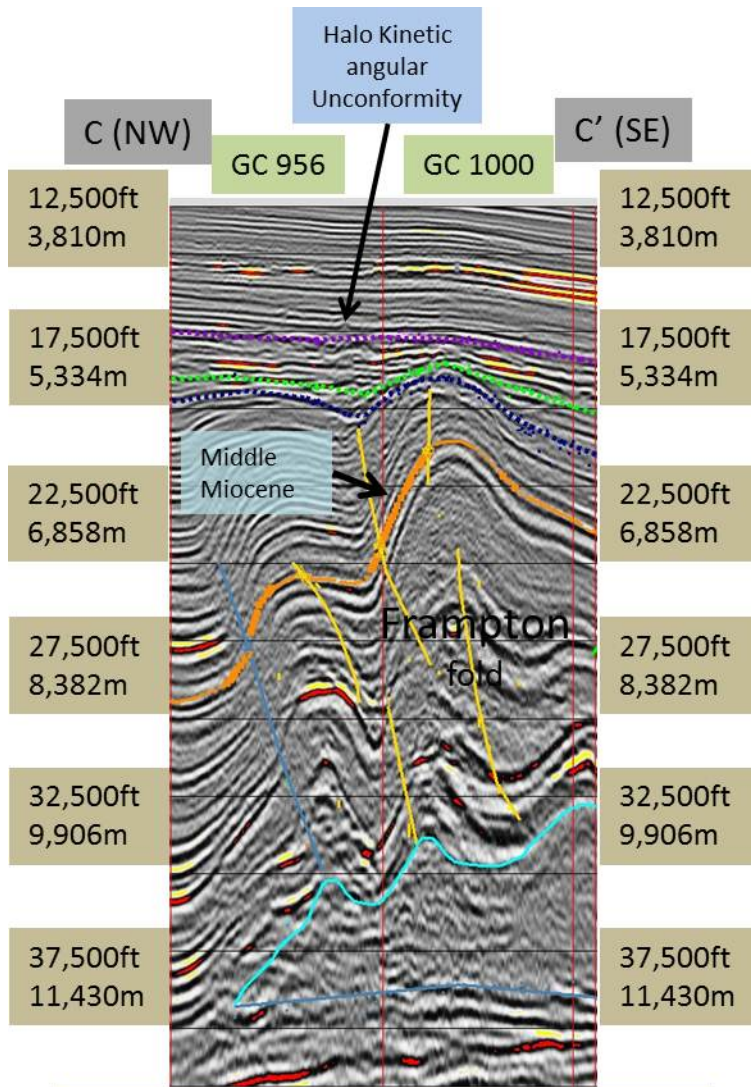


**Figure 10a.**  
 Depth Survey I96\_002\_dm2 Kirchhoff migrated  
 Courtesy of WesternGeco

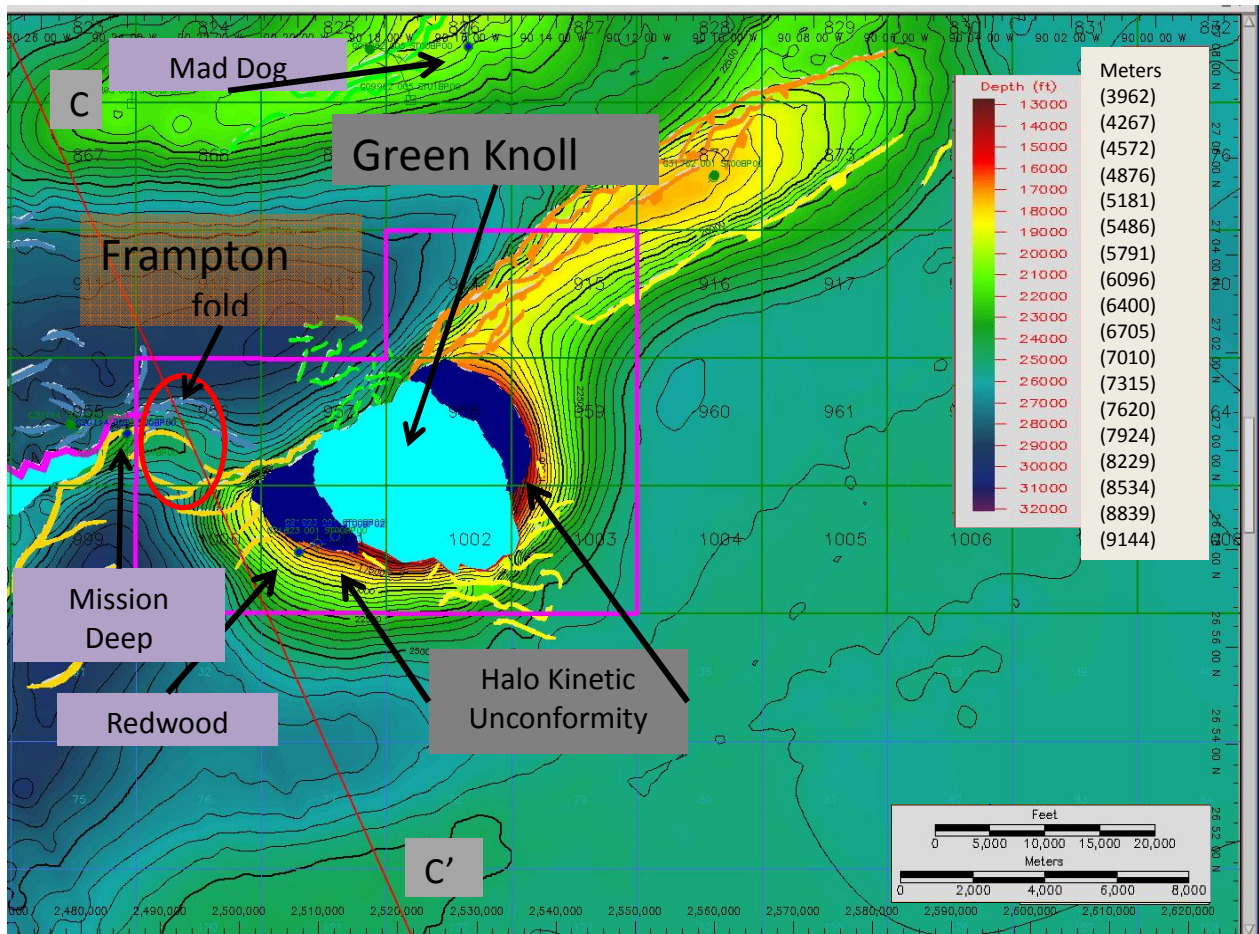


**Figure 10a & 10b.** The seismic line and basemap with the associated traverse that exhibits the halo kinetic angular unconformity. The purple dashed line is the main termination surface and the green dashed line is a secondary termination surface that developed during the growth of the salt dome. The image is annotated with the transect direction and the blocks that the data is covering. Structure Map of the Middle Miocene Depth Survey 196\_002\_dm2 Kirchhoff migrated (Courtesy of WesternGeco).

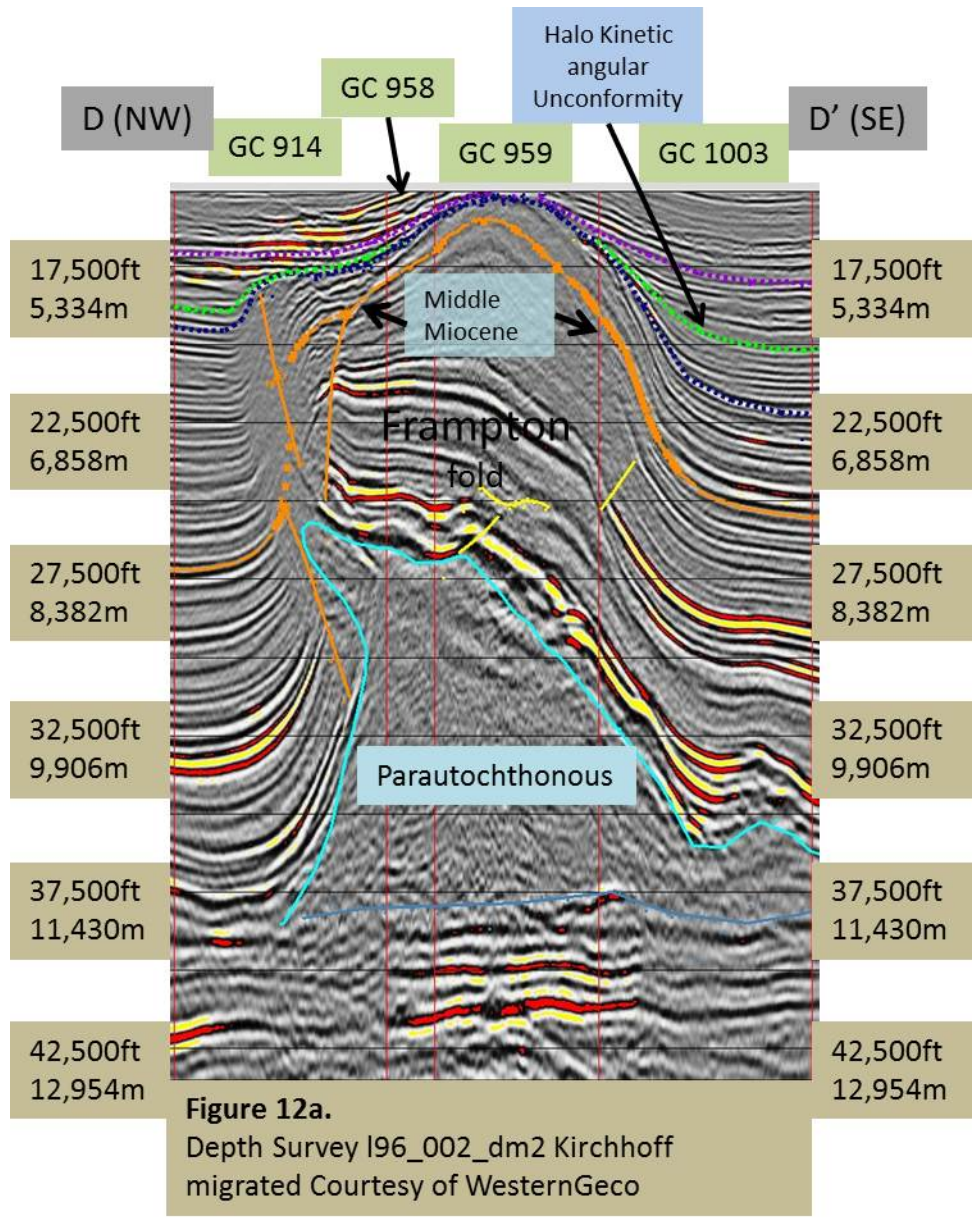




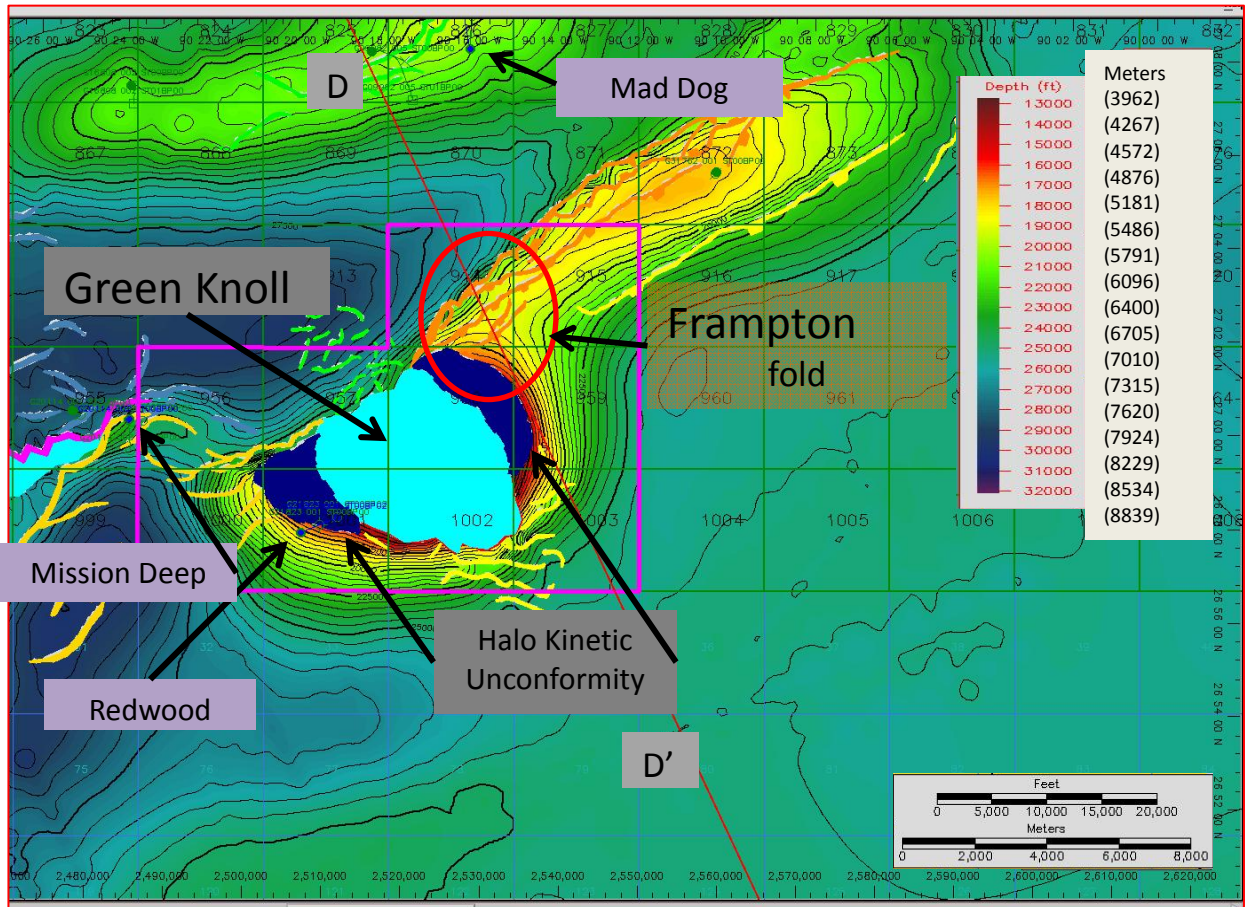
**Figure 11a.**  
 Depth Survey I96\_002\_dm2 Kirchhoff migrated  
 Courtesy of WesternGeco



**Figures 11a. & 11b.** The seismic line and the basemap with the associated traverse of the Frampton fold belt located on the west side of The Green Knoll. Notice the halo kinetic unconformity located at the top of the Frampton fold. The image is annotated with the transect direction and the blocks that the data is covering. Structure Map of the Middle Miocene Depth Survey 196\_002\_dm2 Kirchhoff migrated (Courtesy of WesternGeco).







**Figures 12a. & 12b.** The seismic line and the basemap with the associated traverse of the Frampton fold belt located on the east side of The Green Knoll. Notice the halo kinetic unconformity located at the top of the Frampton fold. The east side of the fold belt is the more prominent section of this geological feature. The image is annotated with the transect direction and the blocks that the data is covering. Structure Map of the Middle Miocene Depth Survey 196\_002\_dm2 Kirchoff migrated (Courtesy of WesternGeco).

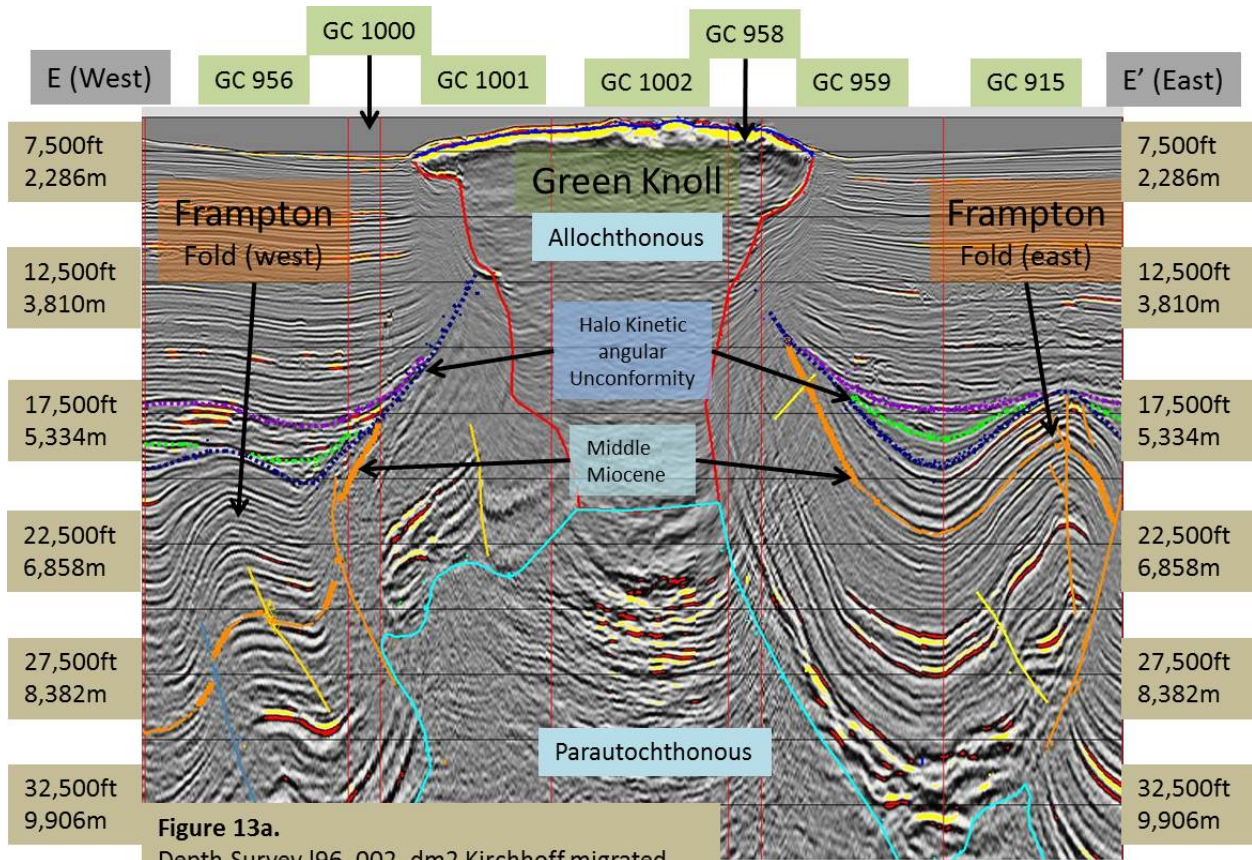


**Figure 13a.**  
 Depth Survey I96\_002\_dm2 Kirchoff migrated  
 Courtesy of WesternGeco



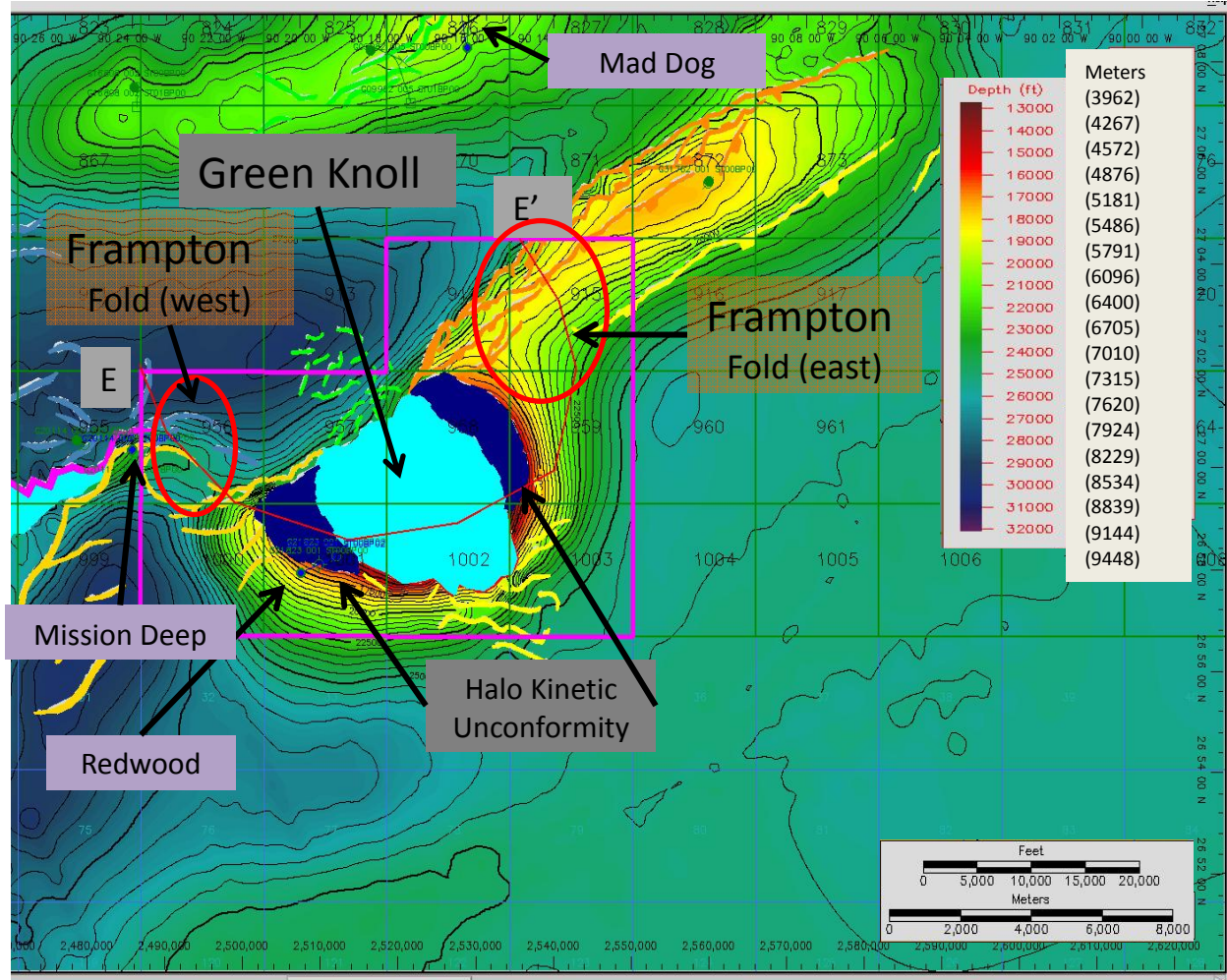


**Figure 13a & 13b.** The seismic line and basemap with the associated traverse for a graphic of The Green Knoll Salt Dome. The seismic line shows The Frampton Fold on both the east and west sides of the salt diapir. This is another example exhibiting the larger and more prominent east side as opposed to the west side of the salt diapir. The image is annotated with the transect direction and the blocks that the data is covering. Structure Map of the Middle Miocene Depth Survey 196\_002\_dm2 Kirchhoff migrated (Courtesy of WesternGeco).



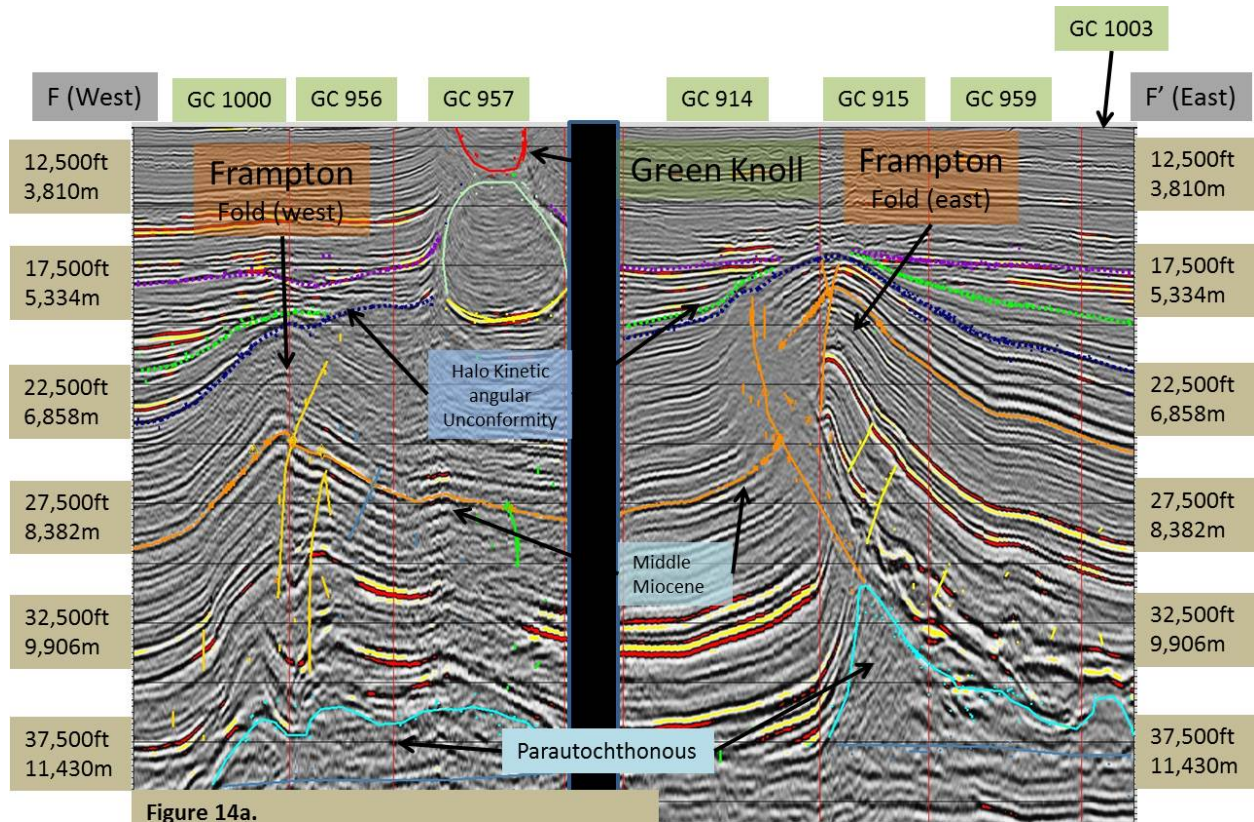


**Figure 14a.**  
 Depth Survey I96\_002\_dm2 Kirchhoff migrated  
 Courtesy of WesternGeco

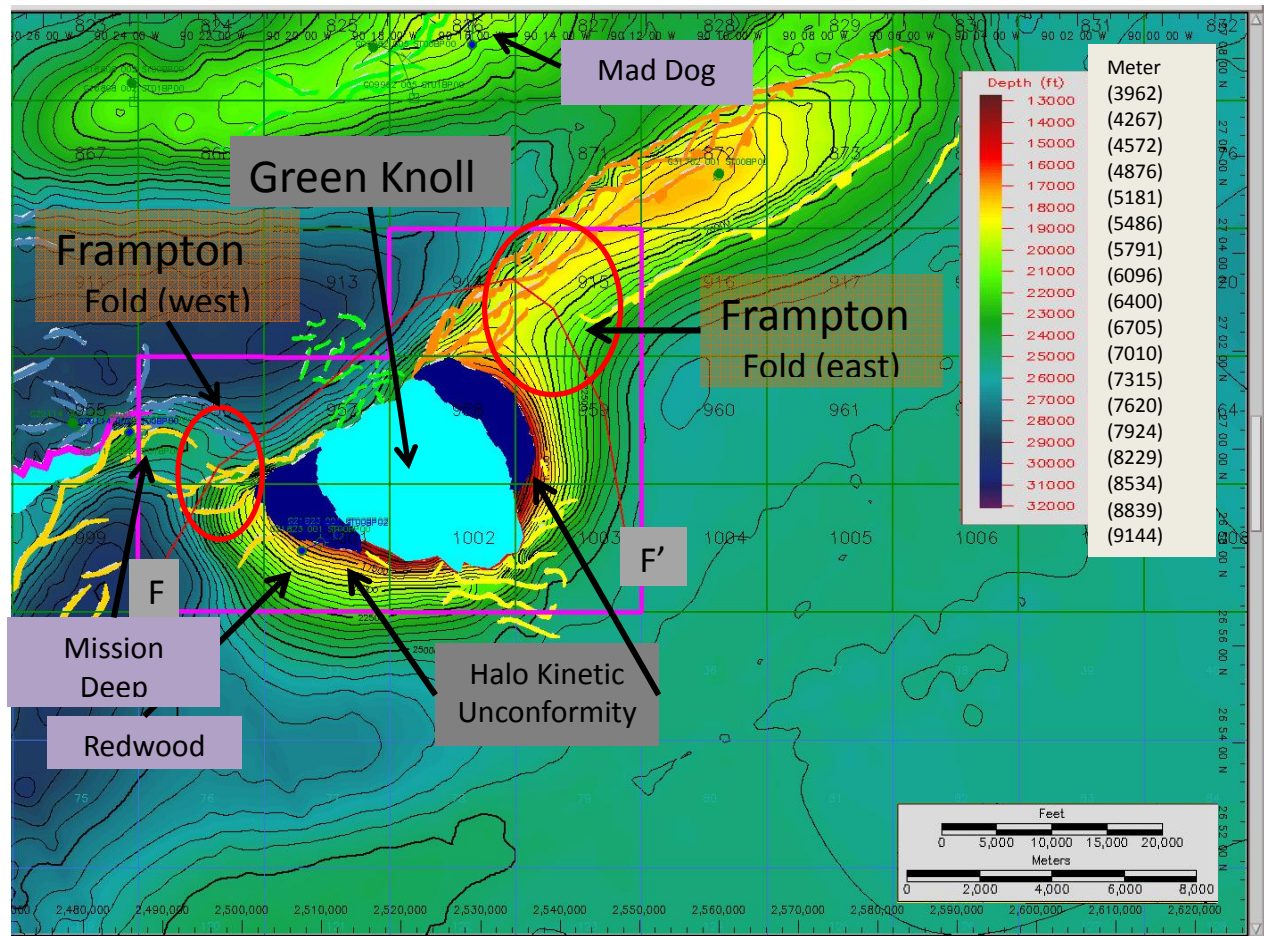


**Figure 14a & 14b.** The seismic line and basemap with the associated traverse for a graphic of The Green Knoll Salt Dome. The seismic line shows The Frampton Fold on both the east and west sides of the salt diapir, the traverse travels from west to east through the north side of the diapir. This is another example exhibiting the larger and more prominent east side as opposed to the west side of the salt diapir. The image is annotated with the transect direction and the blocks that the data is covering. Structure Map of the Middle Miocene Depth Survey I96\_002\_dm2 Kirchhoff migrated (Courtesy of WesternGeco).



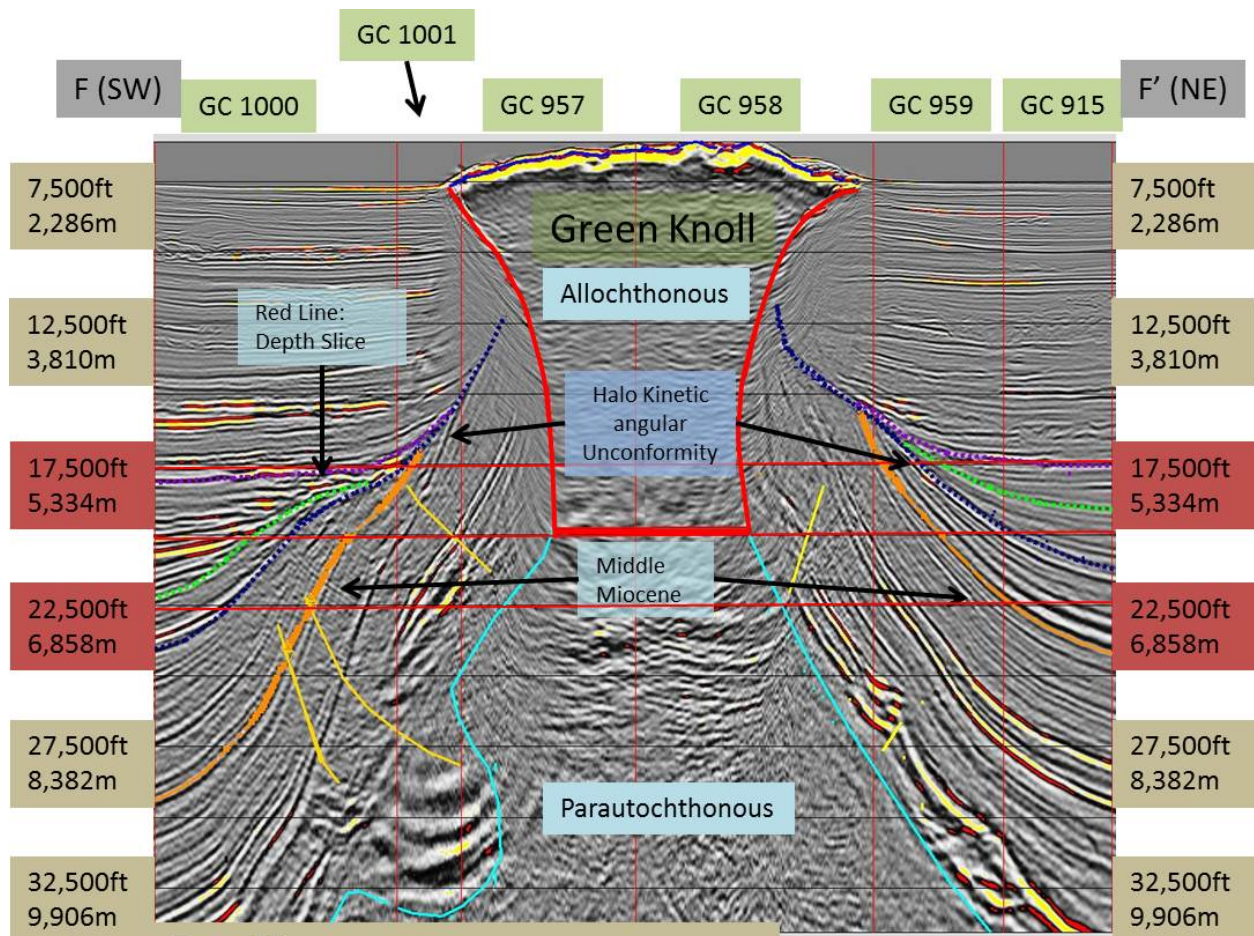


**Figure 15a.**  
 Depth Survey I96\_002\_dm2 Kirchhoff migrated  
 Courtesy of WesternGeco

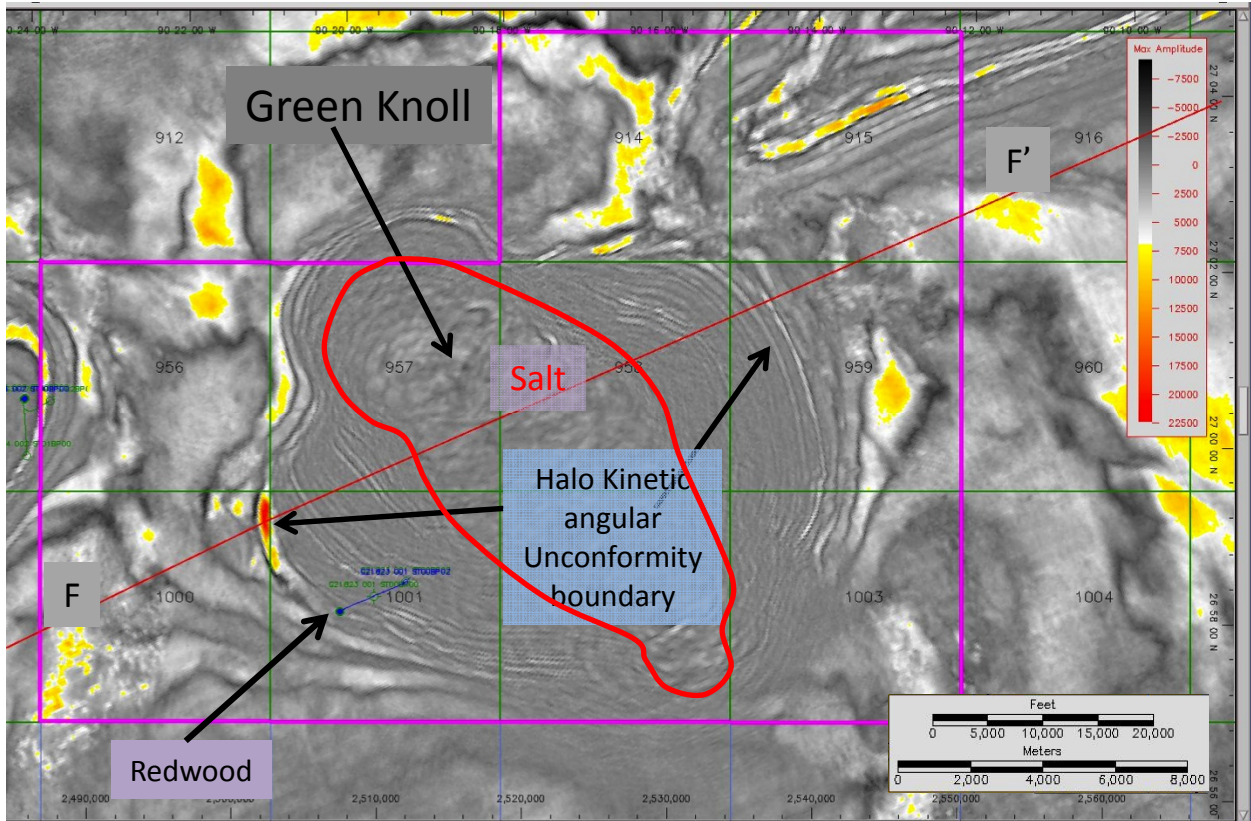


**Figure 15b.**  
 Depth Survey I96\_002\_dm2 Kirchhoff  
 17,500 ft max-amp extraction  
 migrated Courtesy of WesternGeco



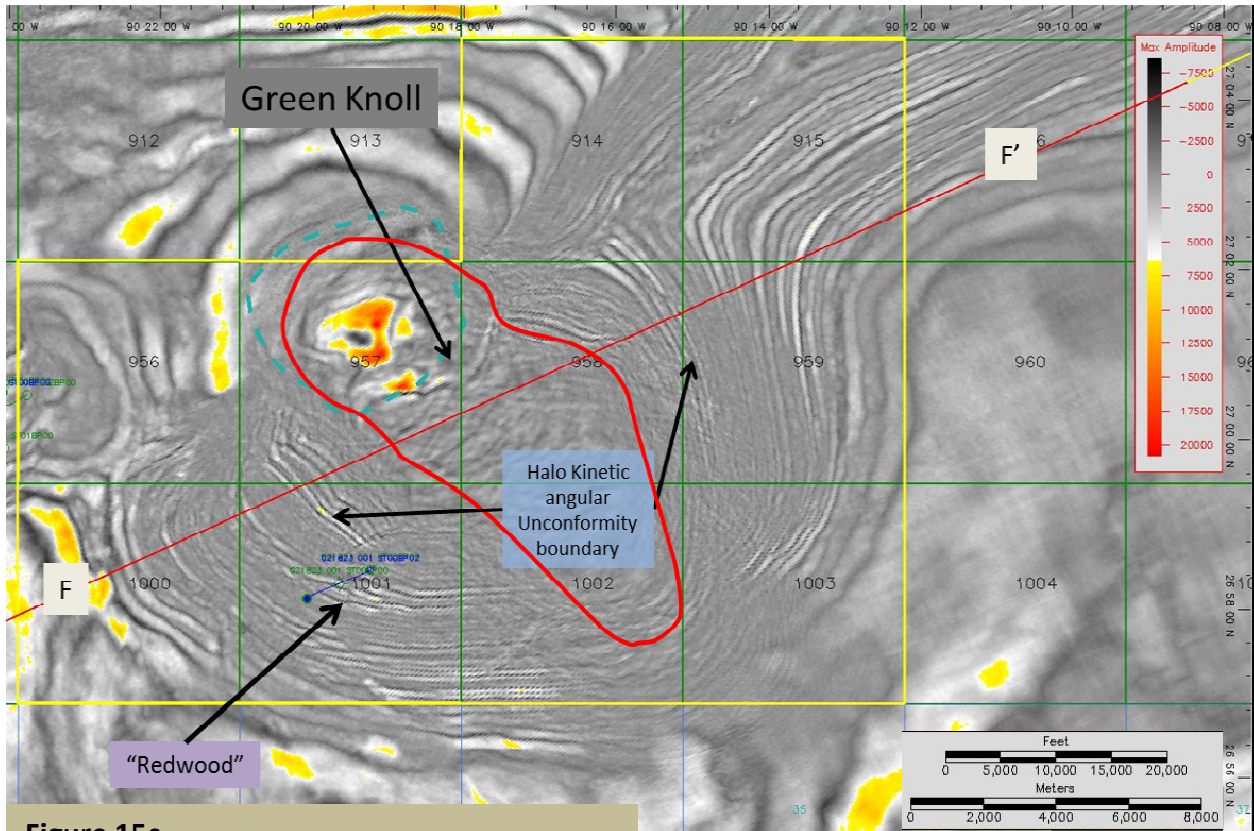


**Figure 15c.**  
 Depth Survey I96\_002\_dm2 Kirchhoff  
 20,000 ft max-amp extraction  
 migrated Courtesy of WesternGeco

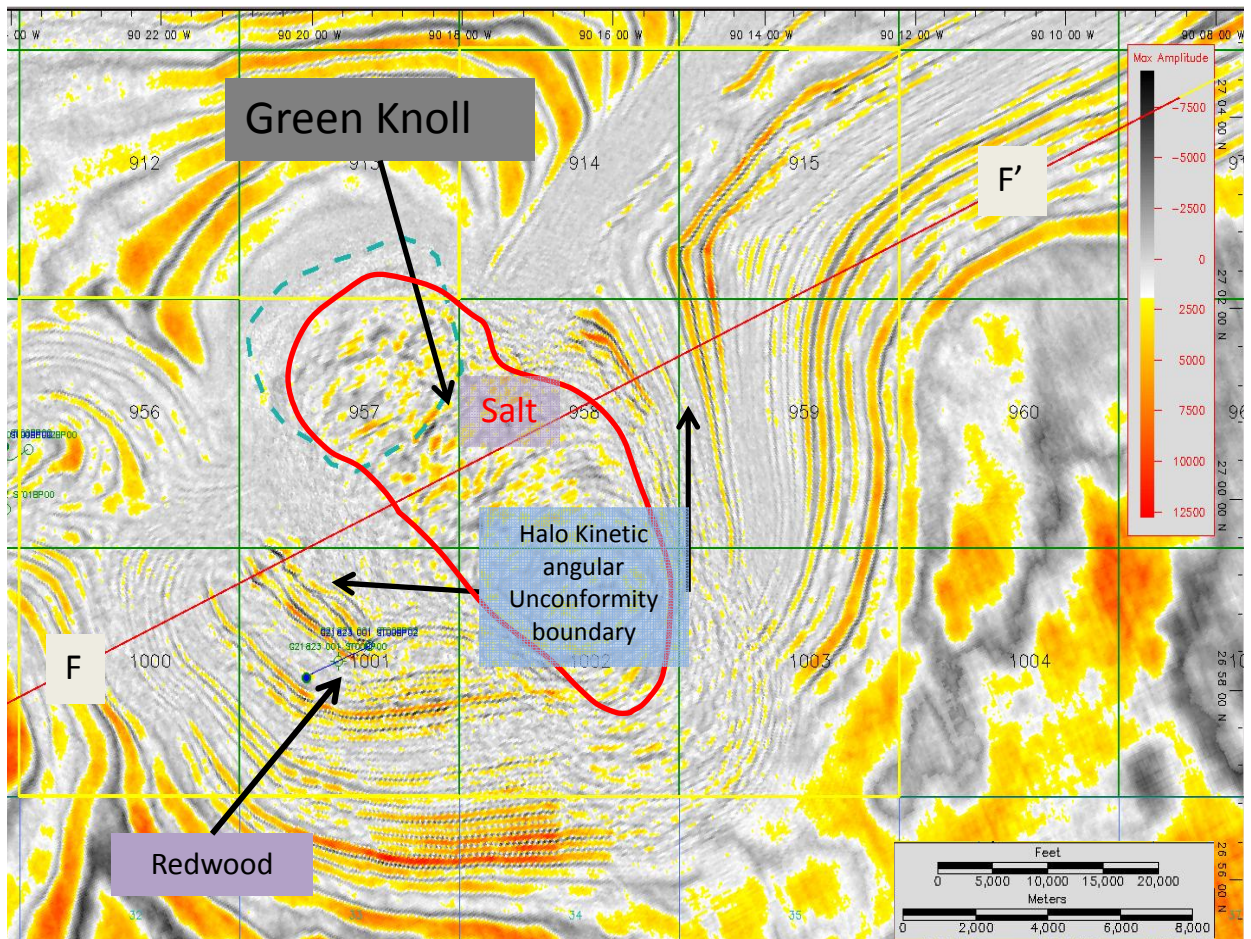


**Figure 15a & 15b, 15c, 15d.** Maximum amplitude map of the 22,500ft depth survey 196\_002\_dm2 Kirchhoff migrated courtesy of WesternGeco. The seismic line and associated basemap with the traverse travelling through The Green Knoll Salt Dome from the southwest to the northeast. The 3 depths associated with the 3 max-amp maps are annotated in red in Fig 11a. The display on the base map for Fig 11b is a depth slice of the max amplitude at 17,500ft. The display on the basemap for Fig 11c is a depth slice of the max amplitude at 20,000ft. The display on the basemap for Fig 11d is a depth slice of the max amplitude at 22,500ft. The red line is the boundary between the sediment and the salt. The image is annotated with the transect direction and the blocks that the data is covering.

## **Structural Restoration**

A 2-dimensional palinspastic structural restoration was attempted on the Green Knoll Salt Dome. A seismic line perpendicular to the salt diapir was extracted and imported into Midland Valley's MOVE program. The salt dome was mapped with an undefined fault polygon because the Move modules need faults to interact with the sediments during the modeling process, and the choices of fault styles are limited. The timing and growth intervals of the salt diapir are crucial to further analyses of the flanks of the Green Knoll for hydrocarbon exploration. As mentioned previously in the literature review section of this work, Grando et al. (2004) performed a palinspastic structural restoration on the Frampton fold belt. The restoration on the Green Knoll was an attempt to test the hypothesis that the timing of the growth periods is linked between Frampton Fold Belt and the Green Knoll Salt Dome.

## **Methods**

The two algorithms used for the palinspastic structural restoration were the decompaction module and the unfolding module. The decompaction module algorithm uses the lithology percentages, porosity and the porosity-depth coefficient of each aged section (Table 3 - 4). The unfolding module algorithm is purely geometric and does not use any parameters from the rock properties data table.

The modeling process began with establishing the stratigraphy and lithological components to the certain aged sediments. These values were obtained from seismic interpretations and well log interpretations. The seismic interpretations were performed in the earlier portion of this work (Figures 9a – 15a), and the two well logs used were Redwood (Green Canyon 1001) and Mission Deep (Green Canyon 955) (Figure 4). Refer to Figures 9b – 15b for spatial reference of where the wells are located. Table 3 shows the generalized stratigraphy of the beds and the thicknesses of the intervals. The lithological values are generalized and are applicable to similar geological compressional settings like the Green Knoll area, refer to Table 4. A seismic line was imported into Midland Valley's Move software using the correct georeferencing procedures. The x and y coordinates of the seismic volume were extracted from the top left and bottom right of the 2D seismic line using IESX mapping software. The seismic



line lies in the northern UTM zone 15 and the x and y coordinates are as follows: top left x2489177.351, y9883474.754 and the bottom left x2549083.390, y9752136.360. The interpreted section is about 10,000 ft (3125 m) wide and about 35,000 ft (10,937.5 m) in height.

Sequentially restoring each horizon is the best method for performing a complete in-depth structural analysis. The method used for the restoration involved a series of decompactions coupled with unfolding techniques. The 2D decompact tool in the Move module was used for the decompactions throughout the restoration. The decompaction curve that was used is known as the Sclater-Christie curve. The Sclater-Christie decompaction model is used to derive long term compaction rates and is used in many basin models (Sclater and Christie 1980). The compaction curves of shale and sand that Sclater and Christie calculated in their work, North Sea Continental Stretching, were compared to other basins like the Gulf of Mexico, Oklahoma and Venezuela basins (Sclater and Christie 1980). The porosities and the porosity-depth coefficients are calculated by determining the surface porosities and their respective depth coefficients for sandstone, shale and limestone located at the top of the rock property database (Table 4). The lithology percentages are plugged in for each aged section and the corresponding porosity and depth coefficients are calculated for each interval (Table 4). The surface porosity and depth coefficient values were used from the generalized porosity-depth graphs from the Sclater and Christie (1980) work. The mud logs used to calculate the lithology percentages for the rock properties data table are the Redwood (GC 1001) and Mission Deep (GC 955) (Figure 4).

The porosity depth coefficients are calculated using the following equation (Sclater and Christie, 1980).

$$f = f^{\circ}(e^{-cy})$$

where:

$f$  = the present day porosity at depth

$f^{\circ}$  = the porosity at the surface

$c$  = the porosity-depth coefficient ( $km^{-1}$ )

$y$  = depth (m)

Polygons are used to calculate the decompaction. The horizon being decompacted is collected into the top bed area, the rest of the horizons and polygons are collected into the active/intermediate area except for the base, which is collected into the base area.

The parameters used are that of the databases discussed in the earlier paragraph Table 3 and 4. Airy isostasy is the isostatic relief parameter used and it is an isostatic response to vertical accommodation with water load variations figured into it, as opposed to flexural isostasy which attributes strength laterally to the lithosphere. Sub-marine load was selected since this model takes place in a marine setting and the load bulk density has been averaged for the Gulf of Mexico and it is 2200 kg/m<sup>3</sup> (Jackson et al. 2010). The default mantle density of 3300 kg/m<sup>3</sup> is used as well (Jackson et al. 2010).

	1:Horizon	2:Colour	3:Rock Type	4:Age	5:Thickness	6:Active
1	Top		PL	0.0000	100.0	
2	Upper Pleistocene		PL	0.2000	1100.0	
3	Middle Pleistocene		PL	0.7800	800.0	
4	Lower Pleistocene		PL	1.7700	700.0	
5	Pliocene		PL	5.3200	500.0	
6	Mio-Pliocene		PL	7.0000	500.0	
7	Upper Miocene		PL	10.5000	1000.0	
8	Miocene		PL	15.5000	1100.0	
9	Lower Miocene		PL	21.5000	400.0	
10	Oligocene		PL	30.0000	250.0	
11	Eocene		PL	36.0000	700.0	
12	Cretaceous-Paleocene		PL	58.5000	1100.0	
13	Mid Cretaceous		PL	94.0000	900.0	
16	Base		PL	150.0000	100.0	

**Table 3.** Stratigraphy table. The Age is in millions of years, and the Thickness is in meters.

The 2D unfolding tool in the Move module was used for the unfolding techniques throughout the restoration. The restoration style algorithms assume a certain deformation style, and in this case the flexural slip style is used because it is associated with compressional features as opposed to simple shear, which is associated with extension.

The datum is unfolded to a specified depth which is the top of the shallowest portion of the horizon. Polygons to unfold seismic is toggled on. Objects to be unfolded contain template beds. These template beds are the beds being unfolded after decompaction including the passive objects which consist of the rest of the beds. A pin was inserted through the center of strata on both sides of the salt dome. The template and other beds are unfolded along a slip system parallel to the template beds and perpendicular to the pine line.

Rock Type	Sandstone(%)	Shale(%)	Limestone(%)	Porosity	Depth Coefficient
Sandstone	100			0.5	0.27
Shale		100		0.4	0.52
Limestone			100	0.3	0.4
Units	%	%	%	fraction	1/km
Default				0.2	0.39
ShalySand				0.2	0.39
Salt				0	0
Top				0.01	0.01
SeaBed				0.2	0
PL	40	50	10	0.43	0.408
5.5 M-P	40	40	20	0.42	0.42
10.5 MU	50	40	10	0.44	0.375
15.5 MM	60	35	5	0.45	0.364
21.5 ML	70	30	0	0.47	0.345
30 OL	30	60	10	0.42	0.433
TE	60	35	5	0.45	0.364
TP	50	50	0	0.45	0.395
Cret	30	30	40	0.39	0.397
Base	0	0	0	0.01	0.01

**Table 4.** Rock properties table.

The section around the pin remains fixed and the slip system established for the passive objects slips the rest of the section away from the pin. The unfolding technique was used separately for both sides of the salt diapir.

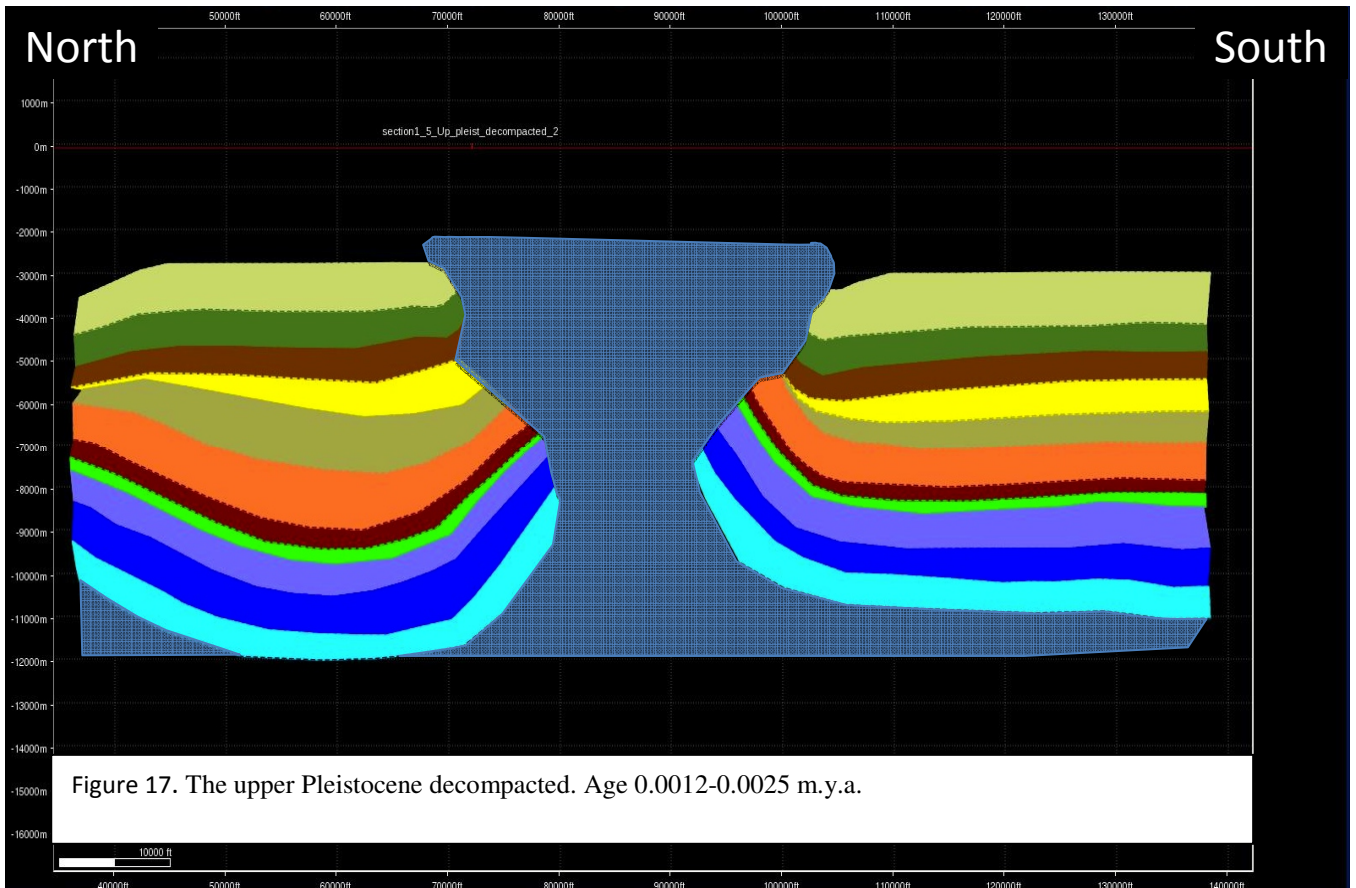
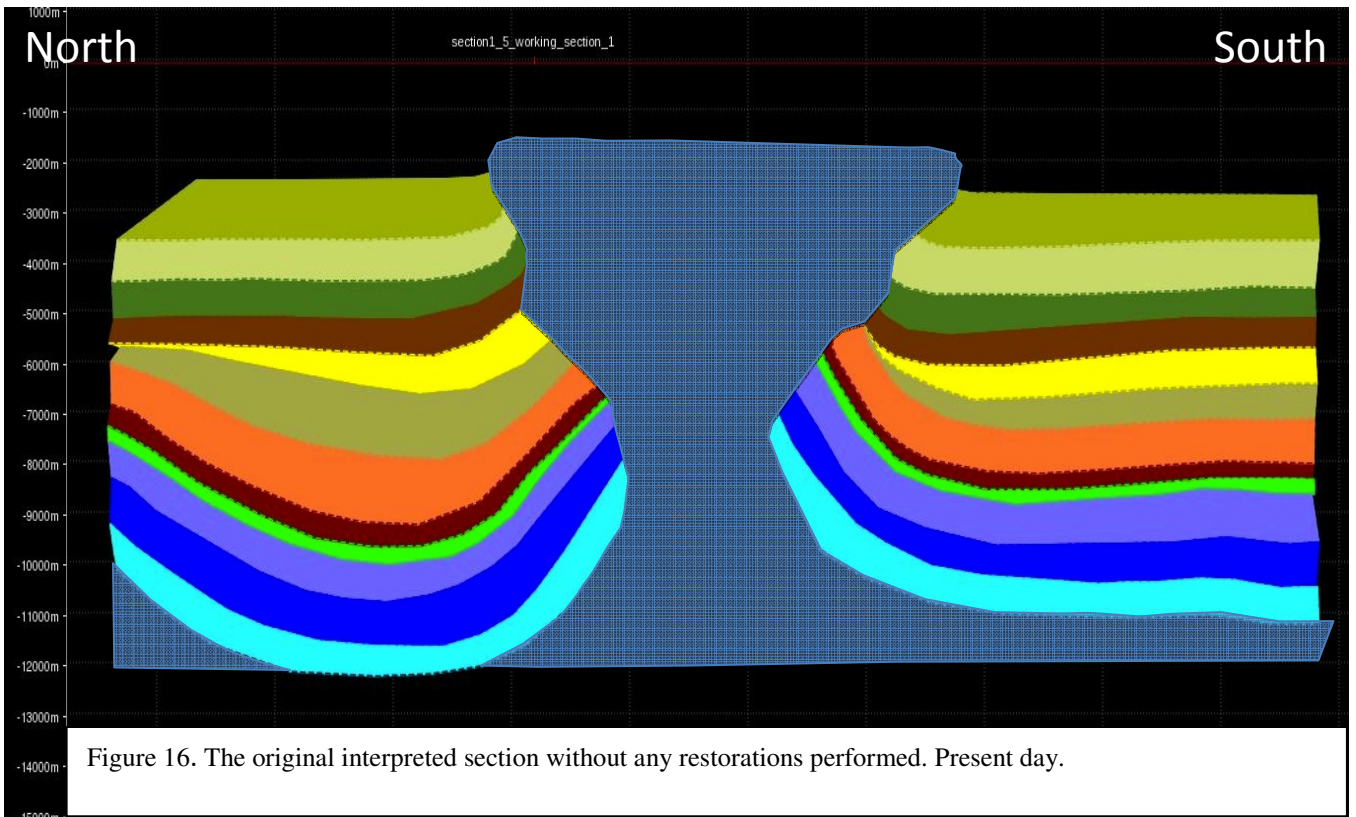
## Interpretation

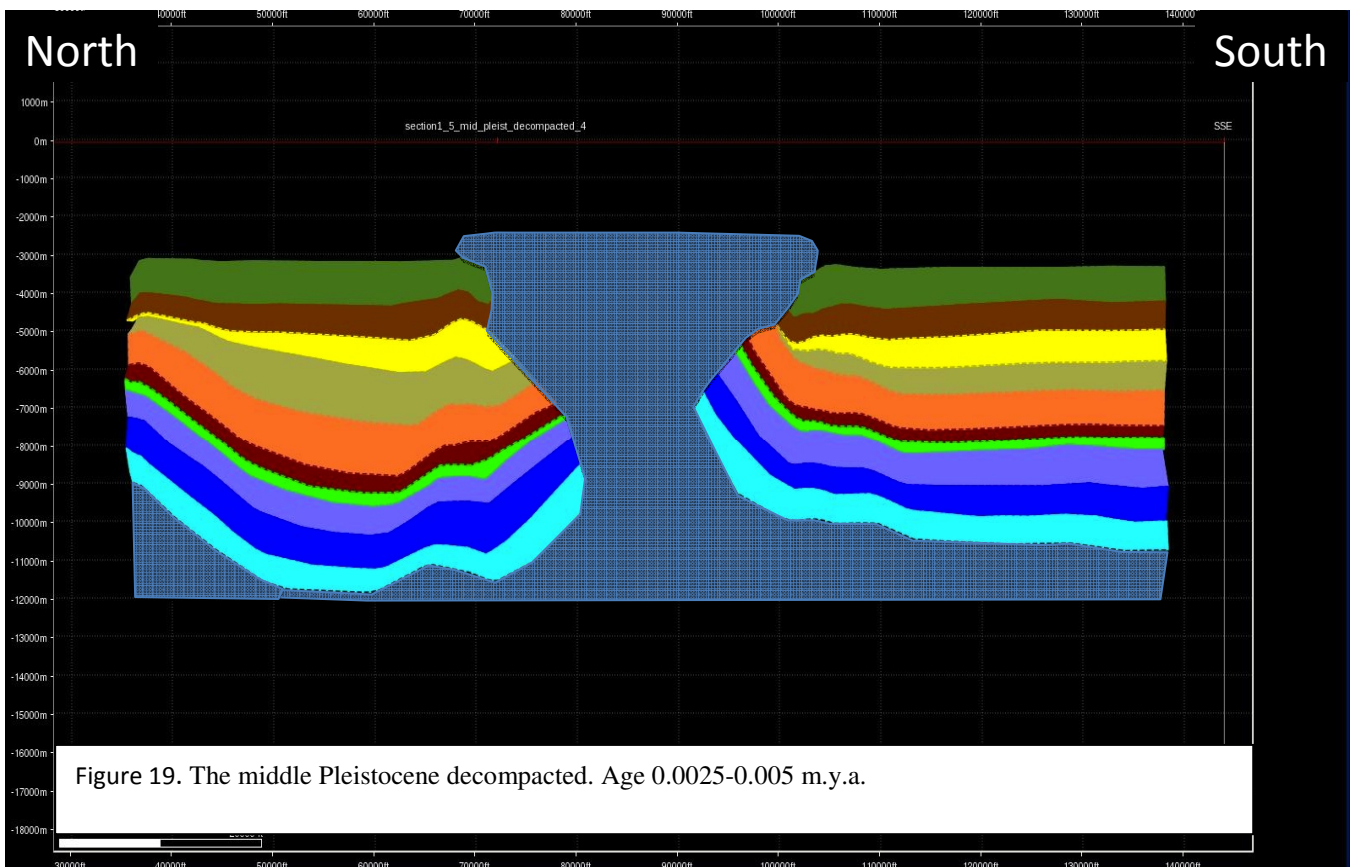
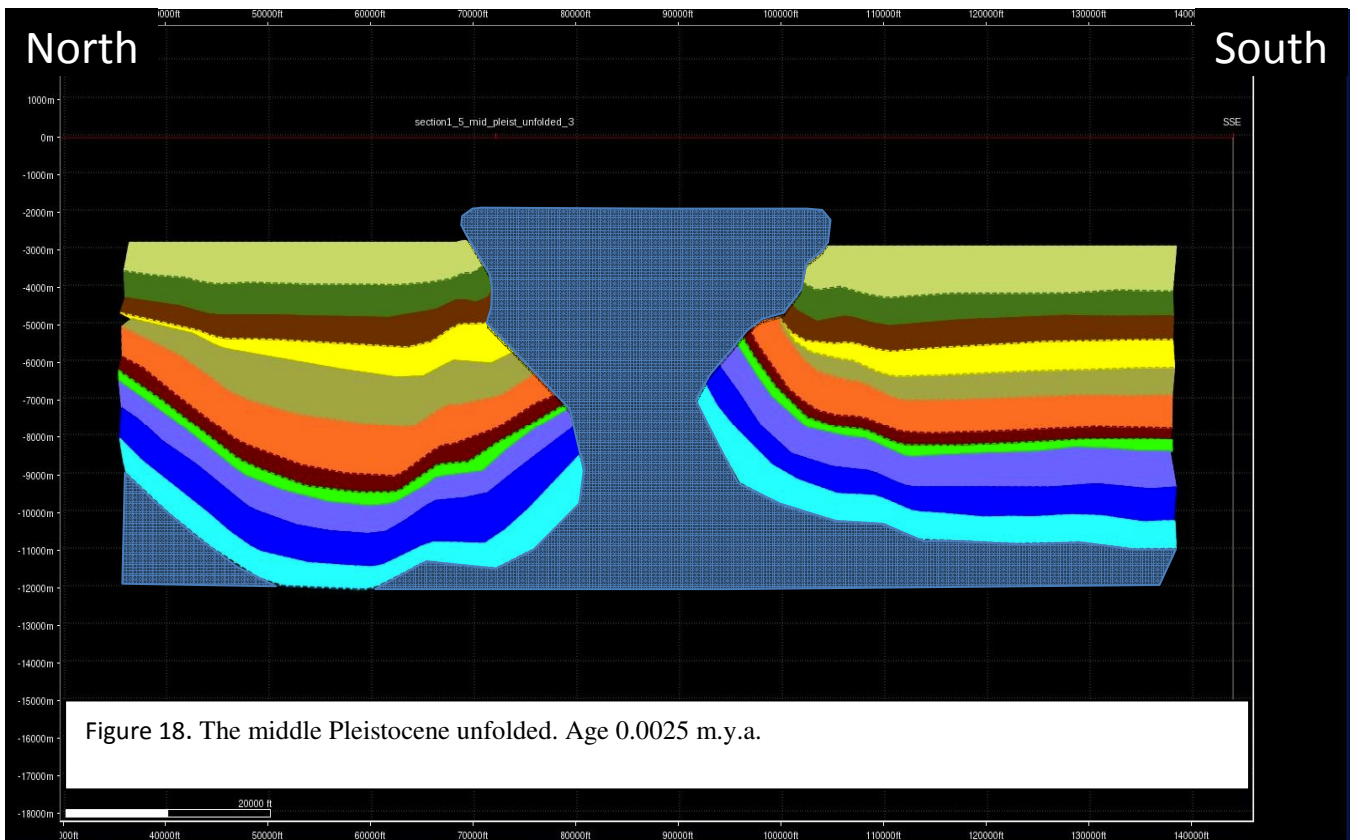
Jackson and Vendeville (1994) state that salt is weaker than other lithologies under both compression and tension. Salt is viscous in nature which means it forms a constant strength. It forms a weak layer between normal sedimentary layers whose strength increases with depth. (Vendeville and Jackson 1992) Rowan (2000) came to the conclusion that salt serves as an excellent detachment surface into which faults can form. Since salt has a constant density regardless of depth, salt is denser than its surrounding strata at the surface, but less dense than other lithologies once it is buried beneath 1000-1500 m of sediment (Jackson and Talbot, 1986). As the density of salt is constant with depth; salt will not compact nor decompact at depths greater than 1500 m. This is why a salt layer horizon was not included in this restoration. Using an undefined fault for the salt provided a “body” for which the sediment could interact with and vice versa. The original undefined salt body started to develop extremely odd shapes throughout the restoration since the out of plane movement of the salt could not be captured. The salt seen in Figures 16-37 was annotated in to show the reader a more true representation of what the salt may have looked like throughout the restoration process.

Salt is very difficult to model, especially with a 2D restoration. For simplicity the implications on the out of plane movement that the salt undergoes will be explained geologically. As the parautochthonous salt migrated basin ward sediment loading created a welded syncline to form on the landward (northern) side of the diapir, while on the basin ward side the toe of the salt pinches out below Cretaceous beds. The emplacement of salt controlled the differing geometries of the strata packages surrounding it. Since the salt diapir and the fold belt are connected by the same parautochthonous salt body, the geometries of strata on the north and south side of the diapir represented what the strata was doing in the fold belt as they were forming. Panning through the restoration images one will see the correlation between the two. The nature of the landward-vergent reverse fault in the Frampton fold belt starts to appear around the Pliocene deposode.

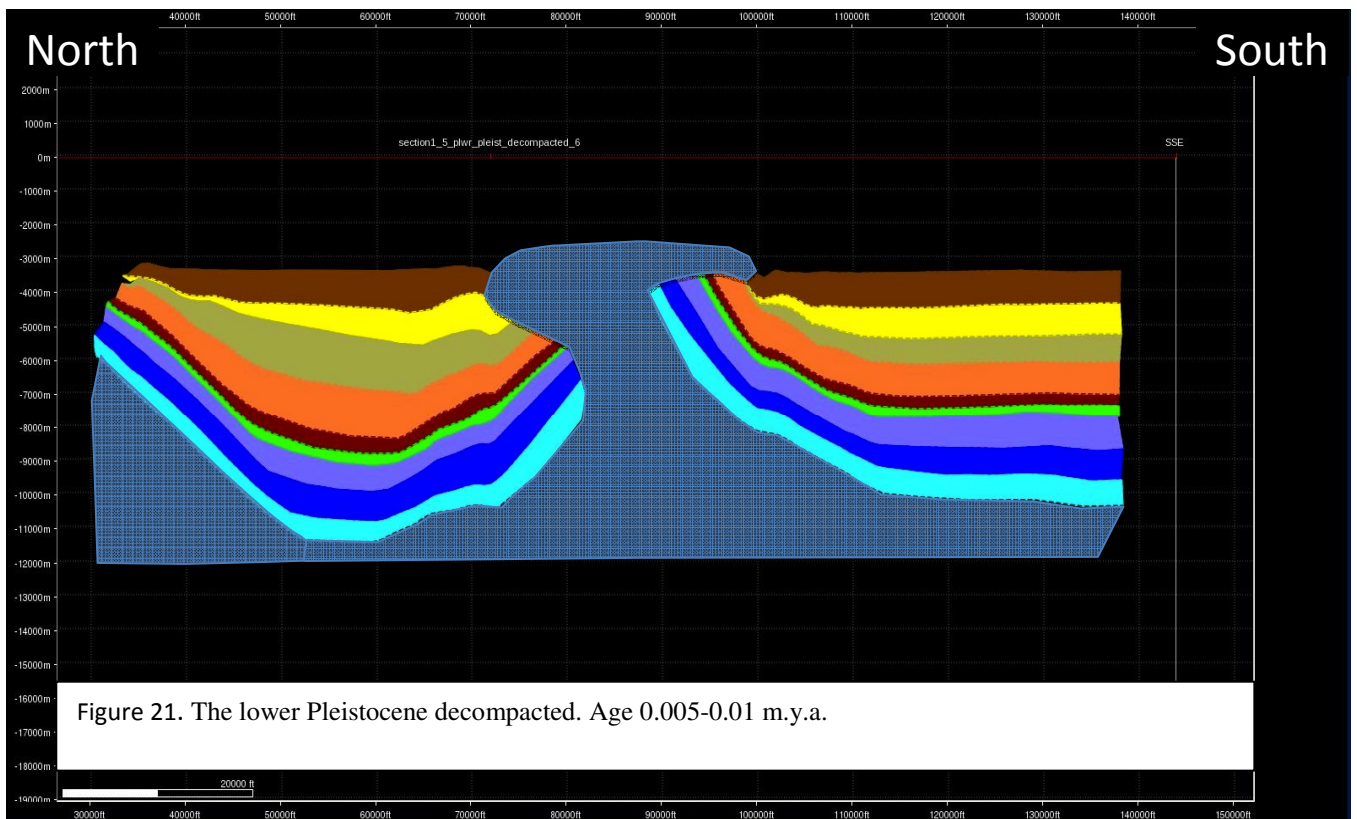
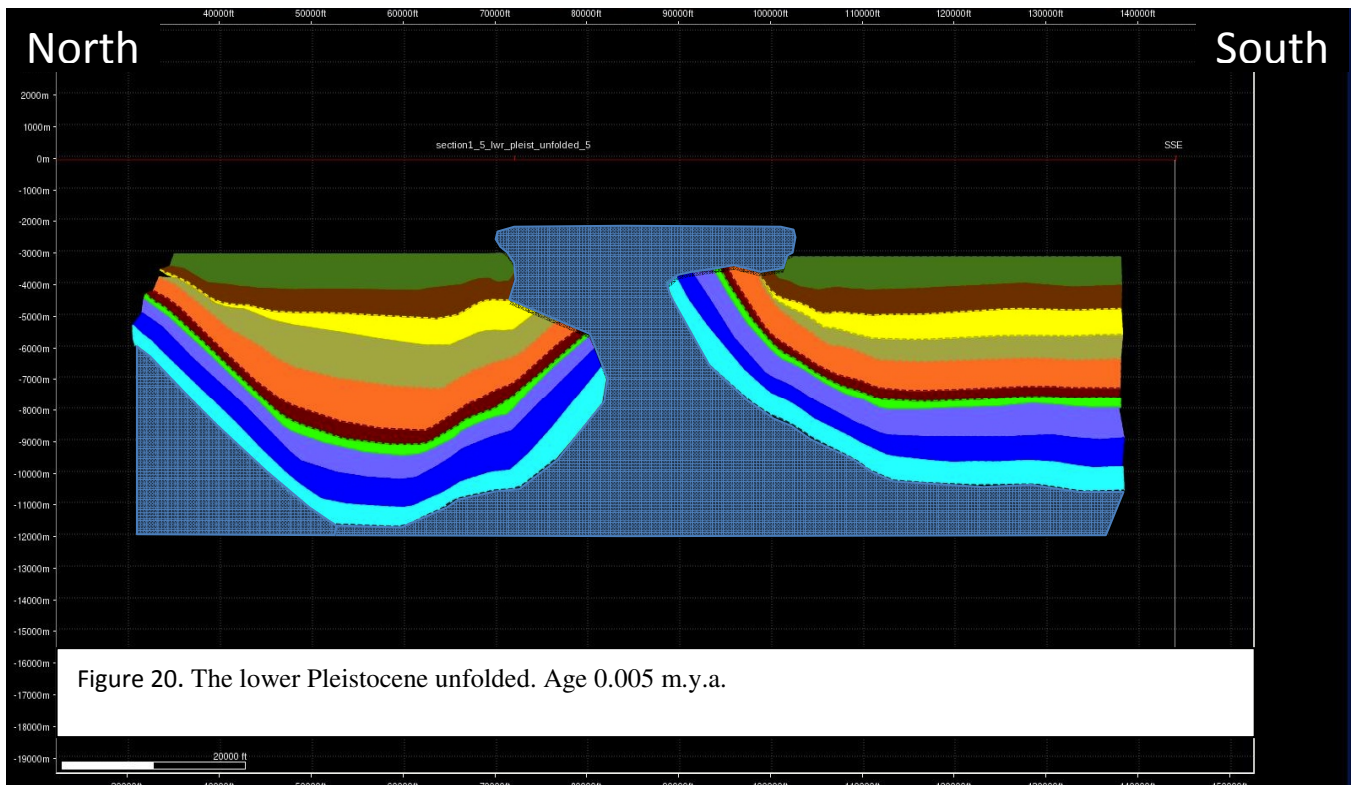
As sediment is deposited the parautochthonous salt is squeezed and begins to migrate upwards, which created shortening on both sides. The beds become steepened as synclinal structures form, which creates a salt weld at the base on the north side (Figure 18).

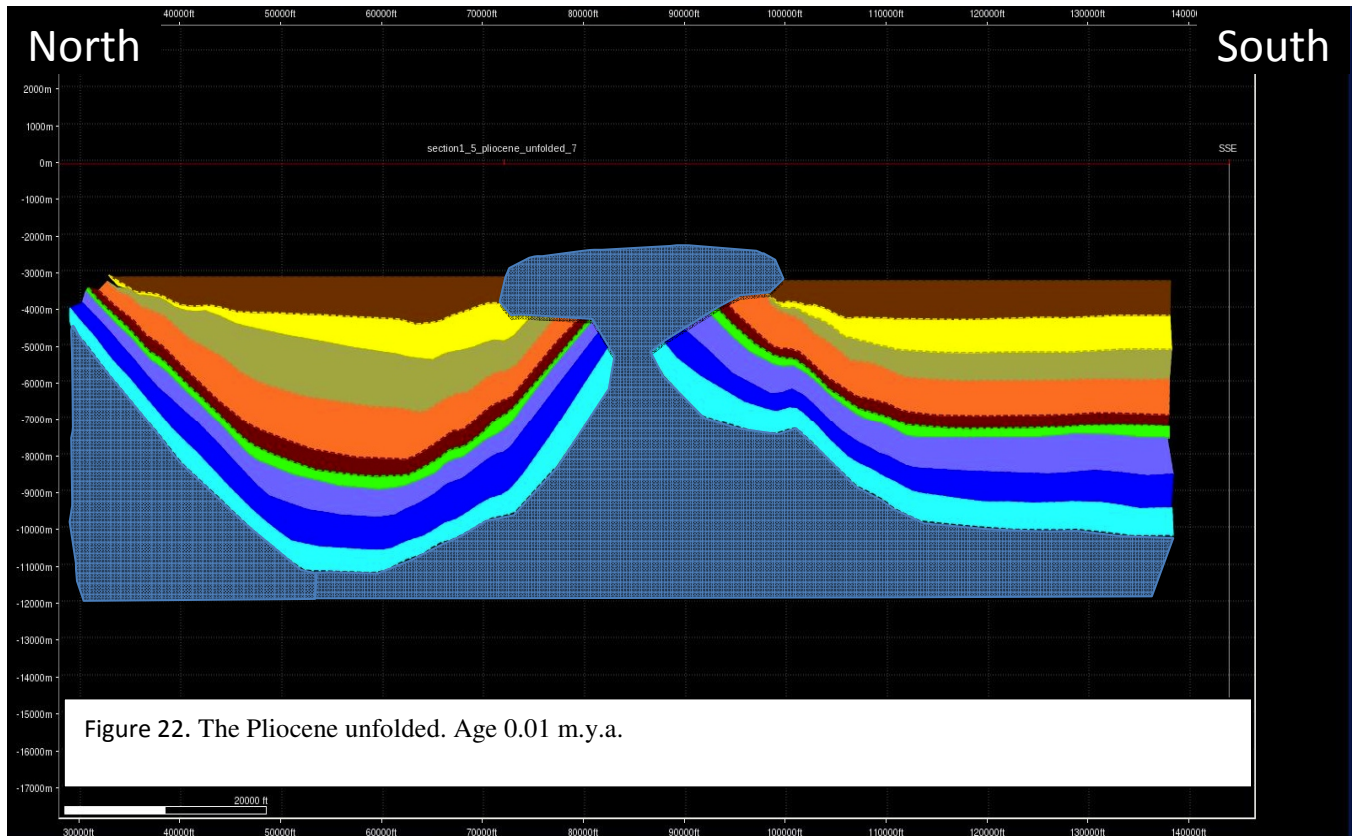
The explanation for salt being added to the structure as opposed to being subtracted during the restoration process can be simplified by keeping the volume of salt consistent during the Cretaceous the same as the present. So it is not a question of whether salt was added or subtracted to the model, but rather how did the salt migrate and influence the structure as sediment was deposited. It would be too difficult to measure the volume of salt being added and lost as this feature formed. From Figure 25 to Figure 24 the Miocene-Pliocene package is deposited and the salt can be seen billowing out more rapidly and in a larger amount. The halokinetic unconformity on the northern side has a different geometry than the unconformity on the south side; hence they are not symmetrical when looking at the section. The north side is being controlled by an allochthonous salt tongue that billowed out during the Miocene Pliocene deposide at depth creating a pinch out distally from the salt diapir. The unconformity on the south side did not have any salt billowing out laterally as growth occurred, so the unconformity causes the Miocene Pliocene interval to pinch in toward the salt diapir, which represents what most of the surrounding flanks look like (Figures 18 – 25). A major growth period of the salt occurs as it billows upward in large amounts, which is after the deposition of the lower and middle Pleistocene (Figure 19 – 18). Another major structural change happens after the Pliocene is deposited (Figure 22 – 21). This is where the restoration reveals the basinward dipping reverse fault that dominates the Frampton anticline presently. According to the restoration the salt broke through the weakest portion of the sediment after the deposition of the lower Miocene (Figures 30 – 29). The significance of the timing exhibited in the restoration confirms the hypothesis that the Frampton Fold Belt and the Green Knoll Salt Dome share the same structural timing. The migration of the salt into the domal structure it is in present day has implications on hydrocarbon migration. Since the restoration is simplistic the faulting that occurs throughout the flanks of the salt dome as a result of the structure forming provided the pathway for hydrocarbons to migrate from Jurassic and Cretaceous source rocks into potential traps. These traps could exist in a couple of different ways: as a 3-way trap against the stock of the salt dome, and/or as a stratigraphic trap within in the Miocene Pliocene unconformity downdip from where the Redwood (GC 1001) well was drilled.

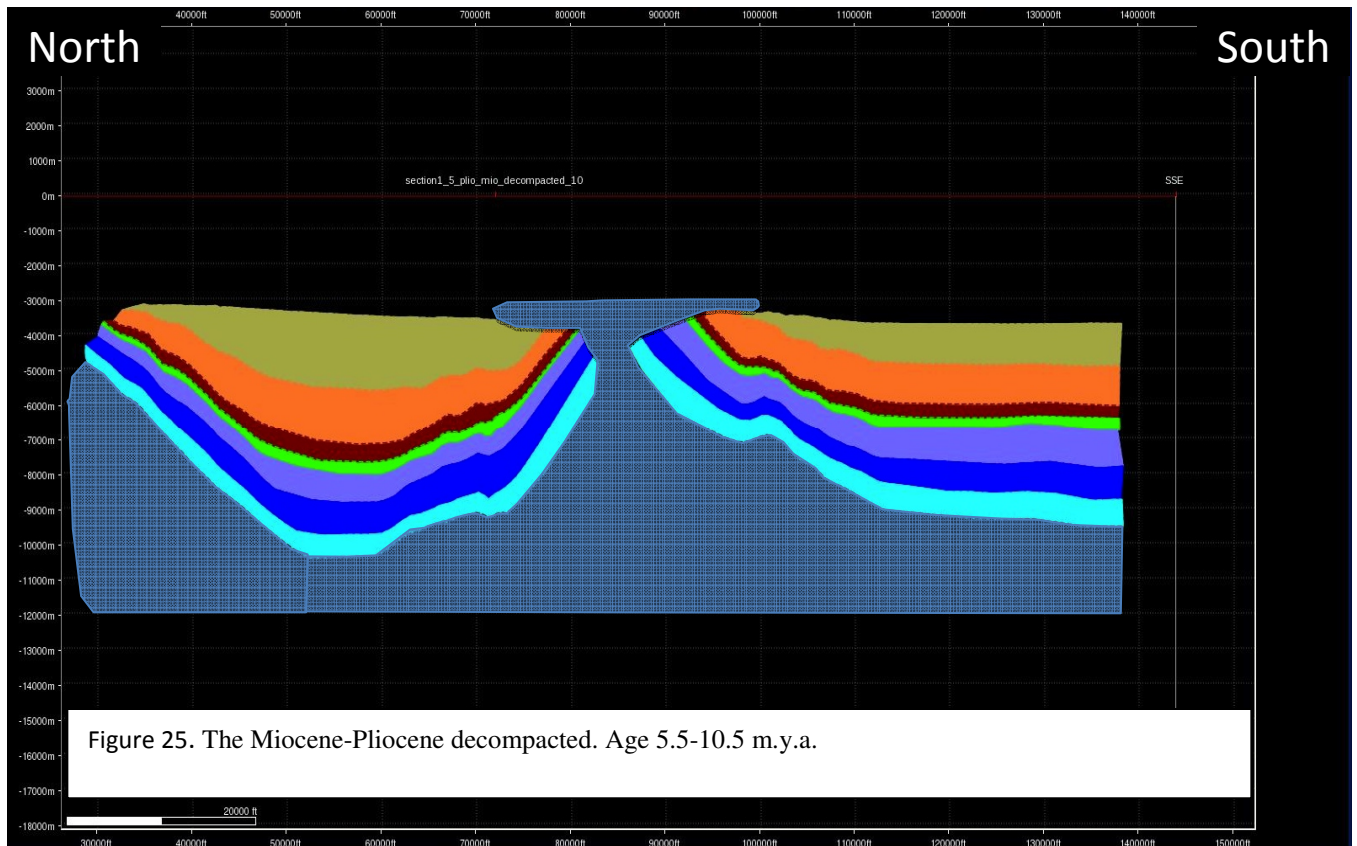
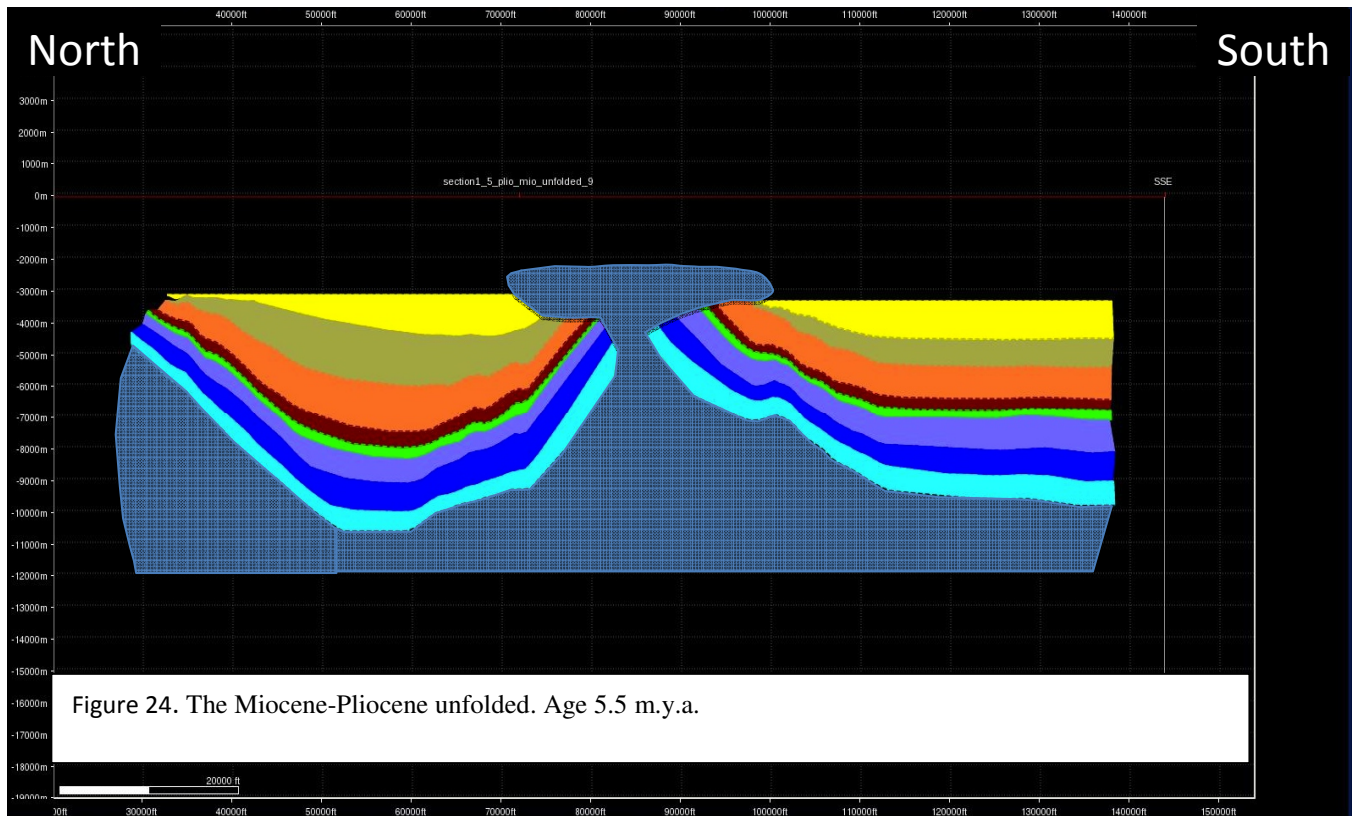




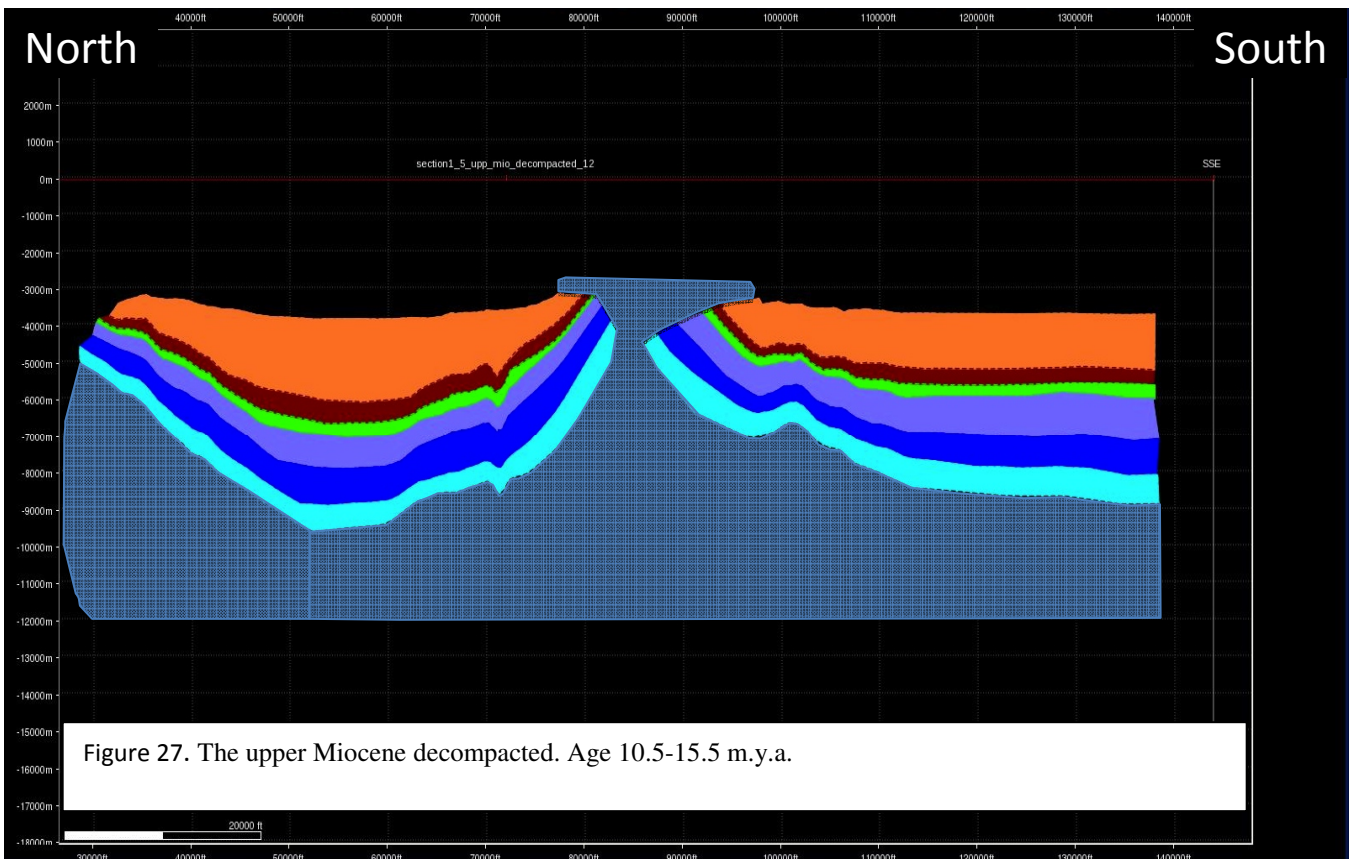


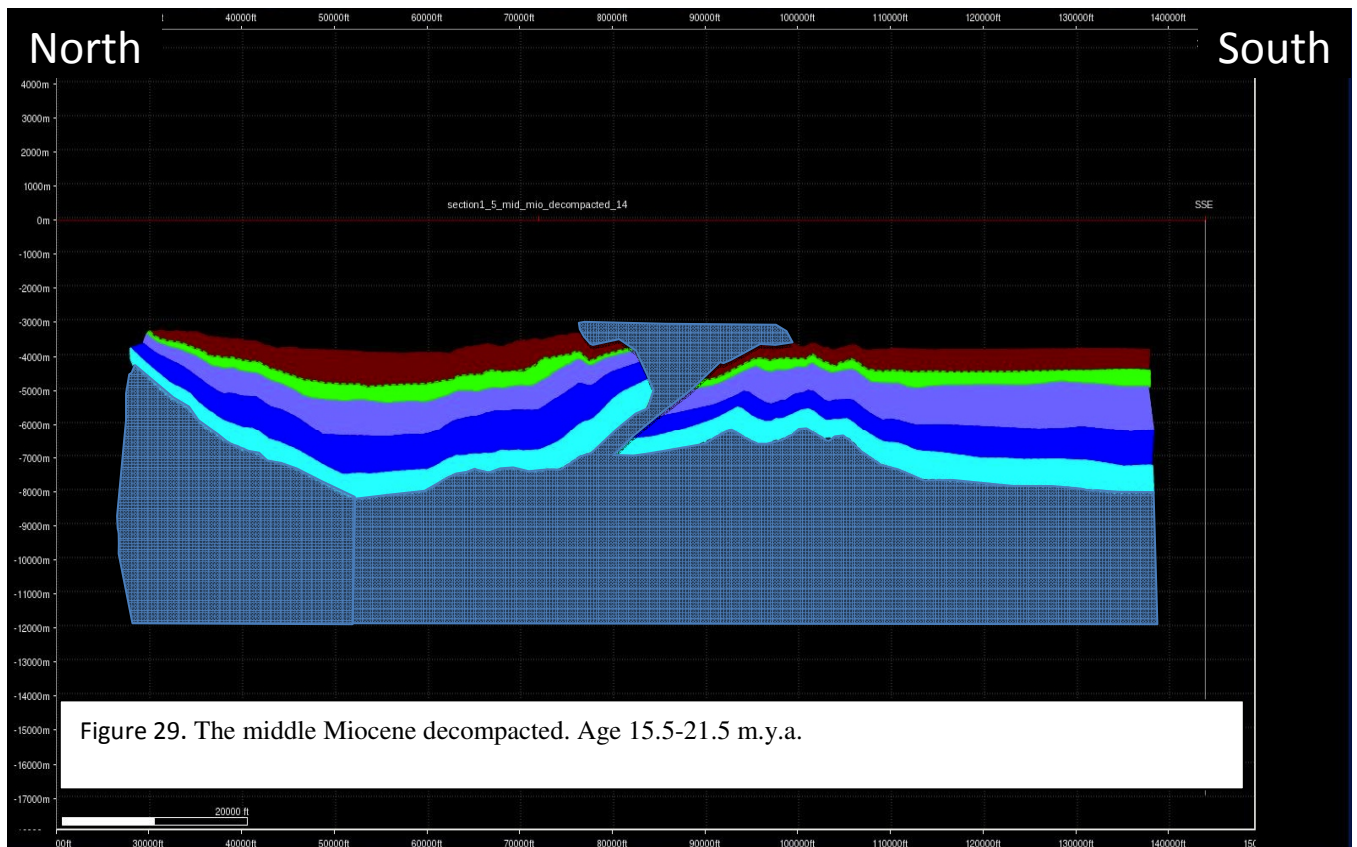
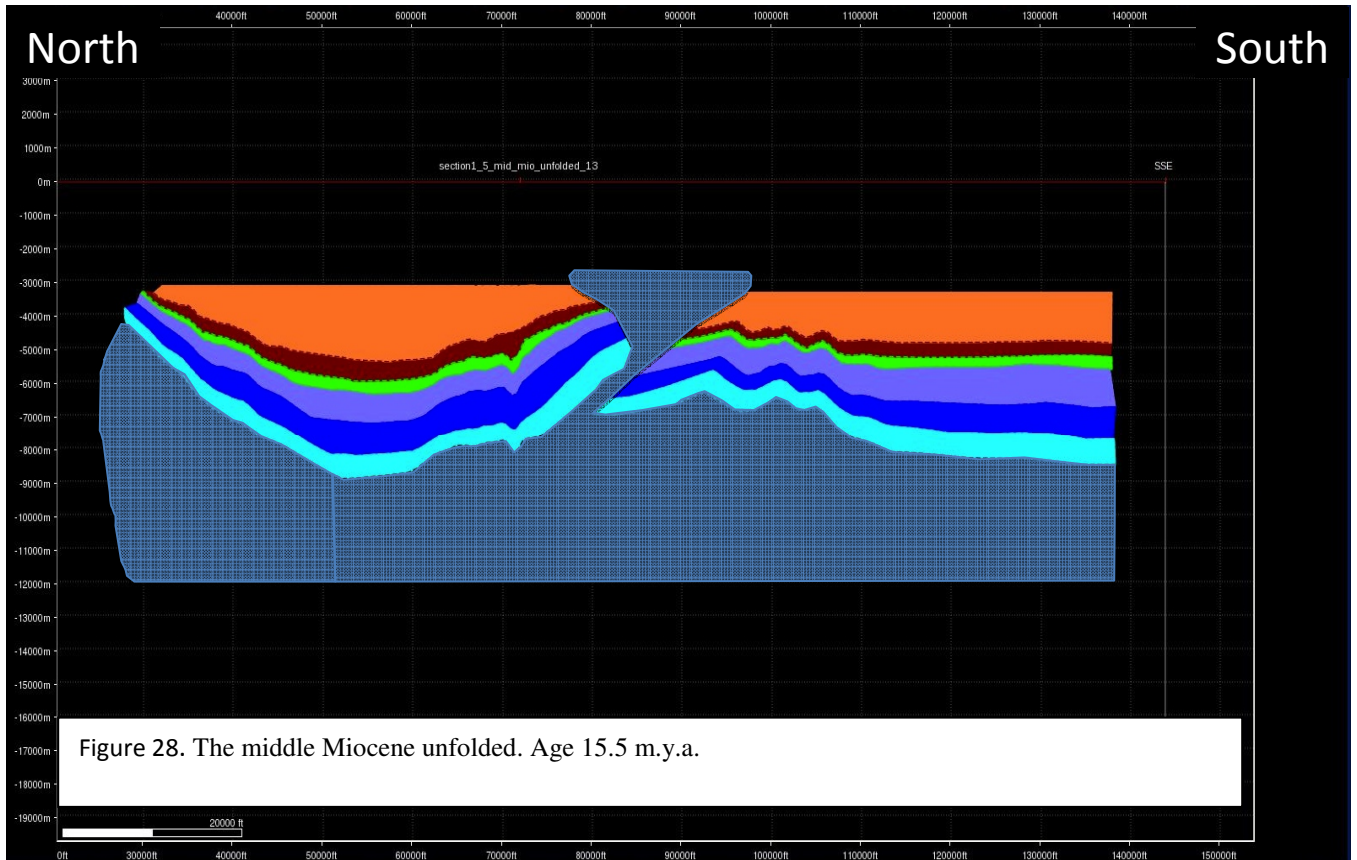


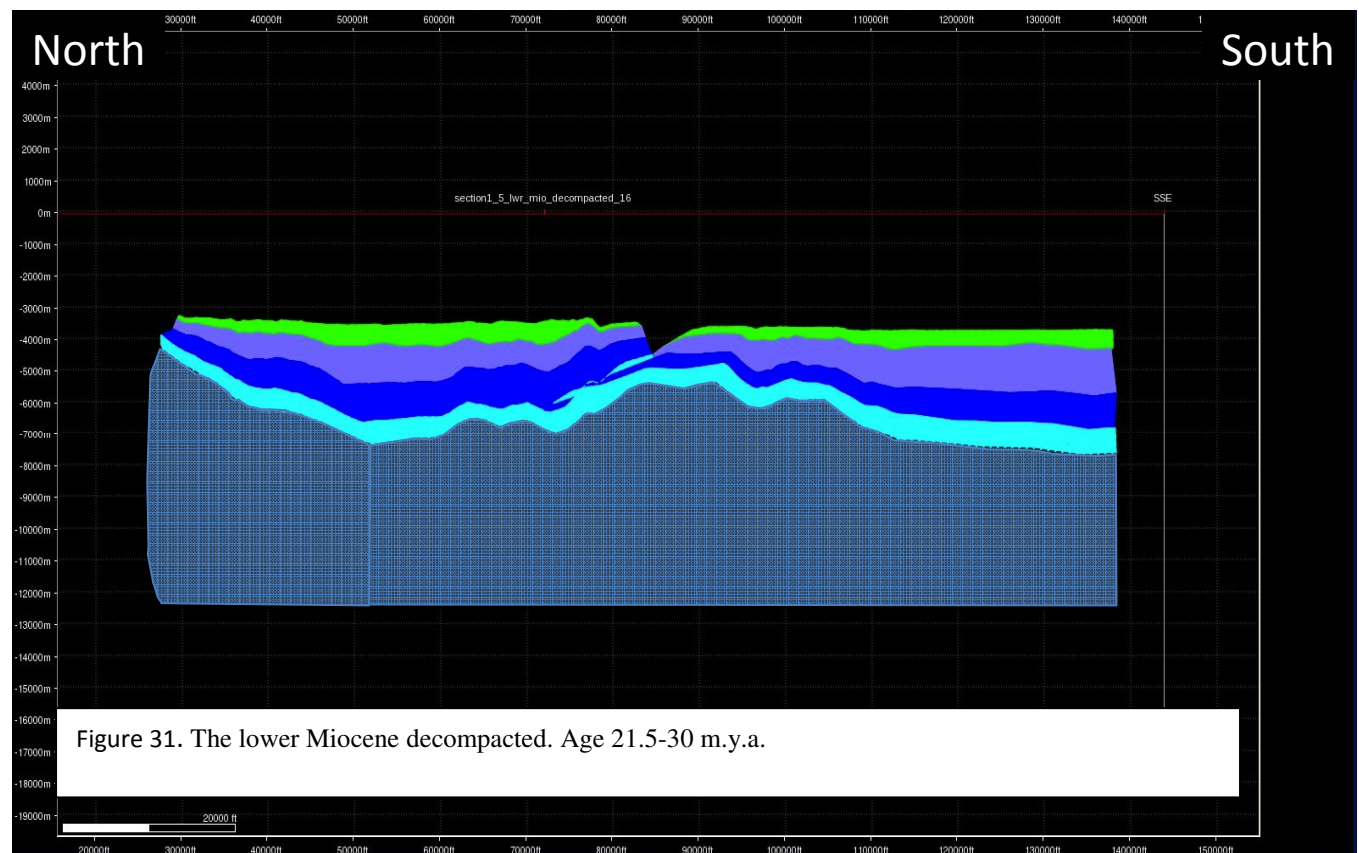
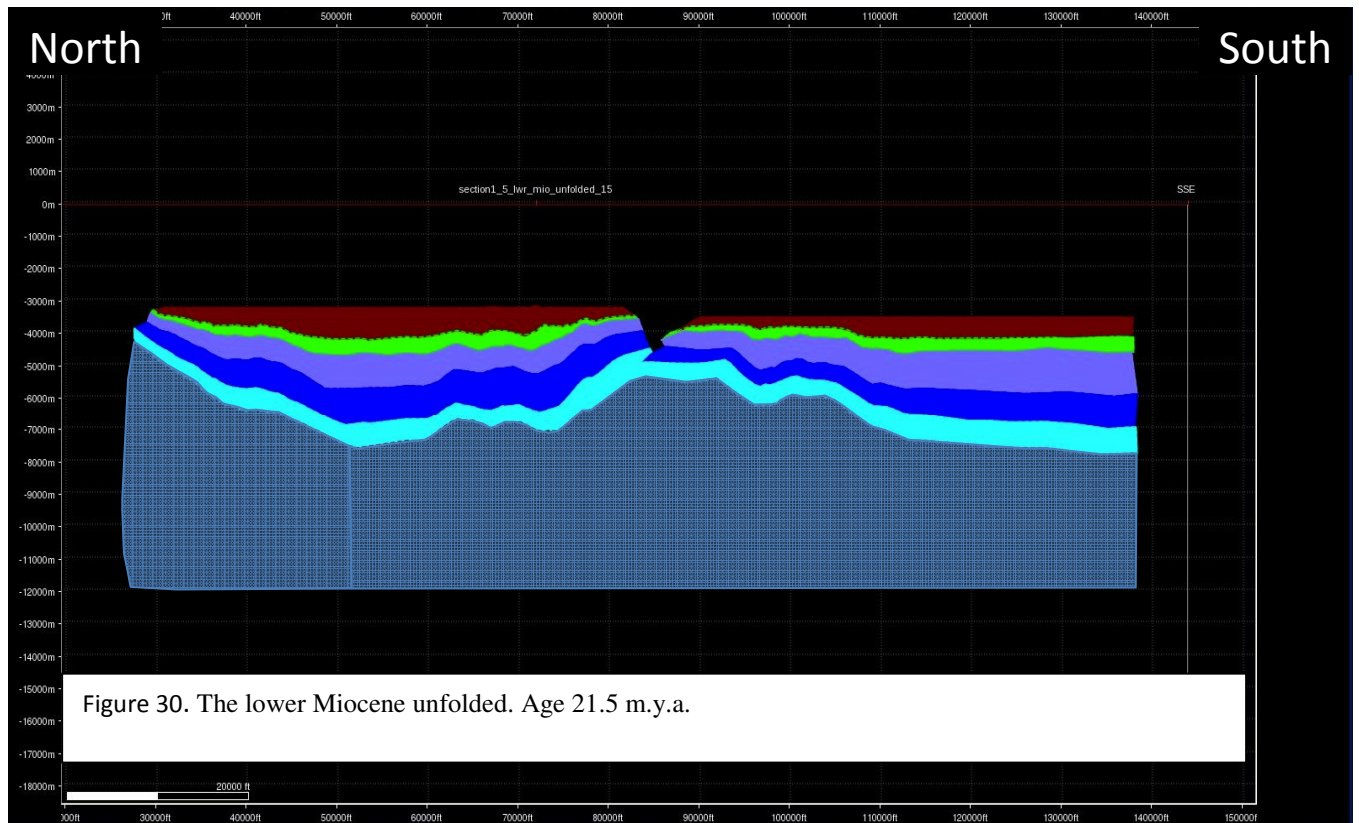




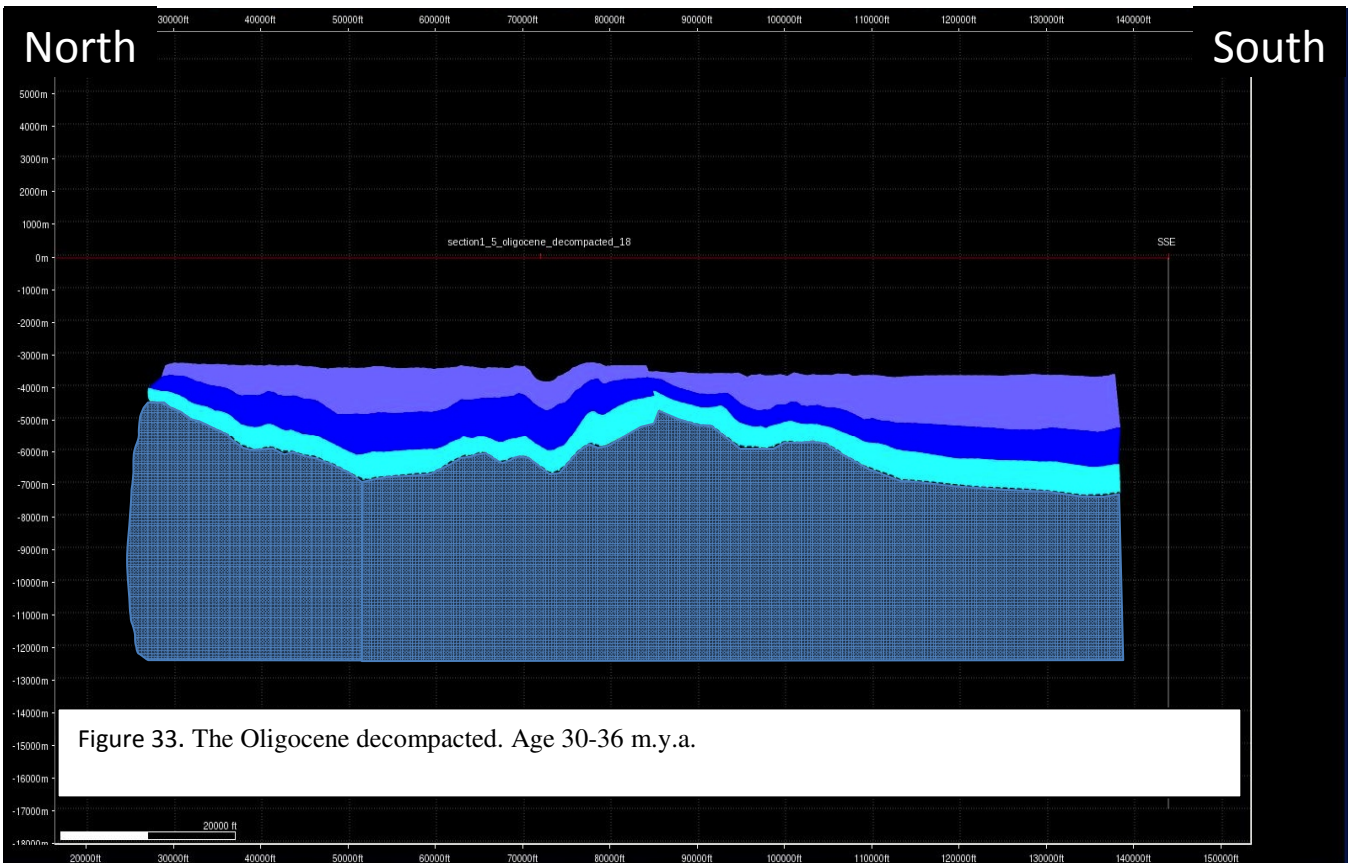
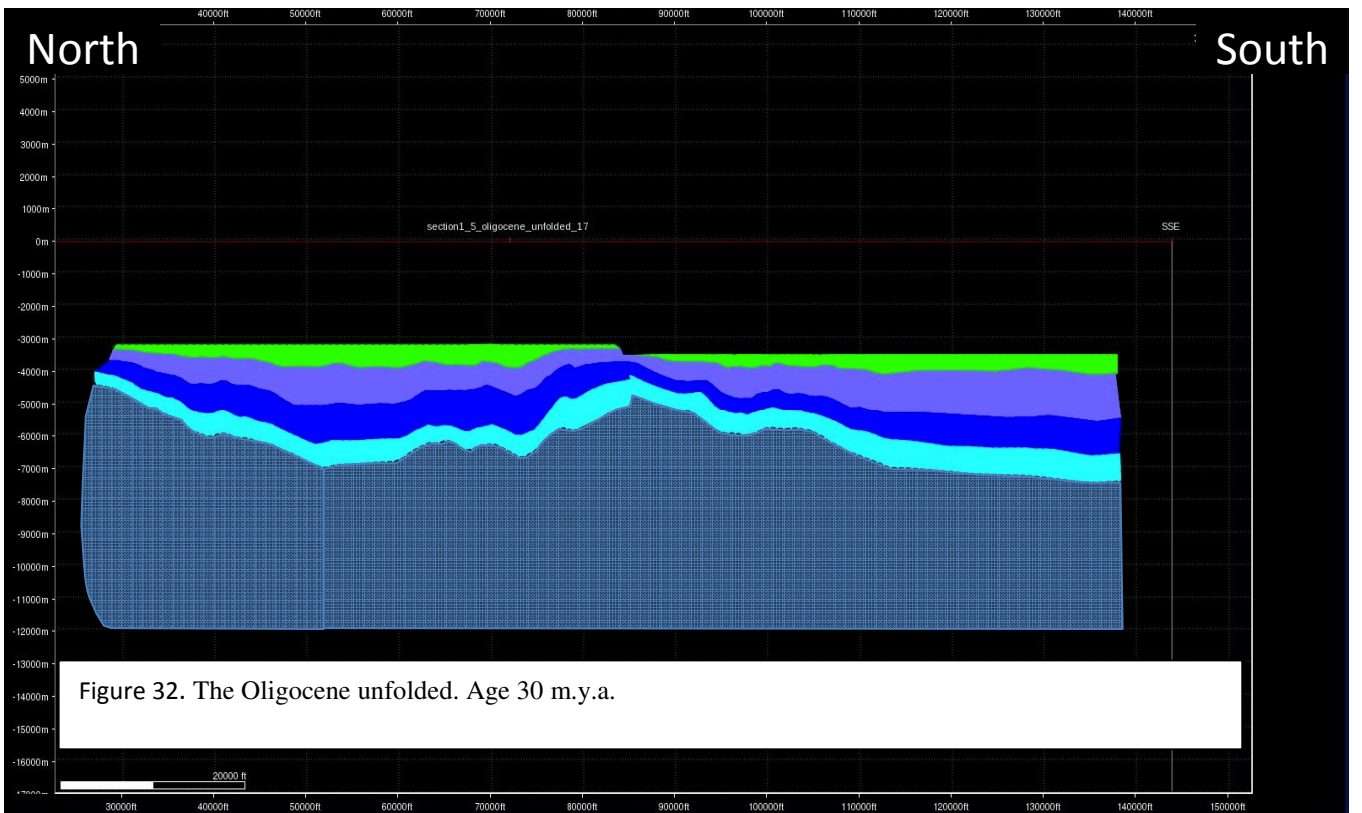




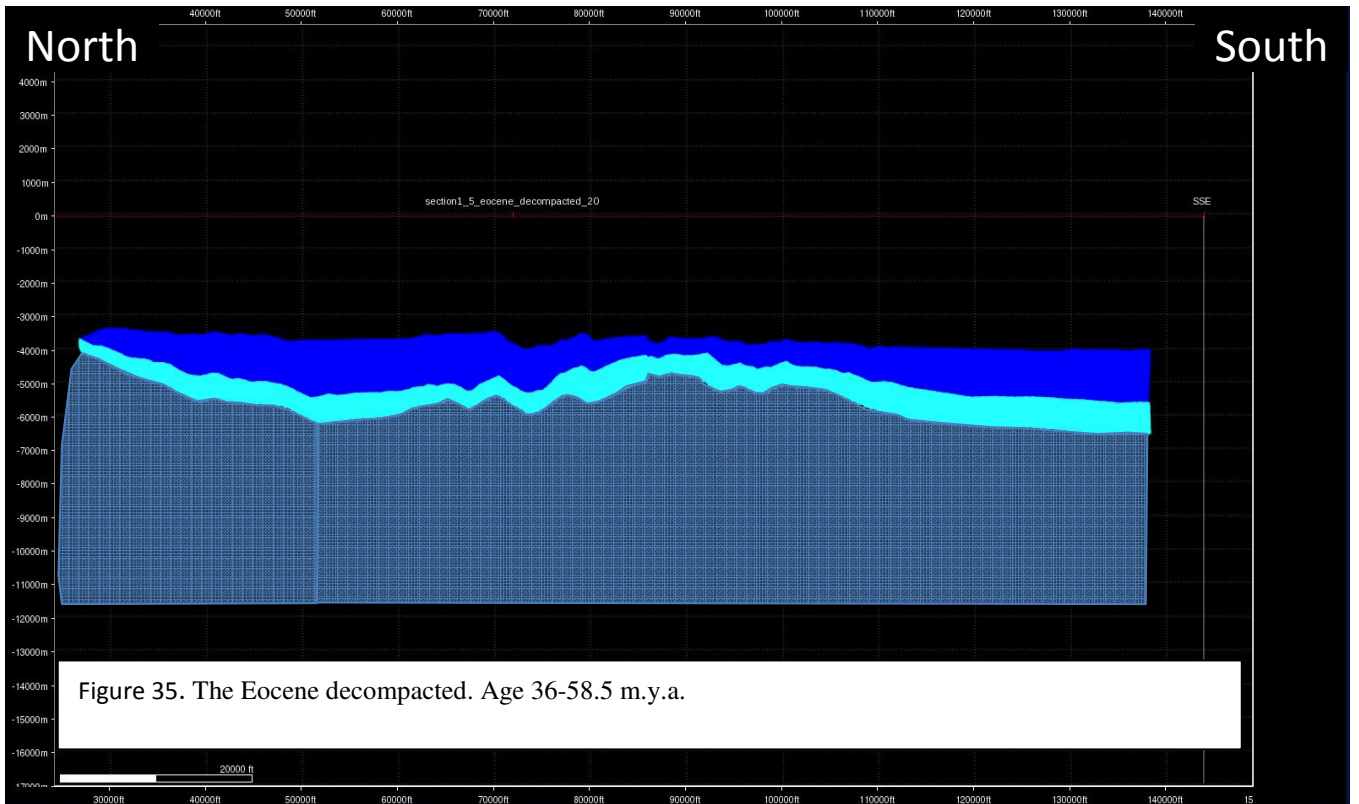
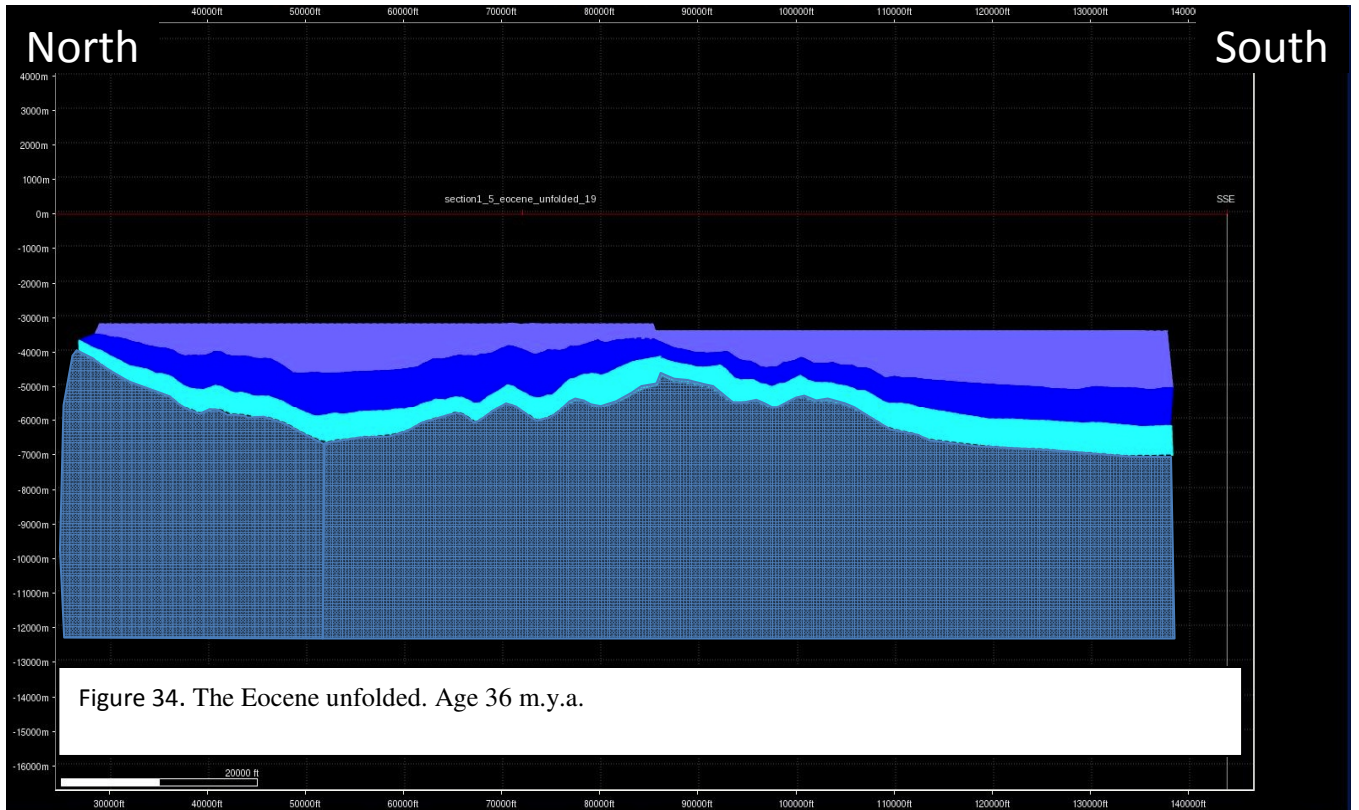


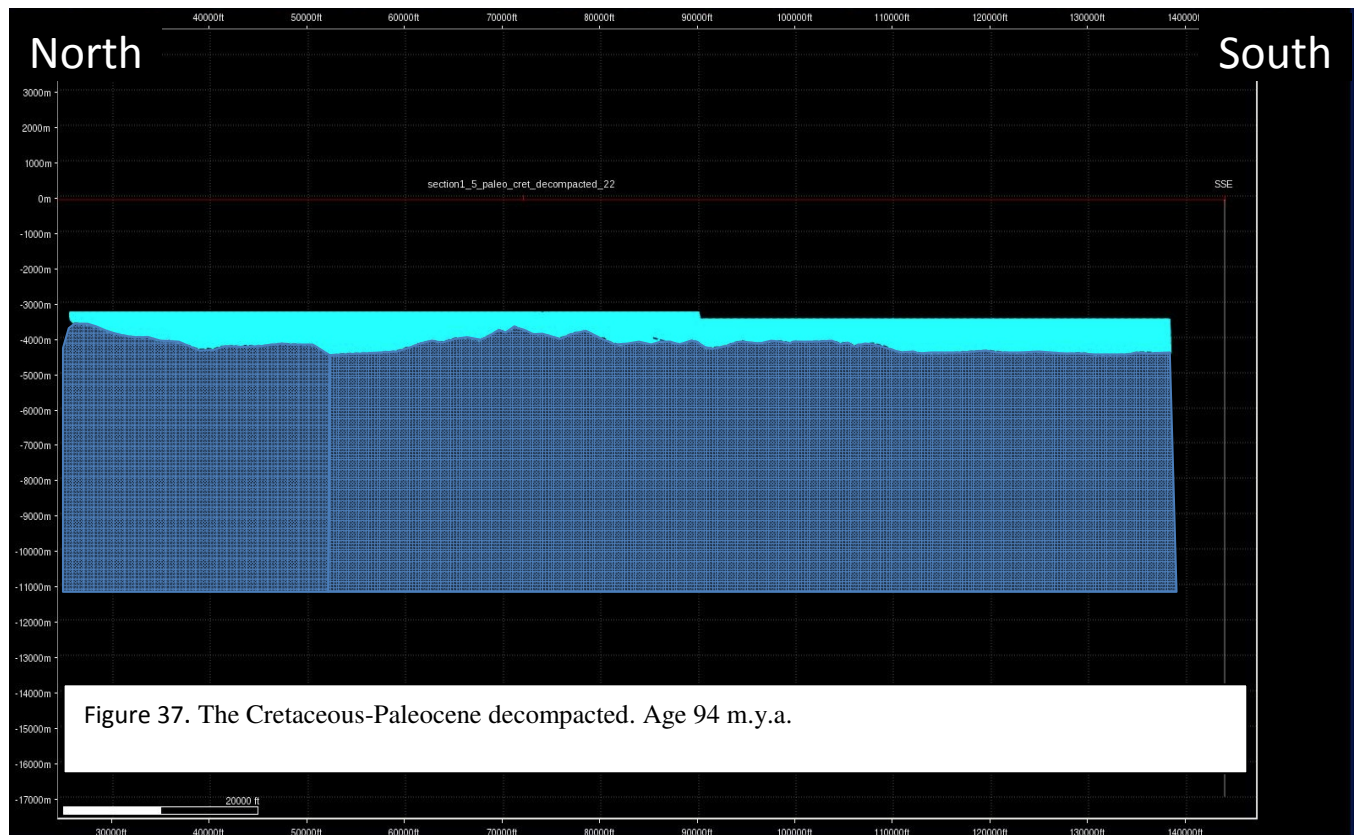
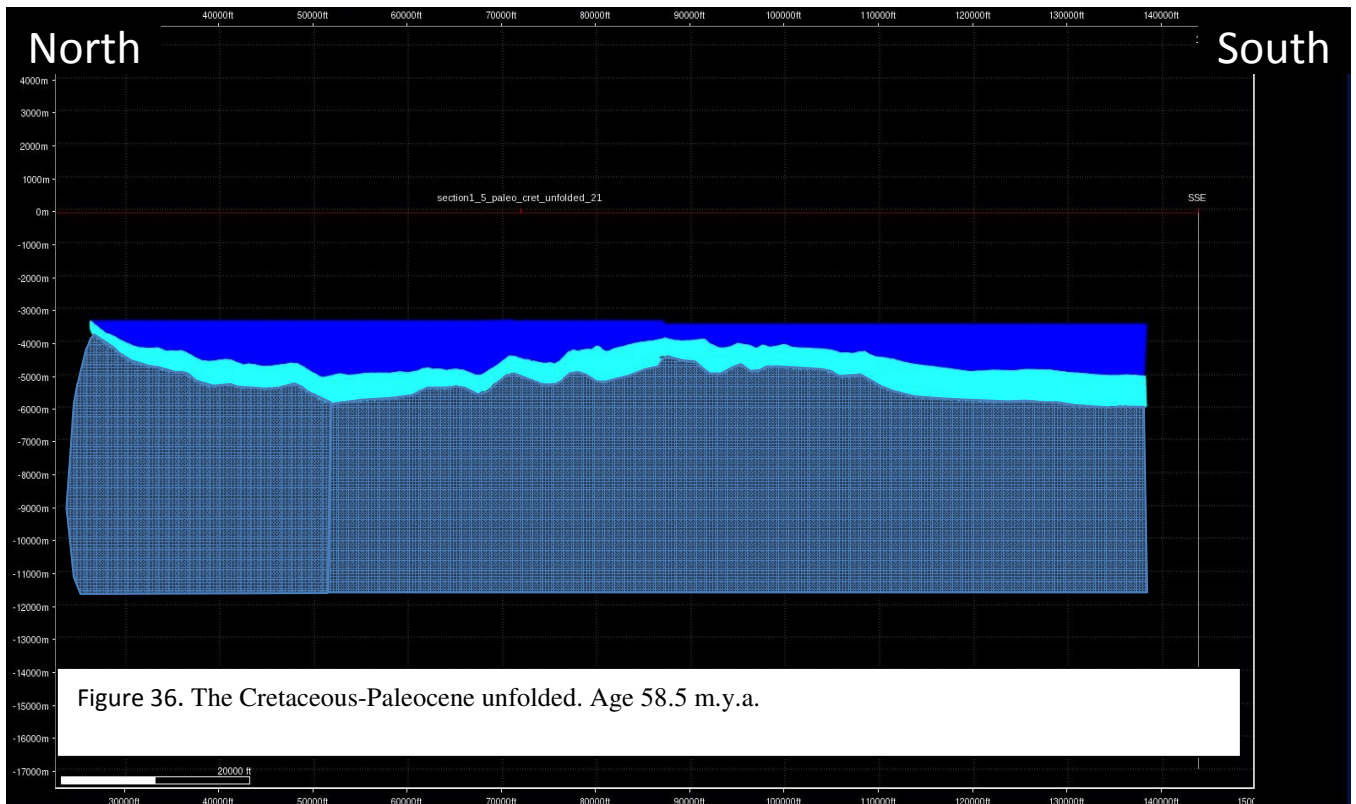












## Conclusion

The Green Knoll Salt Dome is an attractive feature for hydrocarbon exploration. Even though it is located in the deep waters of the Gulf of Mexico, making it a much more expensive operation, this area located near the Sigsbee Escarpment still has a lot of potential for more hydrocarbon discovery. The “Redwood” Prospect missed the objective Miocene sands on the flank of the salt diapir as a result of the halo kinetic angular unconformity. This angular unconformity was not fully recognized because of the poor seismic clarity at the time. At depth seismic clarity was so low in this area around the late 1990s and early 2000s that geoscientists could not properly image the beds on the side of the salt diapir. There also appears to be a sand package that bounds a potential limestone (old chemosynthetic community), which ‘seems’ to exist around the boundary of the angular unconformity which would not provide the necessary seal for hydrocarbons, hence the seepage of hydrocarbons through the limestone creating a chemosynthetic community. This is purely speculative because there is no evidence of a chemosynthetic community existing other than observational analysis from the Redwood mud log. Even though a proper seal for hydrocarbon accumulation does not exist at Redwood, the sands are so thin and the section is so condensed that it would not be economical. However, the well log reveals the existence of shale beds which could provide the potential for traps down dip from the original borehole location. The productive middle Miocene sands are also present further down dip terminating against the discontinuity surfaces possibly containing hydrocarbons with potential commercial traps.

The structural restoration revealed some of the same timing events as the Frampton fold belt, but it was not distinct. It revealed a more accurate depiction of the unconformity on the north and south side because it was easier to see the different geometries which lead to a better understanding on the formation of the Green Knoll. The restoration did exhibit the predicted growth and formation of a salt dome and the deformation it would cause to the surrounding sediment as deposition took place. Some limitations include the coarse and general nature of the 2D restoration. Another problem is modeling salt, since it is difficult to model the in plane out of plane movement as well as the volume of salt being added or subtracted to the system.

The Gulf of Mexico is a prolific petroleum basin that has been studied and analyzed intensely over the past few decades. Since seismic quality has increased in the past 10 years, there will be more to contribute to the petroleum geology interpretations on many of the more complex geological components that make up the Gulf of Mexico. The shallow salt canopy makes seismic imaging difficult for the underlying geology because salt creates a “washout” effect. It is also difficult to distinguish between the salt and sediment interface where strata rides onto the salt, which is the case in this study. An analysis of these relationships is important to furthering the understanding of the geology in this salt dominating basin.

## Works Cited

- Brown, F. L., Loucks, R. G., & Trevino, R. H. (2005). Site-specific sequence-stratigraphic section benchmark charts are key to regional chronostratigraphic systems tract analysis in growth-faulted basins. *AAPG Bulletin*, v. 89 No. 6, p. 715-724.
- Combellas-Bigott, R. I. (2002). Origin and Evolution of the Middle Miocene Submarine-Fan System, East-Central Gulf of Mexico. *GCAGS*, v. 52, p. 151-163.
- Combellas-Bigott, R. I. (2006). Depositional and structural evolution of the middle Miocene depositional episode, east-central Gulf of Mexico. *The American Association of Petroleum Geologists*, v. 9, p. 335-362.
- Combellas-Bigott, R. I., & Galloway, W. E. (2002). Origin and Evolution of the Middle Miocene Submarine-Fan System, East-Central Gulf of Mexico. *GCAGS*, v. 52, p. 151-163.
- Diegel, F. A., Karlo, J. F., Schuster, D. C., Shoup, R. C., & Tauvers, P. R. (1995). Cenozoic Structural Evolution and Tectono-Stratigraphic Framework of the Northern Gulf Coast Continental Margin. *Salt Tectonics: a global perspective AAPG Memoir* v. 65, p. 109-151.
- Dooley, T. P., Jackson, M. A., & Hudec, M. (2013). Coeval extension and shortening above and below salt canopies on an uplifted, continental margin: Application to the northern Gulf of Mexico. *AAPG*, v. 97, p. 1737-1764.
- Fillon, R. H., & Lawless, P. N. (1999). Paleocene-Lower Miocene Sequences in the Northern Gulf: Progradational Slope Salt-Basin Deposition and Diminishing Slope-Bypass Deposition in the Deep Basin. *GCAGS*, v. 49, p. 224-241.
- Galloway, W. E., Ganey-Curry, P. E., Li, X., & Buffler, R. T. (2000). Cenozoic depositional history of the Gulf of Mexico basin. *AAPG Bulletin*, v. 84 no. 11, p.1743-1774.
- Galloway, W. T., Whiteaker, T. L., & Ganey-Curry, P. (2011, August). History of The North American drainage basin evolution, sediment yield, and accumulation in the Gulf of Mexico basin. *Geosphere*, v. 7 No. 4, p. 938-973.
- Grando, G., & McClay, K. (2003, December 8). Structural Evolution of the Frampton growth fold system, Atwater Valley-Southern Green Canyon area, deep water Gulf of Mexico. *Marine and Petroleum Geology*, v. 21, p. 889-910.
- Hall, S. H. (2002). The role of autochthonous salt inflation and deflation in the northern Gulf of Mexico. *Marine and Petroleum Geology*, v. 19, p. 649-682.
- Hood, K. C., Wenger, L. M., Gross, O. P., & Harrison, S. C. (2002). Hydrocarbon systems analysis of the northern Gulf of Mexico: Delineation of hydrocarbon migration pathways using seeps and seismic imaging, in Surface exploration case histories: Application of geochemistry, magnetics, and remote sensing. (D. S. LeSchack, Ed.) *AAPG*, v. 48 No. 11, p. 25-40.



- Hossack, J. (1995). Geometric rules of section balancing for salt structures, in M. P. A. Jackson, D. G. Roberts, and S. Snelson, eds. *Salt tectonics: a global perspective: AAPG Memoir v. 65*, p. 29-40.
- Hudec, M. R., & Jackson, M. A. (2011). *The salt mine: a digital atlas of salt tectonics*. Austin: University of Texas at Austin, Bureau of Economic Geology, Udden Book Series No. 5; AAPG Memoir, p. 305
- Hudec, M. R., Jackson, M. A., & Peel, F. J. (2013). Influence of deep Louann structure on the evolution of the northern Gulf of Mexico. *AAPG*, v. 97, p. 1711-1735.
- Hudec, M. R., Norton, I. O., Jackson, M. A., & Peel, F. J. (2013). Jurassic evolution of the Gulf of Mexico salt basin. *AAPG*, v. 97 No. 10, 1683-1710.
- Jackson, M. A., & Talbot, C. J. (1986). External shapes, strain rates, and dynamics of salt structures. *Geological Society of America Bulletin*, v. 97, p. 305-325.
- Jackson, M. A., Hudec, M. R., & Dooley, T. P. (2010). Some emerging concepts in salt tectonics in the deepwater Gulf of Mexico: intrusive plumes, canopy-margin thrusts, minibasin triggers and allochthonous fragments. *Petroleum Geology Conference series*, v. 7, p. 899-912.
- Jackson, M. P. (1994). Regional extension as a geological trigger for diapirism. *Geological Society of America Bulletin*, v. 106, p. 88-113.
- Lawless, P. N., Fillon, R. H., & Lytton III, R. G. (1997). Gulf of Mexico Cenozoic Biostratigraphic, Lithostratigraphic, and Sequence Stratigraphy Event Chronology. *Gulf Coast Association of Geological Societies Transaction*, Vol. 47.
- Luo, G., Nikolinakou, M. A., Flemings, P. B., & Hudec, M. R. (2012). Geomechanical modeling of stresses adjacent to salt bodies: Part 1 - Uncoupled models. *AAPG*, v. 96, p. 43-64.
- Martin, J., Weimer, P., & Bouroullec, R. (2004). Sequence Stratigraphy of Upper Miocene to Upper Pliocene Sediments of West-Central Mississippi Canyon and Northern Atwater Valley, Northern Gulf of Mexico. *GCAGS*, v. 54, p. 425-441.
- Mercier, E., Rafini, S., & Ahmadi, R. (2007). Fold Kinematics in "Fold-and-Thrust Belts" the "Hinge Migration" Question, A Review. Thrust Belts and Foreland Basins. *Frontiers in Earth Science Part 4*, p. 135-147
- Morris, P. L., & Weimer, P. (2004). Structural Geology of the Mississippi Fan Fold Belt, Northern Deep Gulf of Mexico, Part 1: Geometry and Restorations. *Gulf Coast Association of Geological Societies Transactions* v. 64, 461-481p.
- Mount, V. S., Mahon, K. I., & Mentemeier, S. H. (2010). Structural Restoration and Basin Modeling in North-Central Gulf of Mexico Deepwater Subsalt Plays. *Gulf Coast Association of Geological Societies Transactions*, v. 60, p. 503-510.

- Nikolinakou, M. A., Luo, G., Hudec, M. R., & Flemings, P. B. (2012). Geomechanical modeling of stresses adjacent to salt bodies: Part 2 - Poroelastoplasticity and coupled overpressures. *AAPG*, v. 96, p. 65-85.
- Pilcher, R. S., Kilsdonk, B., & Trude, J. (2011). Primary basins and their boundaries in the deep-water northern Gulf of Mexico: Origin, trap types, and petroleum system implications. *AAPG Bulletin*, v. 95 No. 2, p. 219-240.
- Posamentier, H. W., & Venkatarathnan, K. (2003). Seismic Geomorphology and Stratigraphy of Depositional Elements in Deep-Water Settings. *Journal of Sedimentary Research*, v. 3 No. 3, p. 367-388.
- Prather, B. E., Booth, J. R., Steffens, G. S., & Craig, P. A. (1998). Classification, Lithological Calibration, and Stratigraphic Succession of Seismic Facies of Intraslope Basins, Deep-Water Gulf of Mexico. *AAPG Bulletin*, v. 82 No. 5A, p. 701-728.
- Rowan, M. G., & Vendeville, B. C. (2006, April 10). Foldbelts with early salt withdrawal and diapirism: Physical model and examples from the northern Gulf of Mexico and the Flinders Ranges, Australia. *Marine and Petroleum Geology*, v. 23, p. 871-891.
- Rowan, M. G., Jackson, M. P., & Trudgill, B. D. (1999). Salt-Related Fault Families and Fault Welds in the Northern Gulf of Mexico. *AAPG Bulletin*, v. 83 No. 9, p. 1454-1484.
- Rowan, M. G., Trudgill, B. D., & Fiduk, J. C. (2000). Deep water salt-cored fold belts: lessons from the Mississippi Fan and Perdido Foldbelts, Northern Gulf of Mexico. *Atlantic Rifts and Continental Margins. American Geophysical Union Geophysical Monograph*, v. 115, p. 173-191.
- Slater, J. G., & Christie, P. F. (1980). Continental stretching: an explanation of the post-mid-Cretaceous subsidence of the central North Sea basin. *Journal of Geophysical Research*, v. 85, p. 3711-3739.
- Stephens, B. P. (2009). Basement Controls on Subsurface Geologic Patterns and Coastal Geomorphology across the Northern Gulf of Mexico: Implications for Subsidence Studies and Coastal Restoration. *Gulf Coast Association of Geological Societies Transactions*, v. 59, p. 729-751.
- Stern, R. J., & Dickinson, W. R. (2010). The Gulf of Mexico is a backarc basin. *Geosphere*, v. 6 No. 6, p. 739-754.
- Trudgill, B. D. (1999). The Perdido Fold Belt, Northwestern Deep Gulf of Mexico: Part 1. Structural Geometry, Evolution and Regional Implications. *AAPG Bulletin*, v. 83, p. 88-113.
- Vendeville, B. C., & Jackson, M. A. (1992). The rise of diapirs during thin-skinned extension. *Marine Petroleum Geology*, v. 9, p. 331-353.
- Vinje, V. C. (2010, Volume 7 Issue 4). *Depth Imaging - Seeing the Invisible*. Retrieved February 2013, from Geo ExPro Depth Imaging: [http://www.geoexpro.com/article/Depth\\_Imaging\\_Seeing\\_the\\_Invisible/361f7888.aspx](http://www.geoexpro.com/article/Depth_Imaging_Seeing_the_Invisible/361f7888.aspx)

- Weimer, P. (1990). Sequence Stratigraphy, Facies Geometries, and Depositional History of the Mississippi Fan, Gulf of Mexico. *AAPG Bulletin*, v. 74 No. 4, p. 425-453.
- Witrock, R., Nixon, B., Post, P. J., & Ross, K. M. (2003). Biostratigraphic chart of the Gulf of Mexico offshore region, Jurassic to Quaternary. *U. S. Department of the Interior, Bureau of Ocean Energy Management, Regulation and Enforcement, New Orleans*, [http://www.data.boem.gov/homepg/data\\_center/gandg/biochart.pdf](http://www.data.boem.gov/homepg/data_center/gandg/biochart.pdf). Retrieved from BOEM.gov.
- Wu, Y., Loudon, K. E., Funck, T., Jackson, R. H., & Dehler, S. A. (2006). Crustal structure of the central Nova Scotia margin off Eastern Canada. *Geophys. J. Int.*, v. 166, p. 878-906.

## Vita

Randy Broussard was born in New Orleans, Louisiana in 1983. He moved to Houston in 1999 where he completed his schoolwork at Stephen F. Austin High School in 2003. Randy finished a year of core college credits at Wharton County Junior College and then attended the University of New Orleans (UNO) where he graduated with a double major in business administration and marketing as well as a minor in finance in 2008. He discovered his passion while taking an Earth Science class and continued his education by receiving a Bachelor's in Earth Science from UNO in 2011. During his tenure as a Geology Bachelor's student in the Earth Sciences program he worked for the Bureau of Ocean Energy Management (BOEM, former MMS) as an intern for biologists and physical scientists. Randy entered the Earth Sciences graduate school at UNO in 2011, and BOEM promoted him to a student trainee geology position in their Geophysical and Geological Unit in 2011.